TECHNISCHE UNIVERSITÄT DRESDEN

Fakultät Umweltwissenschaften

Recharge and residence times in an arid area aquifer

Dissertation zur Erlangung des akademischen Grades Doktoringenieur (Dr.-Ing.)

vorgelegt von
Müller, Thomas, Dipl.-Ing.

Gutachter:

Herr Prof. Dr. Rudolf Liedl
Technische Universität Dresden

Herr Prof. Dr. Werner Aeschbach-Hertig
Universität Heidelberg

Herr Prof. Dr. Johannes Barth
Universität Erlangen-Nürnberg

Dresden, 13. Dezember 2012

Erklärung

Erklärung des Promovenden

Die Übereinstimmung dieses Exemplars mit dem Original der Dissertation zum Thema:

Recharge and residence times in an arid area aquifer

wird hiermit bestätigt.

.....
Ort, Datum

.....
Unterschrift (Vorname Name)

COMITTEE

Head of the Committee:

Herr Prof. Dr. Christian Bernhofer
Technische Universität Dresden

1. Reviewer:

Herr Prof. Dr. Rudolf Liedl
Technische Universität Dresden

2. Reviewer:

Herr Prof. Dr. Werner Aeschbach-Hertig
Universität Heidelberg

3. Reviewer:

Herr Prof. Dr. Johannes Barth
Universität Erlangen-Nürnberg

Day of the defense: 19.04.2013

Signature of the head of the PhD committee:

Still, it was worth it.

Acknowledgements

First and foremost, I would like to thank Dr. Gerhard Strauch for the last three and a half years of working together. Thank you, especially for taking responsibility, for always giving me support and for encouraging me throughout the dissertation (but also for ignoring me when becoming too fundamental with my criticism!). I hope I will never forget your ability to look ahead with enthusiasm and curiosity.

Outstanding was the time at the USGS in Reston. Even it was only 3 months, the experiences I made there were of crucial importance for this work. By working together with Ward Sanford I had the chance to learn a lot about groundwater modelling and age dating, but also about how to do science in general and what good scientific practice is. Thank you Ward.

I would also like to thank Professor Rudolf Liedl for his willingness to become the supervisor of this work, even though I was already half-way into my dissertation. The discussions and meetings we had were very valuable for me.

During many visits in Oman I had the chance to experience the warm hospitality of the Omani people which I hope I will always remember. Many people supported my data collection and field work. Dr. Khalid Al-Mashaikhi, Dr. Abduallah Al-Bawain, Dr. Tariq Helmi and Dr. Abdulaziz Ali-Al-Mashaikhi shall be named here in representation of the Ministry of Regional Municipalities and Water Resources and of all those involved.

For the critical reviews and discussions on the dating section I would like to thank Dr. Stephan Weise and Dr. Karsten Osenbrück. Also,

the discussions with Professor Peter Fritz, Professor Werner Aeschbach-Hertig and Dr. Wolfgang Gossel have been very valuable for me. Thank you for that. Thanks also to Edda, Jan and Jan, Andreas and Christian for giving me feedback to parts of this thesis.

This work was funded through the Federal German Ministry of Education and Research (BMBF). So, many thanks go out to our society, the taxpayers, but also to our educational system wich provides opportunities for personal development. Many thanks to the team International Postgraduate Studies in Water and Technology (IPSWaT) for their financial support and benefits without which this work would not have been possible.

Thanks to Stefan Pavetich for the analysis and discussion of the ^{36}Cl-data. Thanks also to David Huenlich and Jessica Plummer for corrections to my English. Many others have been helpful in different ways: Armin and Agnes for sure, Nico and Fred.

Thanks also to the Helmholtz-Centre for Environmental Research - UFZ and here especially the Department of Hydrogeology for allowing me an enormous amount of freedom and independence, and for providing financial and technical support when necessary. The Helmholtz Interdisciplinary Graduate School for Environmental Research (HIGRADE) gave me the chance to participate in lectures and seminars which helped to expand my horizon beyond the water and modelling sector. Thanks for that and for the uncomplicated handling of financial support.

How can I express my gratitude to the people important in my life? My sister Grit, Anton und Paula, my friends Ines, Christian and Martin? You all know how happy I am to have you - but it probably won't hurt to say that again. Sorry for my difficulties to properly set my priorities.

Sarah, that I met you during this PhD journey was the best that could happen. While the PhD is (almost) over, we can go on. Isn't this just great?

Thesen

1. Rain and surface water flow occur from time to time in the arid climate of today's Najd. They are possible sources for groundwater recharge.
2. Modern groundwater recharge to the deep groundwaters - the lower Umm Er Radhuma aquifers - in the Najd does occur.
3. The deep Najd groundwaters are part of an active flow system. Modern recharge must exist to maintain the observed groundwater levels in the Najd.
4. Calculations of the mean groundwater residence times based on radiocarbon data underestimate the groundwater residence times of the deep Najd groundwaters.
5. ^{36}Cl and ^{4}He proove to be more robust tracers for the age dating of the deep aquifers in the Najd.
6. The mean groundwater residence times of the lower Umm Er Radhuma aquifers in the central Najd are in the range of 550,000 years. The resulting flow velocities are below 0.5 m a^{-1}.

Thesen

1. Regen und Oberflächenabfluss treten im heutigen ariden Najd in unregelmässigen Abständen auf. Damit steht Wasser für Grundwasserneubildung zur Verfügung.
2. Es erfolgt eine Grundwasserneubildung in die tiefen Grundwasserleiter der Umm Er Radhuma Formation im Najd.
3. Die tiefen Grundwasserleiter im Najd sind Teil eines aktiven Fließsystems. Rezente Grundwasserneubildung ist notwendig um die aktuell gemessenen Grundwasserstände in den tiefen Grundwasserleitern zu halten.
4. Die Berechnungen der Grundwasseralter basierend auf C-14 Daten unterschätzen die mittleren Verweilzeiten der tiefen Grundwasser im Najd.
5. Chlor-36 und Helium-4 erscheinen im Vergleich mit C-14 die zuverlässigeren Tracer für die Datierung der tiefen Grundwasser im Najd zu sein.
6. Im zentralen Najd können die Grundwasseralter im tiefen Umm Er Radhuma Grundwasserleiter im Bereich bis zu 550 000 Jahren liegen. Damit ergeben sich Fließgeschwindigkeiten unterhalb 0,5 m a^{-1}.

Abstract

Deteriorating water quality in the face of a rising demand for agricultural products triggered interest in the groundwater resources of the Najd dessert, an arid region of southern Oman.

Groundwater in this area usually is abstracted from one of the largest aquifers on the Arabian Peninsula, the Umm Er Radhuma aquifer. Increased discharge stands in contrast to limited precipitation: the monsoon is an annual event but it is regionally limited; cyclones infrequently occur within the range of three to seven years. Both are possible sources for groundwater recharge in the Najd.

With these preconditions in mind, the present study investigates recharge to the Najd groundwaters as part of an active flow system and evaluates the mean residence time in the deep groundwaters. The tools of choice are a groundwater flow model combined with environmental isotope tracer data.

The two-dimensional flow model replicates the characteristics of the aquifer system from the potential recharge area in the south (Dhofar Mountains) to the discharge area in the north (Sabkha Umm as Sammim). The south-to-north gradients and the observed artesian heads in the confined aquifer are reproduced. Simulation results indicate that changes between wet and dry periods caused transient responses in heads and head gradients lasting for several thousand years.

Based on the used parameters the model calibration indicated, that a recharge rate of around 4 mm a^{-1} is sufficient to reproduce current groundwater levels. Since rising groundwater levels were documented after cyclone Keila in November 2011, modern recharge evidently occurs.

^{36}Cl concentrations and dissolved-helium concentrations indicate that the deep groundwaters in the central Najd are up to 550,000 years old. Thus, radiocarbon values indicating groundwater residence times for the central Najd up to 20,000 years and the northern Najd up to 35,000 years underestimate the groundwater residence times and seem to have been strongly affected by mixing during sampling. Decreasing ^{36}Cl and increasing ^{4}He concentrations confirm the expected trend in the direction of groundwater flow and prove to be more robust tracers for age dating of Najd groundwaters.

Backward pathline tracking was used to simulate the groundwater ages. The tracking results show that a total porosity value between 15 and 20 % is consistent with the range of the observed chlorine-36 and heliumbased ages.

The results and parameters obtained in the present study provide the basis for future 3D-groundwater models designed to evaluate the water resources available to the Najd's agricultural complex. In addition, the developed 2D-model allows for studies of paleoclimate scenarios and their influence on the groundwater regime.

Kurzfassung

Ein steigender Bedarf nach landwirtschaftlichen Produkten - und damit Wasser - bei gleichzeitiger Abnahme des verfügbaren Wassers in Qualität und Menge in den bisherigen Anbaugebieten, führt zu einer inteniven Nutzung der Grundwasserressourcen der ariden Najd-Region in der Provinz Dhofar, im Süden des Sultanats Oman. Als Quelle dienen die Grundwasservorräte des Umm Er Radhuma-Aquifers, einer der Hauptaquifere auf der arabischen Halbinsel. Der steigenden Nutzung stehen mit dem jährlichen Monsoon, der regional limitiert ist, und unrgelmässigen, zwischen 3 und 7 Jahren auftretenden Unwettern (Zyklonniederschlag) nur begrenzte Niederschlagsmengen als Quellen für eine mögliche Zufuhr von Wasser (Grundwasserneubildung) zum Aquifersystem gegenüber.

Der Ansatz der vorliegenden Arbeit besteht darin, mit Hilfe eines Grundwassermodells und der Einbeziehung von Umweltisotopen das tiefe und zur Nutzung geförderte Grundwasser in der Najd-Region als Teil eines aktiven Fließsystemes zu untersuchen und mittlere Verweilzeiten des Grundwassers abzuleiten.

Ein 2D-Grundwassermodell entlang einer Fließlinie vom Dhofar Gebirge im Süden zur Sabkha Umm as Sammim im Nordosten wurde entwickelt. Das Modell reproduziert den Süd-Nord-Gradienten als auch den aufwärts gerichteten Gradienten mit höheren Grundwasserständen in den tiefen Grundwasserleitern. Die Simulationen zeigen, dass der Wechsel von ariden und humiden Phasen (wenig bzw. viel Grundwasserneubildung) zu Veränderungen der Grundwasseroberfläche führt die mehrere tausend Jahre anhalten können. Das kalibrierte Grundwassermodel zeigt, dass mit einer Neubildungsrate von 4 mm a^{-1} die natürlichen Grundwasserverhältnisse im Najd abgebildet werden können. Dass eine

moderne Grundwasserneubildung stattfindet, konnte mittels Loggermessungen anhand steigender Grundwasserstände im tiefen Aquifersystem nach dem Extremunwetter im November 2011 (Zyklon Keila) eindeutig nachgewiesen werden.

Die Analyse der ^{36}Cl- und ^{4}He-Konzentrationen zeigt, dass die tiefen Grundwasser im zentralen Najdgebiet bis 550 000 Jahren alt sein können. Das bedeutet allerdings, dass die über ^{14}C Daten berechneten Grundwasseralter mit ca. 20 000 Jahren für das zentrale Najdgebiet und bis zu 35 000 Jahren für den nördlichen Najd, die Grundwasseralter deutlich unterschätzen.

Die abnehmenden ^{36}Cl und ansteigenden ^{4}He Konzentrationen zeigen den erwarteten Trend in Grundwasserfließrichtung und können als aussagefähige Tracer für die Bewertung der Verweilzeiten und Alter des fossilen Grundwassers der Najd-Region angesehen werden.

Mit Hilfe des Partickeltrackings wurden die Grundwasseralter, basierend auf den Isotopentracern, im Grundwassermodel simuliert. Die Porosität wurde dabei für das Aquifesystem mit Werten zwischen 15 und 20 % bestimmt.

Die generierten Parameter und das gewonnene Systemverständnis sind eine wichtige Basis für zukünftige 3D-Modellstudien welche die Verfügbarkeit der Wasserresourcen im Najd untersuchen werden. Weitere Anwendungen für das in dieser Studie aufgebaute 2D-Modell sind Untersuchungen zum Paläoklima und dessen Einfluss auf das Grundwassersystem.

List of abbreviations

AMS	accelerator mass spectrometry
amsl	above mean sea level
BP	before present
CHB	Constant head boundary
CSS	Composite Scaled Sensitivity
DAM	Dammam
GHB	General head boundary
ICP-MS	Induced Coupled Plasma-Mass Spectometry
ITCZ	Intertropical Convergence Zone
LGM	Last glacial maximum
LUER	Lower Umm Er Radhuma
MRMWR	Ministry of Regional Municipalities and Water Resources
PCC	Parameter correlation coefficient
pmC	percent modern Carbon
OSL	optical stimulated luminescence
RCH1	Recharge zone 1
RCH2	Recharge zone 2
RUS	Rus
SRTM	Shuttle Radar Topography Mission
TDS	Total dissolved solids
UER	Umm Er Radhuma
UUER	Upper Umm Er Radhuma

Contents

List of Figures

List of Tables

Chapter 1

Introduction

1.1 Motivation

Recent work on groundwater resources in the Dhofar Governorate of the Sultanate of Oman was initiated for practical reasons: water quality in the Batinah region, the main agricultural area, is deteriorating, while the demand for agricultural products has been increasing over the years. As a consequence the ministries of the Sultanate of Oman have planned and installed large industrial farming areas in the arid Najd region in Dhofar within the last 10 years. Consequently, a strong interest in the hydrogeology and hydrologic characteristics of the area developed. The main concern was how much water could actually be taken from subsurface water systems.

From a perspective of water management this leads to the question of how much water is going in and - if so - when does it recharge and what are the sources for this?

The Sultanate belongs to the most arid areas in the world, which is especially true for the inland region of Dhofar, the Najd, with mean air temperatures of 26.3 °C and low rainfall amounts with around 49 mm a^{-1}. The only direct source of rain to the Najd are rare storm events, so-called cyclones, which reoccur infrequently every 3 to 7 years. These sometimes result in heavy surface runoff lasting for several days. Does water infiltrate the ground during these events, and does it reach the deep aquifers, which are the target for the exploration?

Another regional weather event is the monsoon. The monsoon, locally called *khareef*, is unique for the Arabian Peninsula and brings moisture and rain to the south side of the Dhofar Mountains every year between June and September. Could there also be an input to the deep reservoir via the south-western monsoon?

1.2 State of the Field

Several studies on the groundwater resources and climatic conditions in Oman have been conducted in the past. What follows summarizes the major works and their findings with regard to recharge conditions and groundwater residence times.

A first complex study on the groundwater resources in the Dhofar region is provided by Clark in his PhD thesis (Clark, 1987). The study used isotopic and geochemical methods to determine groundwater mean circulation times. Clark concluded that recent recharge to the shallow aquifers takes place during cyclones in the area, whereas groundwaters confined in considerable depth below the Najd were recharged during more humid times in the Holocene pluvial. The residence time of the deep groundwaters in the Najd were determined to be in excess of 10,000 years (Clark et al., 1995). Modern recharge to the Najd by the yearly monsoon could not be identified.

The assumption that storm events can recharge the shallow aquifer system was proven by Macumber who sampled a cyclonic storm in autumn 1992 in the Al-Wusta region in central Oman, approximately 70 km east of the Najd area Macumber et al. (1994). Rainfall, runoff and shallow groundwater were sampled for chemical and isotopic analyses. Macumber concluded that the infiltration is rapid, the losses by evapotranspiration are small and that under the right physical conditions cyclones can produce fresh groundwater resources.

Stable water isotopes, noble gas measurements and radiocarbon data were analyzed and interpreted in a study area in northern Oman (Weyhenmeyer, 2000). The noble gas temperatures indicated a difference in the groundwater recharge temperatures. Combined with the groundwater ages given by the radiocarbon data this was interpreted as a temperature shift of 6.5±0.6 K, that is, from the Late Pleistocene to the higher temperatures today. It was also concluded that the movement of the Intertropical Convergence Zone (ITCZ) during and since the last glacial maximum (LGM) led to different moisture sources recharging the aquifers. These movements also affected southern Oman - and therefore the region under study here.

Speleothems - proxies for paleoclimate studies - have been investigated in caves in northern and southern Oman. These proxies are reliable climate archives, providing information on the periodicity and intensity of the Indian Ocean Monsoon. Studies by Neff (2001), Burns et al. (2002) and Fleitmann et al. (2011) used oxygen-isotope signatures from uranium-thorium dated speleothems to show the variation in the amount of monsoon precipitation over the last 350,000 years, with the last pluvial period dated from around 6.3 to 10.5 ka BP. The works also announce that the extent of monsoon rainfall was more to the north of its present location during those pluvial times.

The most recent studies on groundwater, groundwater residence times and pale-

oclimate in Dhofar are the PhD thesis of Al-Mashaikhi "Evaluation of groundwater recharge in Najd aquifers using hydraulics, hydrochemical and isotope evidences" (Al-Mashaikhi, 2011) and the Master thesis of Herb "Paleoclimate study based on noble gases and other environmental tracers in groundwater in Dhofar (Southern Oman)" (Herb, 2011). Al-Mashaikhi's work focused on sampling, analyzing and interpreting of the groundwater chemistry and groundwater ages by using isotopes (^{18}O, ^{2}H, ^{3}H, ^{14}C). The following three hypotheses were given:

- groundwater recharge is usually related to flood events reflected in the development of the groundwater levels
- the groundwater quality is controlled by active recharge, aquifer matrix, dissolution processes, geological structure and the aquifer characteristics
- the groundwater age and recharge processes over the Najd is the result of changing climate conditions during a period of more than 20 thousand years

Herb focused on the chronology of the paleotemperature record for the Dhofar groundwaters, based on noble gas measurements. He, too, determined the groundwater ages through radiocarbon and tritium dating. The paleotemperature record based on radiocarbon data shows a temperature increase of 6.3±1.7 K since the last glacial period. Herb stated that no recharge area could be detected, which is most likely a result of mixed groundwaters caused by fault zones, long screen depths of the sampled wells and extensive pumping activities. The radiocarbon ages show no age increase in direction of the groundwater flow from the Dhofar Mountains into the Najd, whereas an increasing trend of non-atmospheric helium with the calibrated ages can be observed. Most of the groundwater was recharged during more humid times, recent recharge originates from cyclones and is limited in time and space. The stable isotope data show no sign of evapotranspiration, indicating a fast infiltration of the cyclone-related rain water.

The presented work on the groundwater dynamic and recharge processes can be summarized as follows:

- groundwater ages based on radiocarbon data give ages up to 35,000 years for the Najd area
- storm events can recharge the shallow aquifer system
- rain water infiltrates rapidly into the ground
- the monsoon does not significantly contribute to modern recharge to the Najd
- in the past the ITCZ moved north and south to today's position and therefore changed the extent of the monsoon

1.3 Aim and general research questions

Though many findings have been obtained over the years, some essential questions remain open regarding the underground water reservoir and its connection to an active flow system.

The aim of the present study was to develop a groundwater model that offers the possibility of studying possible recharge scenarios. The implementation of travel times based on environmental isotopes received special attention in the modelling process. Therefore environmental isotopes had to been interpreted. The working hypothesis was that the combination of groundwater flow modeling and environmental tracer interpretations can lead to a better understanding of the groundwater system with its observed behaviour (monitoring, tracer). The present work will show how the combination of several known techniques (numerical modelling, environmental isotopes) leads to a better understanding of the groundwater resources in the Najd. The general research question was:

Are the Najd (deep) groundwaters part of an active flow system?

Further sub-questions to this research question were:

Recent groundwater recharge: Considering today's arid conditions in the Najd and the more humid conditions of its past, when the underground reservoir was most likely filled, raises the question of whether groundwater recharge has taken place at all in recent times. The possible sources are known since monsoons and storm events are documented. But it remains unclear whether they contribute input to the deep aquifer system. Furthermore, if no connection to an active flow system exists - does this mean that natural depletion (falling groundwater levels) is ongoing?

Groundwater residence times: The radiocarbon based groundwater ages of the recent studies show partly contradicting results in themself but also in comparison to prior studies on groundwater ages or climate conditions. By using other tracers the range of groundwater residence times shall be investigated with a higher degree of certainty. If these residence times can be obtained, what are their impacts?

1.4 Thesis outline

The overall research question and the stated sub-questions are answered in the chapters of this thesis. Chapter 2 describes the region under study with a focus on local features like the Indian monsoon and paleoclimate conditions. Chapter 3 documents the available data and the main pillars this study is based on, namely field work and modeling. Chapter 4 provides an analysis on the available data resulting in the conceptual model for the Dhofar area. The implementation of the conceptual idea in a numerical flow model, the development and calibration of the flow model, and the model results are described in chapter 5. Najd groundwaters are dated based on environmental isotopes in chapter 6. Finally, chapter 7 summarizes the answers to the research questions, provides ideas for future work and raises a number of new research questions.

Chapter 2

Region Under Study

This chapter will present basic information about the region under study. It goes into more detail with regard to topics that have a high relevance for the present study. This includes specific local features such as the occurence and extension of the Indian monsoon, or changing environmental conditions such as the change from previously more humid conditions to a currently dryer climate.

2.1 General Description

The Sultanate of Oman is located on the southeastern coast of the Arabian Peninsula, shown in Figure 2.1. The capital of the Sultanate is Muscat, which lies close to the Northern Tropic. The governorate of Dhofar is one of eight main administrative regions of the Sultanate. Dhofar is the southernmost governorate, sharing a border with Yemen in the west and Saudi Arabia in the north. It covers approximately 99,000 km^2, making it the largest governorate in the Sultanate. The capital of Dhofar is Salalah.

Since Sultan Qaboos bin Said came into power in 1970, the Sulanate of Oman has undergone great changes in the course of its transition from a developing to a developed country. Great efforts were made to establish a modern governmental structure, to access and exploit natural resources (especially oil) and to create the necessary infrastructure. At the same time successful attempts were made to improve living conditions including health facilities, food supply and the educational system. The country's growth and the reliance on its own resources lead to an increased demand for water, with 90 % of the total consumption attributable to the agricultural sector (http://www.fao.org).

Apart from the areas close to the mountains where water from the Falaj system (underground channels, for more information see e.g. Al-Marshudi (2001)), or

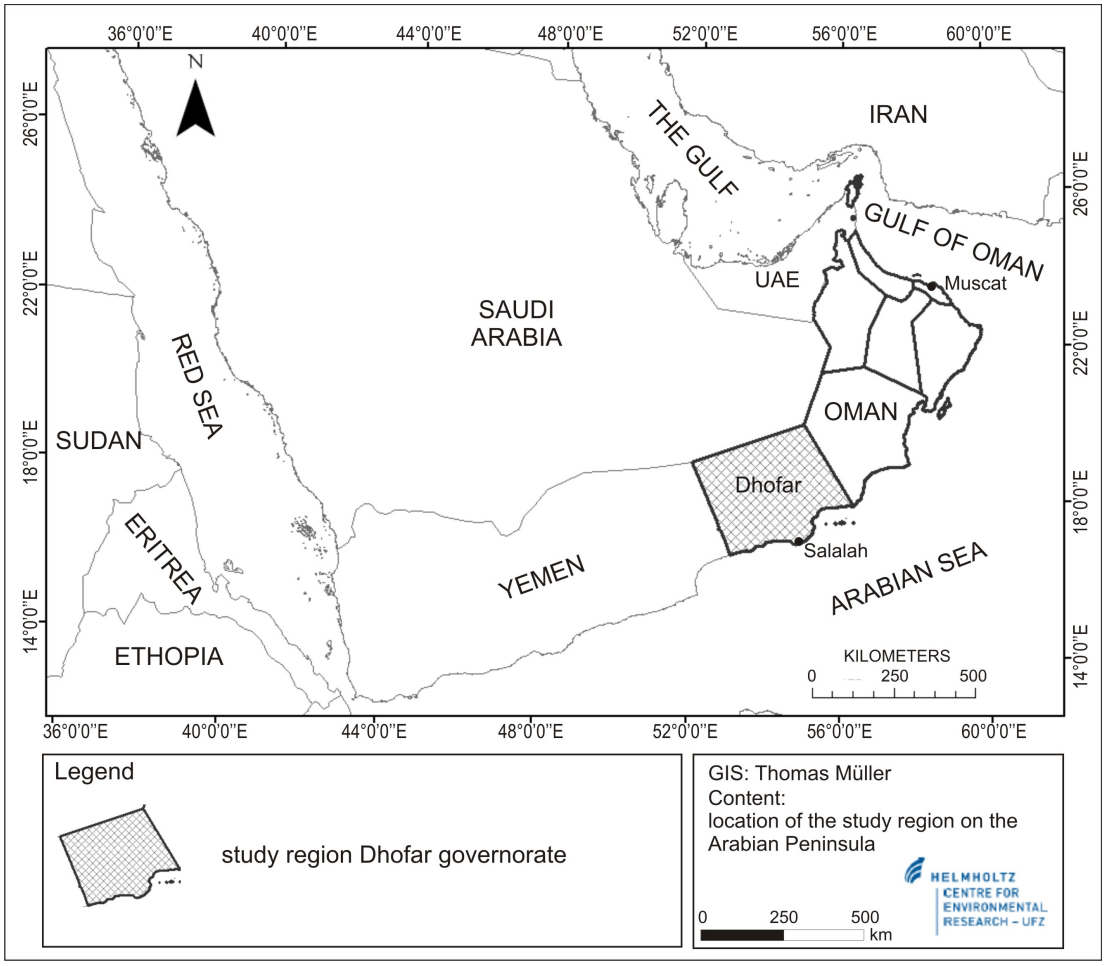

Figure 2.1: The Arabian peninsula with the Sultanate of Oman and the region under study, the Southern Governorate Dhofar.

from springs or dams is available, groundwater became more and more subject to exploration and exploitation. It is by now supplying the majority of the freshwater needs.

With high air temperatures (mean of 26.3 °C for station Thumrait 1986-2009) and small amounts of rainfall (mean 30 mm a^{-1} for station Thumrait 1980-2009) the interior area of Dhofar, the Najd, belongs to the most arid areas in the world. Due to its geographical position on the Arabian Peninsula and the topography of the coastal regions, much of the land receives only small amounts of rainfall. The low rainfall rates and the infrequent occurence of rain make irrigation irreplaceable and, more importantly, sets a limit for the amount of water that can recharge the aquifers. The result is an imbalance between the limited input (recharge) to the reservoir and high water discharge from the reservoir, as usage constantly increases.

2.2 Topography and Geomorphology

Dhofar can be divided into three distinct regions: the coastal plain in the south, the adjacent Dhofar Mountains and the so called Najd - the area north to the mountains reaching up to the Rub Al-Khali desert, as shown in Figure 2.2. The figure also indicates ground elevation in 250 meter intervals. This information was derived from SRTM data with a horizontal resolution of 30 meters (ERSDAC 2011).

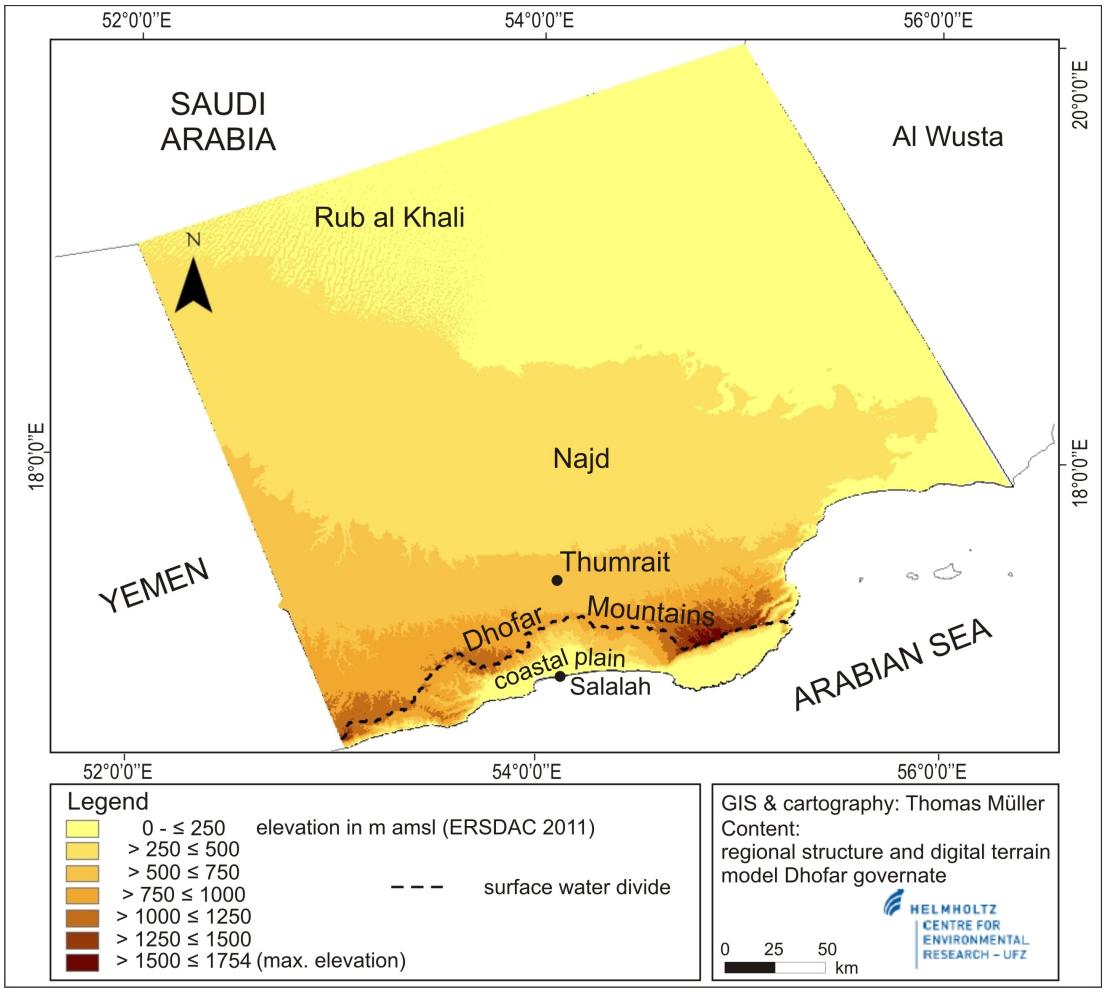

Figure 2.2: Regional structure of the Dhofar governorate with coastal plain, Dhofar Mountains and Najd Region. Dashed line represents surface water divide in the Dhofar Mountains. Ground elevation levels are given in 250 meter intervals based on SRTM data.

Salalah, the capital of the Dhofar governorate, is in the centre of the coastal plain. This area is about 65 km long and 15 km wide at its broadest point. Further to the east there are two other, more narrow coastal plains in Mirbat and Shalim. From the plains, the elevation rises abruptely to more than 1,000 m amsl in the mountains, with higher elevations in the west (Jabal al Qamar, approximately 1,400 m amsl) and east (Jabal Samhan, approximately 1,750 m amsl), than in the centre (Jabal Qara, 1,100 m amsl).

Whereas the southern side has steep slopes, the elevation very gently declines towards the north-east. The Najd area is the main subject of the present study. The terrain in the central Najd is comprised of a stony and sandy plain. Large wadi channels, most likely representing drainage patterns from former pluvial periods, pervade the plain in a south-south-west to north-north-east direction. The northern part of the Najd is covered by large sand dunes which are part of the Rub Al Khali Desert which extends into the Kingdom of Saudi Arabia. The elevations in the far north-east lie between 100 and 200 m amsl.

Vegetation in the Najd is quite sparse, whereas in the Dhofar Mountains there is a natural cover of trees, bushes and grass. Shrubs, grass-tufts, and occasional trees can be found mostly in or close to the wadi beds.

The Najd covers an area of approximately 90,000 km^2 and is bounded by the border to Yemen in the west, the border to Saudi Arabia in the north and the Al-Wusta governorate in the east. The biggest city in the Najd is Thumrait with around 10,000 inhabitants. Smaller villages, farms and individual Bedouine camps are distributed over the Najd. The total number of inhabitants of the Najd is believed to be around 20,000.

2.3 Climate

Previous studies indicate that the groundwater in the Dhofar area was recharged during more humid times in the last 25,000 years (e.g. Al-Mashaikhi (2011); Clark (1987)). Climatic conditions during these humid times were marked by higher quantities of rainfall amounts and lower air temperatures. Studying the groundwater resources of Dhofar, with a focus on the origin of the water, on the mean groundwater residence times, or on recent input to the groundwater system, requires a deeper understanding of the appearance and duration of periods with higher humidity than today. For that reason it is necessary to look at both current climatic conditions and the paleoclimate, going back in time beyond the holocene.

Due to its geographical position between latitudes 17°N and 20°N, Oman is affected by the ITCZ. This low pressure zone is a main driver for the regional climate, determining rainfall amounts, air temperatures and the development of wind systems in the area. The latitudinal position of the ITCZ is variable over

the year, moving northward in spring and southward in autumn. However, it also varies over large periods of time, reaching up to a millenium.

2.3.1 The Current Climate

Todays climate in Dhofar is dry and hot. Annual average temperatures in the south are 26 °C for the coastal plain and 21 °C for the mountains (Bawain, 2012). In the Najd the mean temperature at station Thumrait is 26.3 °C with minimum and maximum values of 6.2 °C and 44.7 °C, respectively (Al-Mashaikhi, 2011). For the far northern area of Dhofar, the dunes of the Rub Al-Khali desert, temperatures up to 50 °C are realistic.

On the south side of the Dhofar Mountains, the yearly amount of rainfall with up to 299 mm a^{-1} is many times the rate of the interior area with a mean value of approximately 50 mm a^{-1}. The main contributor of rain is the monsoon. Rainfall gradually increases from the coastal plain to the top of the Dhofar Mountains yielding mean values of 104 mm a^{-1} in the plain and 299 mm a^{-1} at high elevations, based on monthly data for a 22-year period from 1975 to 1996. For the same time period, the average annual rainfall in the Najd is 49 mm a^{-1} with around 70 mm a^{-1} in the area adjacent to the mountains and around 30 mm a^{-1} in the far north-east (GRC, 2008).

Potential evaporation rates are around 1,660 mm a^{-1} for the coastal plain and 2,200 mm a^{-1} for the interior area. South of the Dhofar Mountains semi-arid conditions prevail, whereas the climate of the Najd is arid.

The ITCZ i.e. the intersection between southern winds from the equator and northern trade winds, is located close to the equator (approximately 5° north to the equator). Over the year the ITCZ follows the zenit position of the sun with a time delay of approximately 4 weeks. Migration above land, at up to ± 25°, is stronger than migration above the ocean where the variation is approximately ± 5° (Neff, 2001). With the warming of the northern hemisphere in spring and summer, the ITCZ moves northward. The northern trade winds are then replaced by the South Westerlies. Consequently, waters at the coast well up, which leads to falling sea temperatures. The warm moist southwesterly winds condense into fogs and drizzling rains, bringing humidity to the landmass. The stronger the winds are, the stronger is the upwelling and with that the intenisty of the precipitation (Neff, 2001).

These humid conditions occurring between mid-June and mid-September mark the annual monsoon season. They are a distinctive feature of the Arabian Peninsula and locally known as the *khareef*. As a result the plain and the south side of the mountains become green, with grass, shrub and tree cover, and in addition, the cloud forest at the Dhofar Mountains regenerates (Bawain, 2012).

The monsoon with its orographic rainfall distribution is the most reliable source of precipitation for the Dhofar area (Hildebrandt et al., 2007). Today, the monsoon does not reach the Najd, the reason for this being an inversion layer limiting the vertical extent of the cloud cover, as can be seen in Figure 2.3.

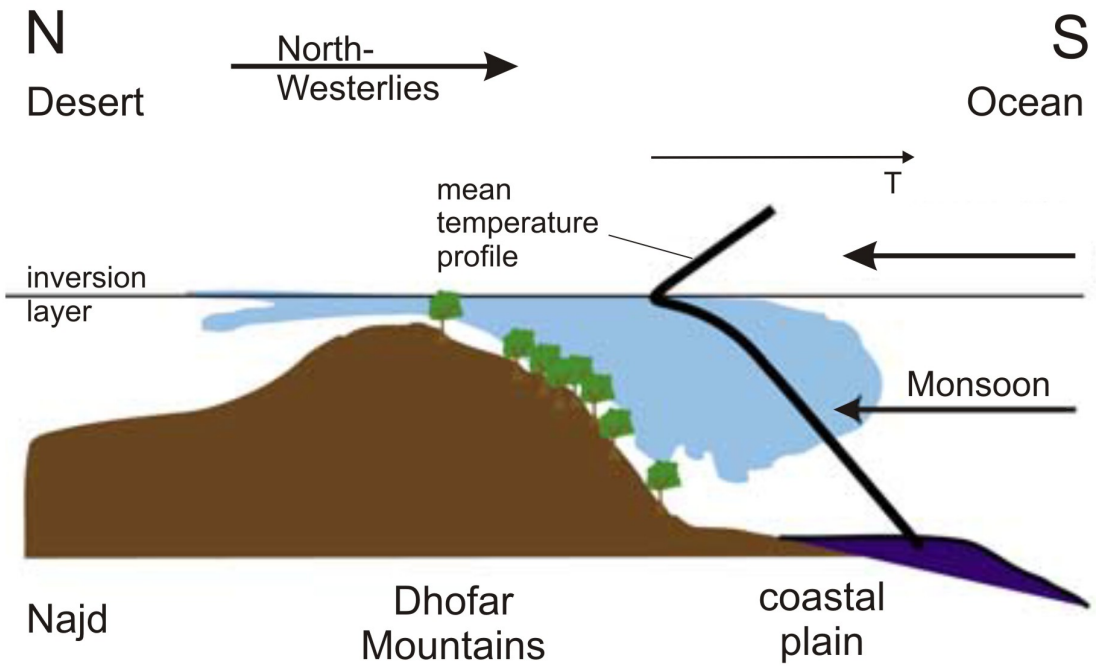

Figure 2.3: Schematic representation of the meteorological situation at the Dhofar Mountains during the monsoon. The extent of the cloud cover is limited to the southern face of the mountains (modified from Hildebrandt et al. (2007)).

Between November and January the ITCZ moves southwards, and winds from the north become dominant. Along with the southern movement of the ITCZ, air temperatures decrease. Since the airmasses come from the land now, they carry less water, resulting in the dry conditions we observe today. Figure 2.4 illustrates the location of the ITCZ in recent times. It shows wind patterns and the location of the ITCZ in summer and winter.

Beside the monsoon two other weather systems deliver rainfall to the Dhofar region: frontal systems originating in the Red Sea or the Mediterranean Sea, and cyclones coming from the Arabian Sea (GRC, 2008). The frontal systems can occur between December and April, the cyclones mostly before that (May and June) and after the monsoon (October and November).

The monsoon and other systems can be further distinguished by their intensity and duration. The monsoon precipitation consists of ongoing light rain, drizzle and

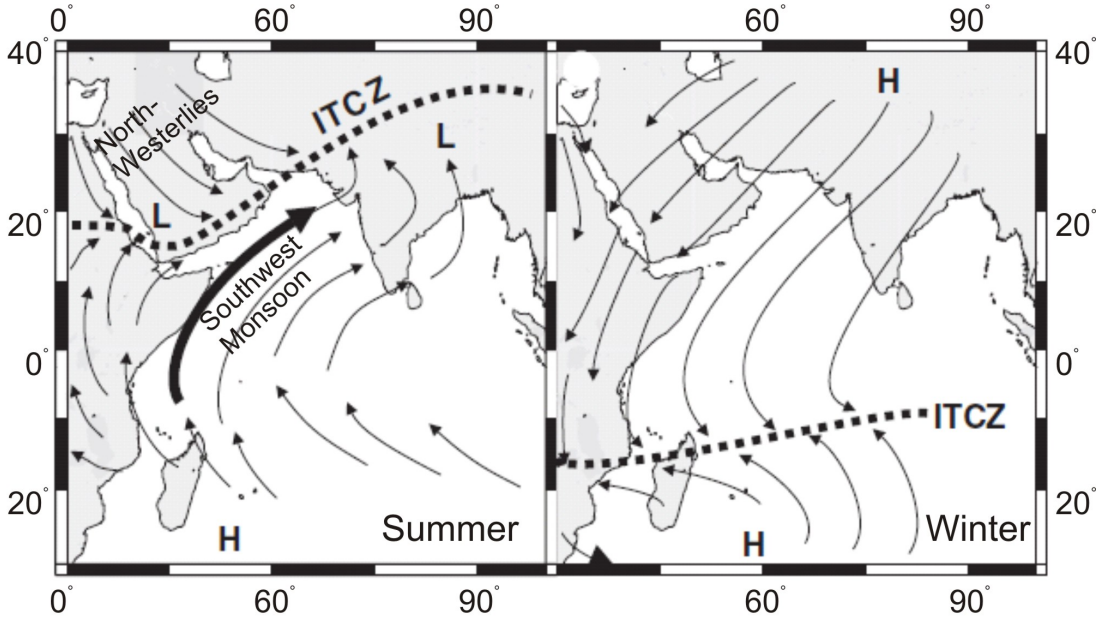

Figure 2.4: Wind patterns and position of the ITCZ over the Arabian Sea and the continent in summer and winter (modified from Fleitmann et al. (2007)). Dashed line marks the location of the ITCZ, L and H are representing areas of Low and High pressure.

mists, which lasts from days up to months. The frontal systems are rather light rains too, which last from minutes to hours. In contrast to these are the cyclone events, which can bring heavy rainfall and huge amounts of water to the area in relatively short time periods and which last hours to days. Apart from intensity and duration, the monsoon and cyclones show distinctive isotopic signatures in their stable water isotopes. This different signature can be used when evaluating the source of the groundwater in the reservoir (see chapter 6).

2.3.2 Paleoclimate

The climate and the occurence and duration of humid conditions during the last 30 ka are of particular interest for the present study because this is the time window during which groundwater recharge took place, according to Clark et al. (1996) and Al-Mashaikhi (2011).

There are indications of more humid conditions in previous times in the south of the Arabian Peninsula, and in the Dhofar region in particular. For example, pluvial wadi channels pervade the ground surface and are observable in the field and on satellite images. These channels begin in the Dhofar Mountains and run

in a northeastern direction. Their course and morphology prove that large surface flows occured in the area long ago.

Numerous studies on the paleoclimate of the Arabian Peninsula and today's territory of the Sultanate of Oman have investigated the fluctuation of wet and dry periods and their intensity (e.g. Burns et al. (2001); Clark and Fontes (1990); Clark (1987); Fleitmann (2003); Fleitmann and Matter (2009); Fleitmann et al. (2007, 2011); Fuchs and Buerkert (2008); Heathcote and King (1998); McClure (1976); Neff (2001); Rosenberg et al. (2011); Weyhenmeyer (2000)). All studies agree that pluvial conditions occured in the past. However, there are different opinions concerning the classification of these periods on the long time scale (10 to 30 ka BP).

Various authors have discovered evidence for major periods of humidity lasting for several thousand years, in contrast to arid periods lasting for some 10,000 years. Figure 2.5 schematically represents the discrepancies in duration between (a) the "wet" (humid) and (b) the "dry" (arid) scenarios constructed by scientists for the last 30 ka before present.

The image reflects the results of different studies, with an emphasis on the humid periods, represented by the black columns in Figure 2.5. Some differences as to the lenghts of the humid periods occur among the different authors. Also, the studies used no uniform definition of humid or transitional periods. However, the intention of Figure 2.5 is to clearly show the differences between the two major theories about the succession of humid and arid periods. In the "dry" scenarios, the models show no humid period between 10 and 30 ka BP.

None of the studies presents data on amounts of precipitation for any period. The studies describe variances in rainfall intensity (humid or transitional) and developments (increasing or decreasing with time), but provide no numbers.

The groundwater ages calculated by Clark et al. (1996) or Al-Mashaikhi (2011) fit roughly in the "wet" scenario (Figure 2.5 (a)). The "dry" scenario (Figure 2.5 (b)), by contrast, would suggest that the groundwater recharge took place sometime in the time period 5 to 10 ka or before 30 ka BP.

The "wet" theory is based on investigations on travertine in northern Oman (based on ^{14}C-dating). The findings reveal pluvial periods in the lower Holocene (13.9 to 6.5 ka BP) and in the upper (31 to 26 ka BP) and late (23.5 to 16.8) Pleistocene (Clark, 1987). These findings are in good agreement with investigations on lake sediments in the Rub Al-Khali desert by McClure (1976). McClure's investigations used radiocarbon dating as evidence for a pluvial period from 36 to 17 ka BP.

The "dry" theory is based on investigations in north and south Oman and Yemen. Humid conditions at the beginning of the Holocene 10.5 to 6 ka BP were detected by dating (^{230}Th) speleothem records in south (Qunf Cave located in the region under study) and north Oman (Burns et al., 2001; Fleitmann, 2003). A

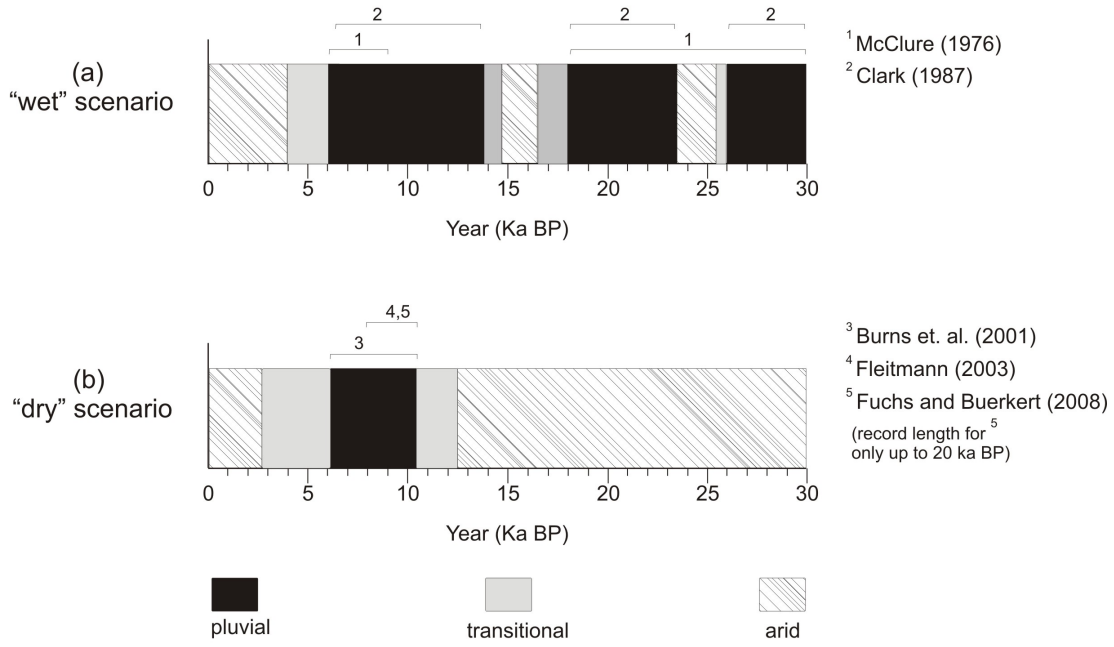

Figure 2.5: Scheme of climatic periods during the last 30 ka for the south-eastern Arabian Peninsula. The bars indicating humid (black), transitional (grey) or arid (hatched) periods. a) "Wet" scenario according to McClure (1976) or Clark (1987) indicating major humid periods between 17 to 30 ka BP. b) "Dry" scenario according to Burns et al. (2001), Fleitmann (2003) or Fuchs and Buerkert (2008) with no humid period between 10 and 30 ka BP. Differences among the authors with regard to the length of the periods are marked with a focus on the humid periods.

sediment record (20 ka, dated by OSL - optical stimulated luminescence) from a mountain range in northern Oman reveals similar results, the period of humidity lasting here from 10.5 ka to 8 ka BP (Fuchs and Buerkert, 2008). Interestingly, no pluvial period could be detected in the $\approx$ 20 ka before that. Moreover, recent works such as Fleitmann et al. (2011) or Rosenberg et al. (2011) point out that no pluvial period occured between 70 to around 10 ka BP. For the present study, this long dry period raises the question of whether or not any groundwater recharge took place.

There is proof that, in previous times the position of the ITCZ differed from that of today. It was farther south during the last glacial maximum (LGM) (Weyhenmeyer, 2000), for example, and further to the north during the humid periods (Neff, 2001).

Figure 2.6 indicates the position of the ITCZ during the humid period 7 ka BP

according to Fleitmann et al. (2007). Compared to today, the ITCZ was positioned much farther north around 7 ka BP (Figure 2.4). This implies that during humid periods the Monsoon also reached further north back then than it does today and was able to bring fresh water to the interior area.

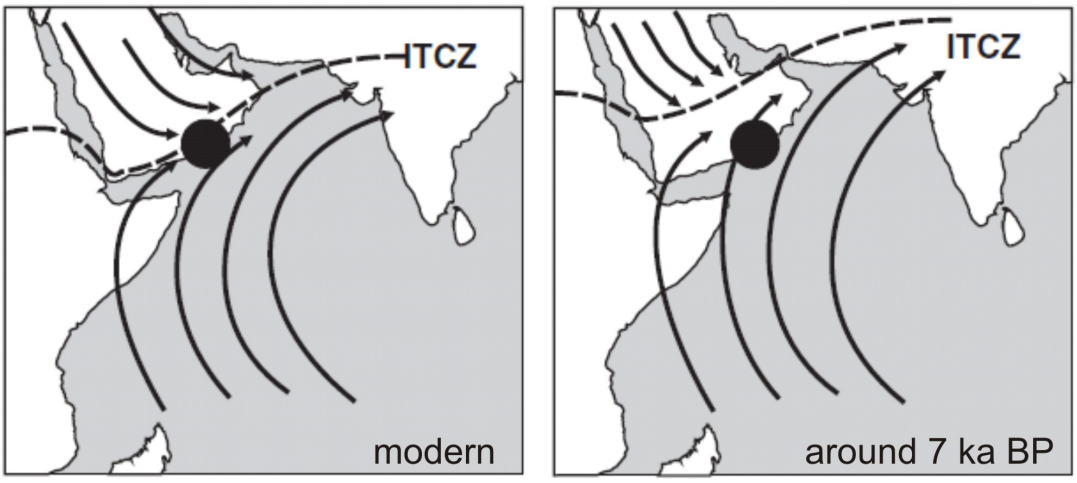

Figure 2.6: Wind patterns and position of the ITCZ over the Arabian Sea and the continent today and during the pluvial time around 7 ka BP modified from Fleitmann et al. (2007). Dashed line marks the location of the ITCZ, black dot the location of the Qunf Cave in Dhofar.

2.4 Hydrology

A number of springs exist in the south at the foot of the mountains. During and after the monsoon, large open water bodies, pools and wadis filled with water accumulate in the south. They disappear within weeks after the monsoon.

In the Najd there are two small open bodies of water, the Uyun pools adjacent to the Dhofar Mountains (elevation 750 m amsl), and the spring in Mudhai (elevation 550 m amsl, 70 km north to the surface water divide). Both are most likely fed by shallow aquifers.

Surface runoff is rare in the Najd and it only occurs as the result of heavy rainfall.

2.4.1 Springs

Springs have been the main water source in the Dhofar Mountains and the Salalah plain prior to 1970. Today they are still an important component of the water budget for the Salalah plain. Spring discharge is measured manually at six springs at the foot of the mountains. Not all of the springs are active throughout the year. Some only contain water some weeks after the beginning of the monsoon.

Previous studies e.g. GRC (2005a), indicate that a large number of springs and open watering holes (approximately 150) exist at the southside of the Dhofar Mountains at higher elevations. However, there is no further information (concerning depth, water level, flow conditions, etc.) on the numerous watering holes, so that an evaluation of this water source is impossible based on current literature.

2.4.2 Wadi

Numerous channels pervading the land surface cross the Najd in a southwest-northeast direction. Close to the Dhofar Mountains they are deeply incised and small; in the northward direction they become wide and flat, before they finally disappear in the sand dunes of the Rub-Al-Khali desert. From time to time surface flow takes place in the Najd caused by cyclone events. Consequently, there is a source for groundwater recharge in the Najd.

2.5 Geology and Hydrogeology

Several studies describing the geological and hydrogeological characteristics of the Dhofar area have been conducted in the last 30 years, i.e. PAWR (1986) or GRC (2008). A very informative description on the geology and the geodynamic evolution of Dhofar is given by Roger et al. (1992). The recent doctoral thesis of Al-Mashaikhi (2011) also gives a general summary. The interested reader should refer to these cited works, since I will only give a brief description of the most crucial features.

2.5.1 Geological structure and hydrogeological units

The formations of interest in this study are from the Eocene and Paleocene eras and belong to the Hadramout group, which is present in large areas of the south and east of the Arabian Peninsula. Predominantly there are up to 900 m thick carbonate sediments, laying uncomformably atop Cretaceous formations in the region under study. In ascending order, the Hadramout group consists of the lower Eocene to Paleocene Umm Er Radhuma (UER), the lower Eocene Rus (RUS), and

the middle to lower Eocene Dammam (DAM) formations. The wadi beds of the Hadramout group are partly covered by thin alluvium deposits which do not act as aquifers. Figure 2.7 shows a schematic cross-section of the region with the mentioned geologic formations.

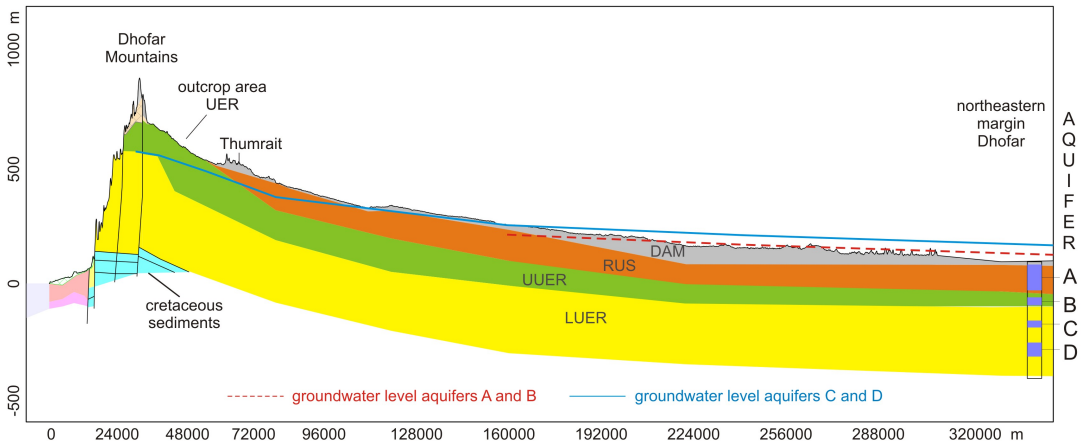

Figure 2.7: Schematic geological cross-section spanning the coastal plain in the south to the northeastern margin of Dhofar. Showing the formations of the Hadramout group: DAM, RUS, UUER, LUER. The four aquifer locations (A, B, C, D) are represented, with higher groundwater levels in the lower aquifers C and D (solid line) than in the upper aquifers A and B (dashed line). Vertical exaggeration: 80x

The Umm Er Radhuma, one of the major aquifer systems on the Arabian Peninsuala, is divided in an upper (UUER) and lower (LUER) part in the Sultanate of Oman, a differentiation not made, for example, in the Kingdom of Saudi Arabia.

The thickness of the formations increases when moving in a northeasterly direction. The thickness, therefore, for Dammam is 10 to 100 m, 30 to 250 m for the RUS, 50 to 300 m for the upper UER and 250 to 300 m for the lower UER. All four formation are mainly comprised of limestone, with varying proportions of marl and shale (DAM), dolomite, marl and gypsum (RUS), biomicrite and blue grey shale (UUER).

The RUS is furthermore characterized by evaporitic and evaporite-associated deposits which are limited to restricted basins. The evaporitic deposits of the RUS are grouped in the Aybut Member (Roger et al., 1992), whereas the Gahit Member lacks evaporitic indicators.

The upper and lower UER can be differentiated by microfossils and lithology. Underlying the Umm Er Radhuma is the Shammar Shale of cretaceous origin,

comprised of black shale and limestone, which acts as an impermeable layer for the overlying aquifers of the tertiary formations.

Whereas the Dhofar Mountains, as part of the Hadramout Arch, represent a major anticlinal structure, the formations in the Najd are in general flat and uniform. They gently dip from the mountains in a northern direction. The outcroppings of the UER lying in the north of the Dhofar Mountains are highly relevant to groundwater hydrology. Most likely they are the result of a second anticlinal structure in the area (PAWR, 1986). The Umm Er Radhuma also has outcroppings at the south-side of the mountains.

Several geological faults affecting the groundwater dynamics of the region have been mentioned in previous works, for example Al-Mashaikhi (2011); Clark (1987) or Herb (2011). However, recent seismic surveys by the oil industry did not confirm all the current theories about the occurence and extension of these structures (Al-Mashaikhi, 2011).

Uncertainties exist about the thickness of the lower and upper UER in the Dhofar Mountains due to cavities of different sizes and depths. In various boreholes at the south-side of the Dhofar Mountains, such cavities were encountered during drilling, leading to loss of the drilling cuttings. For this reason, separation between formations could not be detected (GRC, 2008).

Four aquifers (A, B, C, D) are known in the Najd (Figure 2.7). Aquifer A is unconfined to semi-confined and is located in the DAM and RUS. The aquifers B, C and D are confined and are all located in the UER. B in the upper part (UUER), and C and D in the lower part (LUER). Aquifers A and B are local aquifers. A exists mostly in the central area and B in the central and western Najd. Only aquifer D is distributed over the whole Najd, whereas aquifer C does not extend to the Dhofar Mountains. The city of Thumrait is the rough southern border for C. The water bearing horizons are separated by thin layers of shale (Al-Mashaikhi, 2011).

2.5.2 Groundwater flow

The regional groundwater flow in aquifers C and D is in a northeasterly direction. A special characteristic of the Najd aquifers are the higher groundwater levels to be found in aquifers C and D as compared to A and B. This characteristic can also be viewed in graphic representation in Figure 2.7. Differences in groundwater level up to 50 meter are observable in some places.

Al-Mashaikhi (2011) describes the groundwater hydraulics as follows:

"Recharged groundwater is captured by aquifer D in the Dhofar Mountains and flows in a northeasterly direction. Faults and fractures carry the groundwater from aquifer C to aquifer D, approximately 40 kilometers north of the surface

watershed. Aquifer B and A, in the more central area of the Najd, receive their water from aquifer C."

These zones of connection or leakage must be limited because there is no balancing between the water levels of the aquifers. This is also supported by the fact that, as long as the natural system is not disturbed, even pumping tests on one aquifer have no impact on the water levels of neighbouring aquifers. This indicates that aquifers are sufficiently sealed off by the layers of shale mentioned above.

2.5.3 Groundwater Recharge

In conjunction with the increasing demand for freshwater in the Najd, the question of input to the system, of groundwater recharge, has become more and more pressing. Taking into account the region's current arid conditions, there is the question of whether recent input to the system exists at all. If not, every abstraction would be drawing on these groundwater resources. On the other hand even small inputs of more recent water are important because they would indicate that hydraulic connections to an active flow system exist (Clark and Fritz, 1997).

In section 2.3 I already mentioned that the groundwater system was charged during more humid times in the past. Humid times not only indicate higher amounts of rainfall but also larger areas of precipitation. This inevitably leads to different recharge areas than today. Understanding the Najd groundwater system requires studying of possible recharge processes both in the past and today.

Groundwater recharge takes place at the monsoon-influenced south side of the mountains. This is proven by increasing groundwater levels in the plain and increasing spring water discharge during and after the monsoon season. Further interpretation and calculation of groundwater level response times or parameter distribution for the aquifers is limited, because monitoring wells for groundwater resources only exist in the plain and not on the southern side of the Dhofar Mountains.

To this date, there are no observations that clearly indicate that the monsoon recharge affects or contributes to the groundwater system in the north. In particular, water level observations on the near northern side of the Dhofar Mountains do not exist, and the more distant wells with monitoring records are too far away from the region to provide data that addresses this issue. There are few wells in the interior that have a stable isotope signature close to that of the monsoon, but it is not clear when this water was recharged. Potentially it could represent recharge from an earlier time when the monsoon extended farther to the north.

2.5.4 Discharge

The natural discharge area for the UER aquifers is the Sabkha Umm As Samim, a large inland *sabkha* approximately 250 km away from the north-eastern border of Dhofar, just at the border of the Sultanate of Oman and the Kingdom of Saudi Arabia. The monitored groundwater level and groundwater flow direction show this. It was also proven through water salinity maps that showed gradually increasing TDS in the groundwater flow direction (Al Lamki and Terken, 1996).

Anthropogenic discharge has greater impact on the groundwater reservoir. On one hand, this includes water taken from the reservoir through pumps and artesian wells, as well as open pits dug into the ground to collect water from shallow aquifers. On the other hand, there are also losses caused by insufficient drilling and poorly constructed boreholes which lead to substantial water losses from the aquifers to adjacent formations (GRC, 2008). Especially for the confined aquifers C and D, this means that once the confining layer is penetrated, the water can flow out of the reservoir unhindered. Effective sealing of the boreholes and wells would incur extraordinary costs. Such effort is usually not made.

In the last 10 years, increased efforts have been made by the authorities to enforce guidelines for the drilling of wells. Experiences so far show that the efforts are not sufficient and adequate in all cases (GRC, 2008). Another contributor to uncertain conditions are illegally drilled wells, for which guidelines or rules are of secondary importance. The problem is that even if these wells can be found and closed, the natural system is irretrievably destroyed and the groundwater lost.

Since the 1970s, numerous boreholes have been drilled, most of them to provide water for irrigated agriculture. However, some also serve public, industrial and commercial use. The centers of abstraction are the farm areas of Hanfeet, some commercial users south and north of Thumrait, and the city of Thumrait itself. Numbers on abstraction rates are not published by the authorities. One reason certainly is that in most cases no monitoring for abstraction rates exists. Up until now, wells are usually not equipped with a water meter or anything similar. The other reason is that information and data on ongoing or planned activities related to the groundwater resources are kept secret.

The Food and Agriculture Organization of the United Nations published data for the Sultanate of Oman in the year 2003, indicating a total withdrawal of 1.3 $\times$ 10^9 m^3, with almost 90 % used by the agricultural sector (http://www.fao.org). It must be assumed that the numbers have increased since then, especially in the Dhofar region. Since 2008, there have been ongoing initiatives to install new wellfields in the Najd and to shift part of the agriculture activities from the northern Batinah region to the central Najd area.

Even without detailed numbers it is certain that the withdrawal from the aquifers is higher than all possible modern inputs to the aquifer - if the latter

exist at all. Furthermore, it is certain that there are falling groundwater levels with the greatest decline in the central Najd. Therefore it is a fact no longer to be ignored, that the groundwater in the Najd is being overtaxed.

2.5.5 Fossil groundwater and gradient

Fossil groundwater resources have become more and more a subject in the field of groundwater hydrology in the last 40 years. This is partly due to the development of new investigative tools in groundwater hydrology, such as dating tools and newly invented environmental tracers. People became aware of the relevance of past climatic conditions and their impact on deep groundwater systems in association with increasing knowledge about residence times and time scales. This growing awareness and interest can also be attributed to the fact that in arid areas, it is especially these old or "fossil" groundwaters which are often the only source for fresh water.

One reason that fossil water, and especially fossil gradients, are an important subject of discussion is that in many groundwater basins in arid areas, groundwater gradients exist that seem to be inconsistent with modern recharge rates. Usually this inconsistency is manifested by the presence of zero or small input (recharge) along with relatively steep groundwater gradients. This inconsistency suggests that such groundwater basins may be the remains of a past (or fossil) water resource resulting from more humid conditions. The term "fossil" indicates that large time spans are under investigation, and possibly that the essential climatic conditions changed, especially during the Pleistocene/Holocene transition period. This is the case for the Great Saharian basins in North Africa and for the major basins on the Arabian Peninsula.

Thus far some studies have examined fossil groundwater and fossil groundwater gradients (Bakiewicz et al., 1982; Bourdon, 1977; Faulkner, 1994; Lloyd and Farag, 1978; Lloyd and Miles, 1986). In summary, their findings support the existence of modern recharge. Modern recharge rates can, under certain conditions, be sufficient to explain currently observable groundwater heads. The studies show, furthermore, the possibility that other mechanisms (for example: residual heads, lowering of discharge level, tilting of the basin or compaction) contribute to groundwater gradients in the great basins of the arid regions. The extent to which other mechanisms are involved cannot be answered satisfactorily, because of the vast dimension of the basins, the fragmentary data about them, and the vast time dimension involved for which data is lacking.

Water that infiltrated a long time ago and is still present in the subsurface indicates that, for some reason, the flow through the system is slow. This could indicate the following characteristics: low amounts of recharge, large storage capac-

ities and/or low natural discharge out of the system. Questions remain concerning many of these old groundwater systems and whether what is observed today is the result of past or current conditions. Since the Dhofar groundwater belongs in this category of old groundwater, potentially recharged in more humid times with greater recharge amounts than today, this type of question applies.

Chapter 3

Materials and Methods

3.1 Data availability

Sparsely inhabited regions like the Najd in the Dhofar governorate often lack sufficient monitoring devices for rainfall, surface water flow or climate parameters. Furthermore long-time records, which could provide information about the conditions before the development of the area, are missing.

Today's knowledge of the area is based on explorations and monitoring campaigns which have been gradually conducted since the 1970's. These investigations were initiated by different stakeholders (i.e. oil industry, agriculture, water authorities) with varied interests. This is sometimes reflected in the kind of data and the quality of data retrieved.

Another fact is that not all existing data were available for the present study, because of the structure of authorities and economical reasons (oil industry). The work presented here is based on data and information provided by the Ministry of Regional Municipalities and Water Resources (MRMWR) and own investigations. Although full information could not be provided, for example, access was denied to specific regions in the northern area and to specific sites of recent development, such as new well fields, it can be assumed that the data that were made available for the present study are relevant.

3.1.1 Provided data

The following data were provided by the Ministry of Regional Municipalities and Water Resources (MRMWR):

- records (1981-2006, 2009-2011) for 238 groundwater monitoring wells; 190 on the coastal side, 48 for the Najd area; most of the stations have records

starting in the 1990's; monitoring intervals go from 2 weeks up to 6 months

- flow records (1984-2007) for four wadi stations in the Najd area
- monitoring records for 39 rain stations; 24 coastal side, 15 for the Najd area; most of the stations in the south have records dating back to the 1980's, whereas the majority of the stations in the Najd were installed towards the end of the 1990's
- monitoring records (1986-2008) for 5 springs at the south side; monitoring interval 2 weeks to 3 months
- geological maps (1:100 000; 1:250 000) for the Dhofar governorate
- 62 drilling logs for wells in the Dhofar Mountains and the Najd area
- data on pumping test for 40 wells in the Najd area
- internal reports on geology, groundwater resources and agricultural activities for the Najd area

Also available for this study were data on water chemistry, environmental isotopes and noble gases collected and analyzed during the PhD-thesis of Khalid Al-Mashaikhi (Al-Mashaikhi, 2011) and the master thesis of Christian Herb (Herb, 2011).

3.2 Field work

Chapter 4, below, will present the analysis of the available data and show the major gaps identified during the analysis. To overcome some of the shortcomings of the data, the following field activities were undertaken:

- installation of 14 automatic pressure transducers to monitor the groundwater level continously in groundwater wells in the Najd (beginning in 11/2010)
- installation of 6 automatic pressure transducers to monitor the groundwater level (3) and the spring discharge (3) at the southside of the Dhofar Mountains (beginning in 11/2010)
- sampling campaign for ^{36}Cl measurement along a groundwater flowpath in the Najd (01/2012)
- monthly sampling (^{2}H, ^{18}O) at the springs at the southside of the Dhofar Mountains (06/2011-11/2012)

Primary aim of the measures was to observe possible fluctuation of the groundwater level as a result of influences by the monsoon or cyclonic events. An additional goal was to observe the general groundwater decline and, at the eastern boundary, to observe input to the reservoir from outside. The location of the installed pressure transducers in the groundwater wells will be indicated in the next chapter. The results of these observations of the groundwater heads will be presented for some wells in Chapter 5.

^{36}Cl was sampled and analysed to recheck the contradicting results of the ^{14}C and ^{4}He results for the groundwater residence times in the Najd. This will be discussed in Chapter 6 together with results and an interpretation of the ^{36}Cl.

Yet to be completed is the work regarding response times (groundwater wells and springs) and sources (^{2}H and ^{18}O) of the water at the southside of the Mountains. Results are expected here not before 01/2013 and with that after the present work will be finished.

3.3 Methods

The work flow used in the present study consists of:

Data analysis Aim of the data analysis was the development of a conceptual idea for the groundwater flow in the Najd plus answering the question if under today's dry conditions a sufficient amount of water is available for groundwater recharge.

Numerical groundwater flow model The first perspective of the numerical groundwater flow model was to evaluate on a theoretical base if groundwater recharge to the deep aquifer system in the Najd is possible. Aim of the modeling was furthermore to get a better grip on parameter values and the ratio between them.

Calculation groundwater residence times The concentrations of environmental isotope tracer were used for the analysis of how long the water has been in the system. Discussed together with radiocarbon based groundwater residence times of previous studies, a likely range for the Najd groundwaters will be obtained.

Combining flow model and isotope data Bringing together groundwater flow modeling and isotope based groundwater ages is aimed at the estimation of the aquifer porosity, flow velocity and likely maximum recharge values.

Chapter 4

Data Analysis and Conceptual Model

The main focus of this part of the study lies in the collection, preparation and interpretation of available information about the region under study. I will concentrate on the significant data for groundwater recharge and groundwater dynamics: rain, wadi flow, aquifer parameters and hydraulic heads. It is supplemented by data collected during several field trips in the years 2009 to 2012. A systematic understanding of the groundwater hydrology of Dhofar was developed, resulting in a conceptual model presented at the end of the chapter. The developed conceptual model provides the basis for the work presented in the subsequent chapters.

4.1 Data analysis

In theory, recharge to the Najd aquifer system can occur in two ways: (i) directly from rain (i.e., the Monsoon or Cyclones), or, (ii) indirectly, from the surface flow in the wadis that sometimes follow a Cyclone. However, the infiltration areas for (i) are not that clear. Precipitation could take place in the whole area, but it could also be that infiltration is initiated by local features, such as depressions or swallow holes. The following questions arise among others, if we focus first on possible sources of recharge, and with that on the processes above the land surface:

(i) Is it possible to identify the areas precipitation (recharge) takes place in? What amount or duration of rainfall is needed for infiltration for water to work its way into the deeper ground?

(ii) What are the catchments contributing to surface runoff? Is there a certain threshold of precipitation needed to generate surface flow?

Further observations in the groundwater itself are inevitable (hydraulic head,

water chemistry/ environmental isotopes) to determine whether or not surface processes and subsurface aquifer system are connected.

4.1.1 Rainfall

The only consistent source of rainfall in Dhofar is the annual monsoon. The frontal systems and cyclones mentioned above are irregular in their occurrence. Of special interest for the Najd are the large cyclones, because they are almost the only source of rain in the Najd and trigger heavy rainfalls with up to more than 200 mm per downpour. These downpours occur once in three to four (Brook and Sheen, 2000) or even five to seven years (Bawain, 2012). In Dhofar it is common to call every case of rain outside the monsoon a cyclone, which is in fact not true in a strictly meteorological sense.

Altogether 39 rain stations exist in the Dhofar area; 24 at the southside of the Dhofar Mountains and 15 station in the Najd (see Figure 4.1). Most of the stations in the south have records dating back to the 1980's, whereas the majority of the stations in the Najd were installed between 1998 and 1999. The longest record available for the present study was that for the station Thumrait with data spanning the years 1980 until 2007.

In years without cyclones, more than 75 percent of the annual rainfall occurs during the monsoon (Brook and Sheen, 2000). The records of the rain stations in the south indicate that the distribution of rainfall is quite variable over the area. They also reveal the years with cyclonic storm events. For the monsoon-influenced station Qaroon Hairiti, close to the top of the mountains (873 m amsl), a mean precipitation of 197 mm for the period 1977 to 2007 is reported, with 6 years of rainfall amounts above 300 mm a^{-1} (Al-Mashaikhi, 2011). Variation in the amount of rainfall can furthermore be observed along a westeastern line of 90 km distance, with higher rainfall occurring at the eastern stations.

Figure 4.2 schematically illustrates the rainfall distribution along an idealized cross-section from the Arabian Sea to the northeastern margin of Dhofar (see Figure 4.1 for a position of the cross-section). The figure shows the areas currently influenced by the monsoon: mainly, it affects the south side of the mountains, whereas a cyclonic storm can affect the entire area. The locations marked are six rainfall stations (R1, R2, R3, R4, R6, R7) with continuous rainfall data for the years 2000 to 2009 (apart from station Sahalnawt which lacks data for 2009) as well as the Thumrait station (R5) which has the longest available record for the Najd (1980 to 2007).

The Figures 4.3(a), 4.3(b) and 4.3(c) represent the rainfall distribution for the southern stations Sahalnawt (R1), Rakbayt (R2) and Hagayf (R3). Higher rainfall amounts in the mountains are indicated, as are variations in the amount.

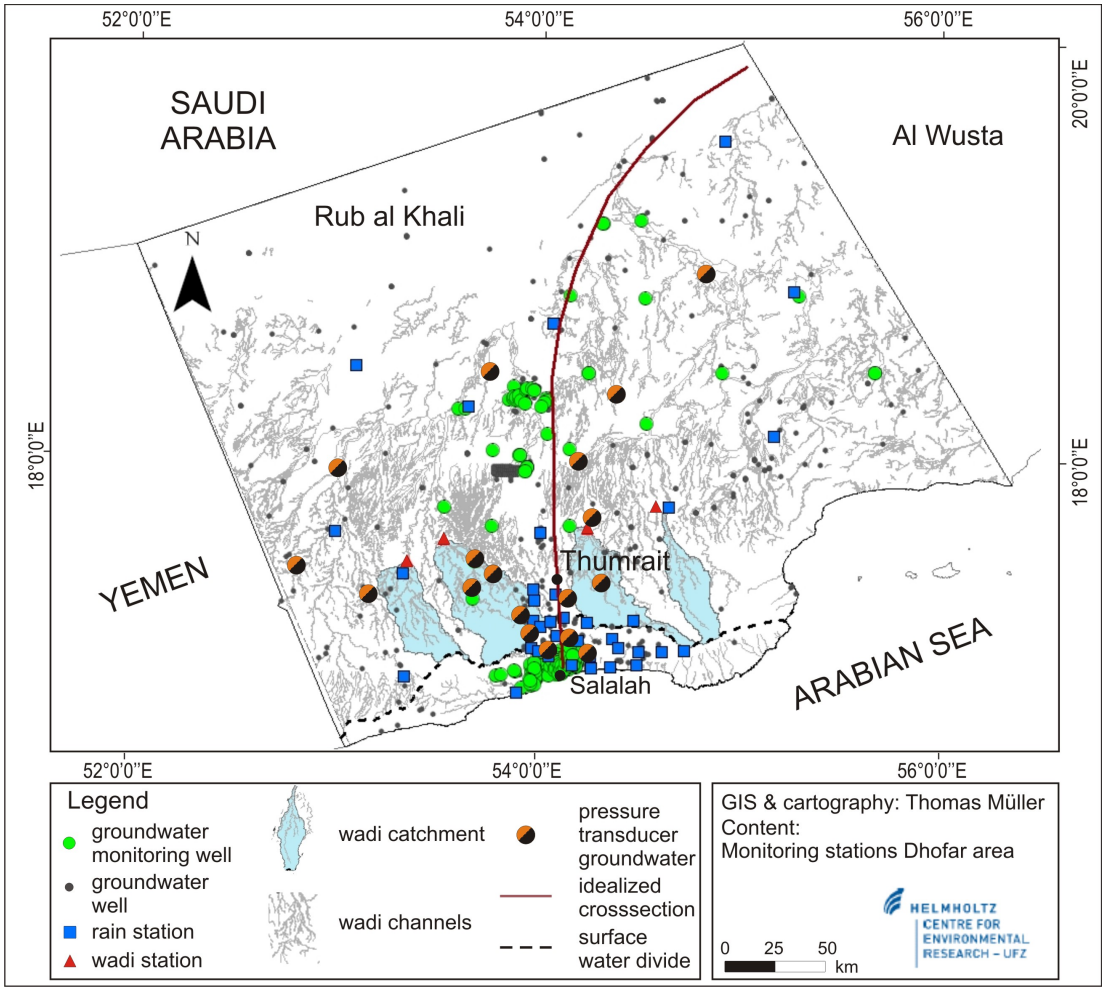

Figure 4.1: Hydrological monitoring stations in the Dhofar area. Circles show the location of groundwater monitoring wells, dots the location of all groundwater wells. The location of the rain stations is represented by the squares, the wadi stations by the triangle. Wadi channels and courses are illustrated by lines.

The data for the period 2000 to 2009 also show that the rainfall amounts at the station Rakbayt at around 500 m amsl were above the rainfall rate at the station Hagayf at 890 m elevation. The same trend could be observed at the station Kanzer (elevation also 500 m amsl, 12 km to the east).

The difference in rainfall amounts between the southern stations (4.3(a) to 4.3(c)) and the northern stations (4.3(d) to 4.3(f)) stands out clearly. The hydrographs for the time period from 2000 to 2009 in Figure 4.3(d) to 4.3(f), document the lower rainfall rates in the Najd and the years without measured rainfall for the station Shisr (2000) and Muqshin (2005, 2008, 2009). The analysis of data

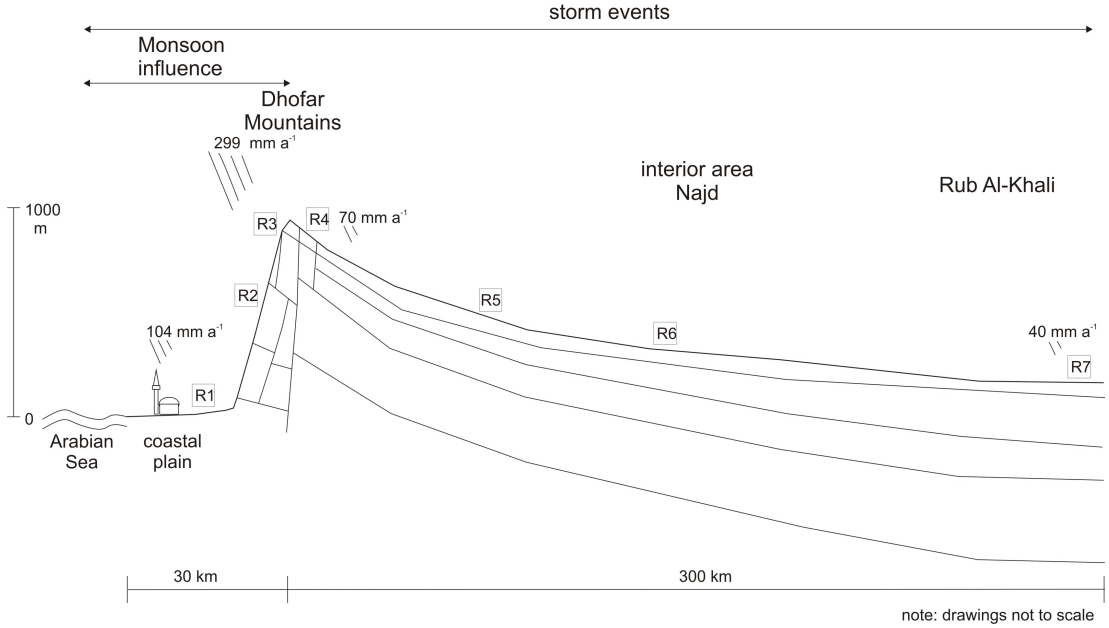

Figure 4.2: Schematic cross-section from the Arabian Sea to the north eastern margin of Dhofar. R1 to R7 represent the locations of the rainfall stations (Figure 4.3(a) to 4.3(f)). Mean precipitation rates according to GRC (2008)

from all stations further indicates that rainfall events in the Najd area can have a distinct local character, also described in previous accounts of the area (GRC, 2005a).

The occurrence of the irregular cyclonic events was also documented by rain stations in the north. At the station Thumrait (R5) there was no rain in the years 1984, 1991, 1998, 2000, 2001 and 2006. However, the records include rainfall amounts above 100 mm a^{-1} for the years 1983 (145 mm a^{-1}), 1989 (227 mm a^{-1}) and 1992 (131 mm a^{-1}) as can be seen in Figure 4.4. In 1989, the year with the highest recorded rainfall, almost 98% of the total amount of precipitation was measured on three days.

Almost all stations have one or several years without any rain or with unexpectedly low amounts of rainfall compared to other years. Years without any rain are conceivable for the Najd, but the inspection in the field showed that other reasons (poor maintenance, failure of the collector) could lead to zero rainfall in the data. Therefore, years with no rain in the data record are not necessarily real dry years. Since the stations in the north are far from each other (often more than 50 km, see Figure 4.1) and because the rainfall events often have restricted local character, it is impossible to note correlations or fill gaps with data from other stations.

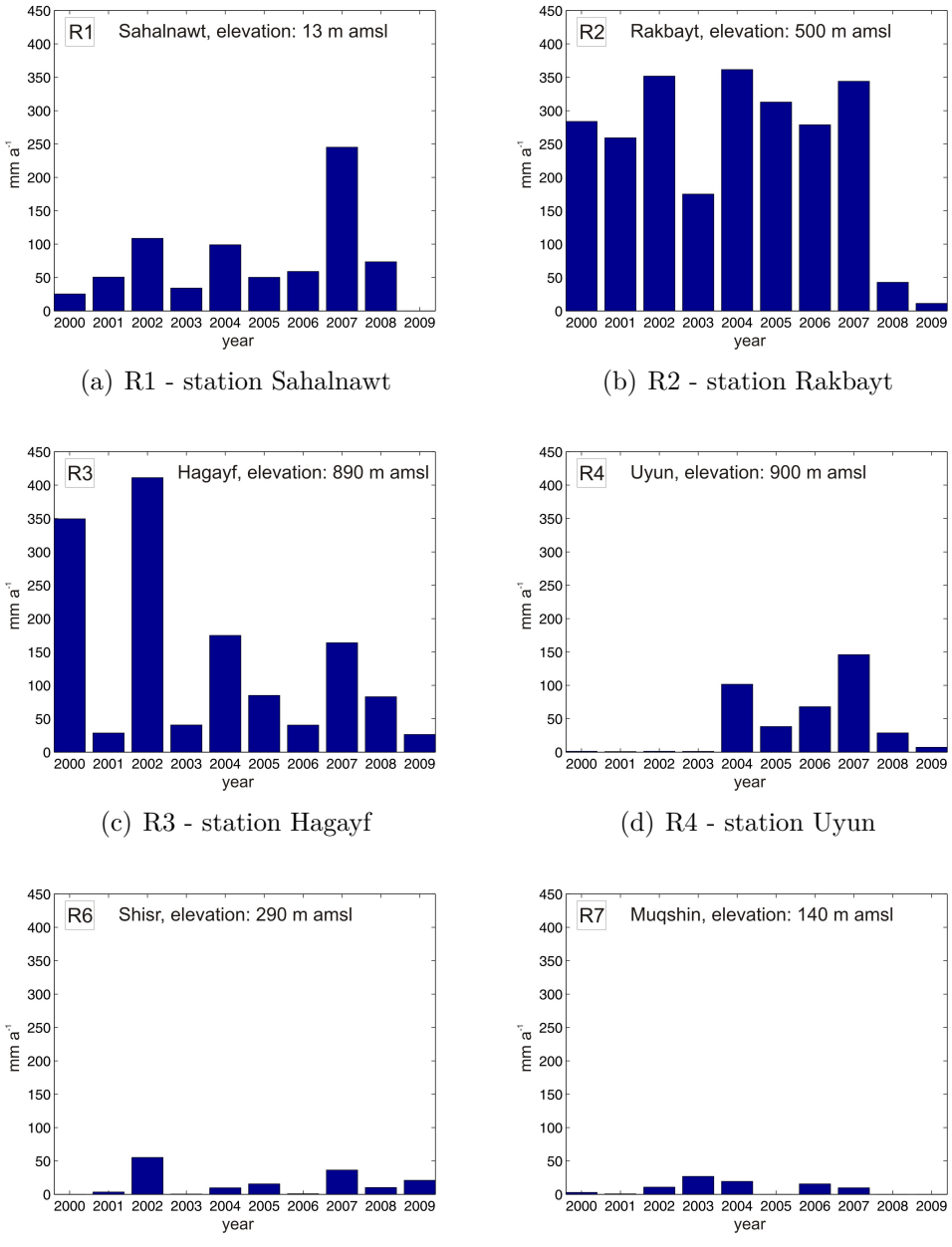

(a) R1 - station Sahalnawt

(b) R2 - station Rakbayt

(c) R3 - station Hagayf

(d) R4 - station Uyun

(e) R6 - station Shisr

(f) R7 - station Muqshin

Figure 4.3: Rainfall rates for the years 2000 to 2009 for the stations along the crosssection from the Salalah plain to the northeastern margin of Dhofar. Location of the stations is shown in Figure 4.2. No data were available for the station Sahalnawt for the year 2009.

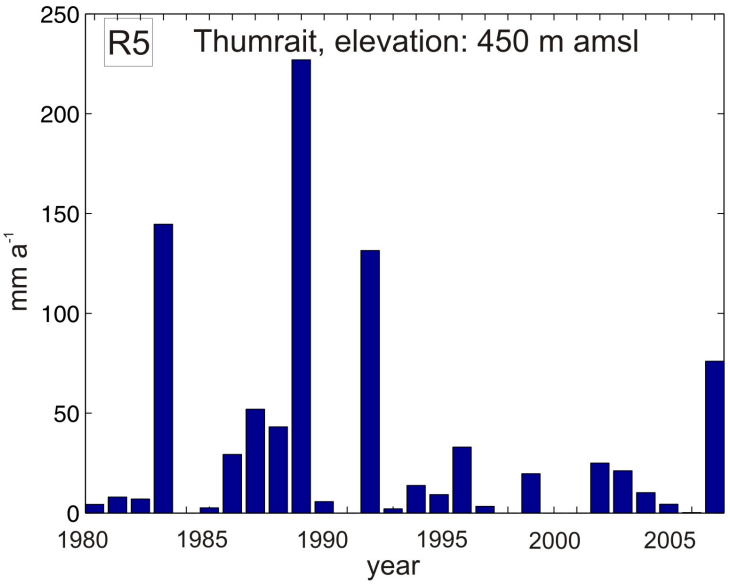

Figure 4.4: Rainfall data for the staion Thumrait for 1980 to 2007. The location of the rainfall station (R5) can be seen in Figure 4.2, the elevation is approximately 450 meters above mean sea level.

Years without any rain in the monsoon-influenced south are most likely an indication for a failure of the station. In this case, the data from surrounding stations can be used to clarify whether (monsoon-) rainfall occurred. However, in the south there are also occurrences of rainfall with restricted local character, which may not allow any conclusions from rainfall at surrounding stations with reference to rainfall at the station under analysis. Furthermore, the microrelief of the southern mountain slope and the distance between the stations (10 to 20 km) make the extrapolation of data to the whole area impermissible.

The rain stations used are standard equipment (tipping bucket) that are able to collect the vertical component of the rain. By contrast, the monsoon is characterized by two components: the vertical component of drizzle and drops and the horizontal component, the so called occult precipitation. Vegetation, especially bushes and trees, "comb" the moisture out of the mist. This also depends on factors such as altitude, topography or crown configuration (Hildebrandt and Eltahir, 2008) or (Bawain, 2012). Water collected this way has to be added to the rainfall measured by the tipping buckets, since rain collectors do not capture this part of the precipitation. GRC (2008) indicates that the rate of rainfall from occult precipitation lies at 20 %. Numbers in the same range were found recently by Abdullah Mohammed Ali Bawain, whose work focused on the significance of tree species and their ability to collect fog water (Bawain, 2012).

4.1.2 Wadi flow

Four wadi gauging stations exist in the Najd, Gharah and Ghadun in the western part and Dhahaban and Andour in the east. They are located 50 to 70 km north of the surface water divide in the Dhofar Mountains. Their location in the Najd and the catchments are illustrated in Figure 4.1. Upstream, a network of smaller tributaries and channels exists, which eventually combine into one big wadi channel with up to several hundred meters width at the location of the stations. The stations, the catchment they cover, and some information on the recorded events are given in Table 4.1. The database on the recorded signals stems from the wadi flow meter. The flow numbers are calculated values from the Ministry of Water Resources (MRMWR). For the station Andour the record covers the time period between end of 1983 and the year 2008. There are some inconsistencies in the record for the time periods 1984 to 1991 and 1993 to 2002, indicating that in the mentioned periods the station was out of order.

The westernmost station Gharah has the highest number of recorded events and days with wadi flow, Andour as the easternmost station has the lowest numbers. The more central stations Ghadun and Dhahaban show almost the same number of recorded events and days. Because of the mentioned inconsistencies in the data of Andour, a west-east gradient in the event frequency cannot be definitely assessed. However, a higher total flow was accumulated during the times of record at the eastern stations Dhahaban and Andour.

The essential message of the presented data is that from time to time surface flow takes place in the Najd. Consequently, there is a source for groundwater recharge in the Najd. However, the numbers attained have to be treated with caution.

Table 4.1: Wadi stations in the Najd area. Summarized flow records for the monitoring period 1984-2007. Flow numbers base on calculations from the Ministry of Water Resources (MRMWR).

Station name	area [a] [km^2]	number events	number days	total flow [Mm^3]	min. flow [m^{3}d^{-1}]	max flow [m^{3}d^{-1}]
Gharah	1109	24	59	19,9	86	6,500,000
Ghadun	1959	17	42	32,2	1	8,400,000
Dhahaban	1405	19	40	115,5	20	42,300,000
Andour	886	8	34	47,4	173	8,900,000

[a] Catchment covered by the Wadi stations. Area size was derived from the Wadi classification of the MRMWR.

It is unknown how these values were calculated, which makes it difficult to be certain about the reliability and meaning of the data. The data for minimum and maximum flow of all stations show a large variance. On the one hand, it is difficult to imagine that low values, like 1 m^3 d^{-1}, are trustworthy - when taking in account that all wadi channels at the location of the recording stations are clearly more than 100 m wide. On the other hand the maximum values cannot be evaluated either. 42 Mm^3 d^{-1}, the maximum value recorded at station Dhahaban, results in a flow rate of 490 m^3 s^{-1}. With a roughly estimated channel width of 250 m (SRTM-data) and a water level of 3 m the flow velocity was calculated as 0.65 m s^{-1}. While this is a very high value, it is not completely unrealistic. Still, the water volume passing through the wadis, and with it the total amount of water, remains unresolved.

4.1.3 Piezometry

Of interest for this study are the hydraulic heads for the main aquifers C and D before the development of the area began in 1970. Today groundwater wells exist in most part of the Najd. This was not the case in the 1970s and 1980s. Especially parts of the northern territory were not surveyed until 15 years ago. Therefore, some assumptions had to be made. For instance, it is assumed that no major change in the hydraulic heads has taken place in the areas far from abstraction wells. Based on such assumptions, a map for the aquifers C and D was constructed. This is because drilling protocols and monitoring campaigns showed that the aquifers have almost the same groundwater heads. Also, many of the boreholes drilled to the lower UER have quite long open hole sections (100 m and more), not allowing a distinction between C and D. A piezometric map of the predevelopment hydraulic heads for most of the Najd area was constructed, using borehole information and early reports about the area (see Figure 4.5).

The highest groundwater levels were found in the Dhofar Mountains above 550 meter amsl, and in the east, at the border to Yemen, at 500 amsl. The direction of groundwater flow runs from the Dhofar Mountains in a northeasterly direction. Figure 4.5 shows the approximate location of the artesian water prior to the development of the area. North of this line, the groundwater in C and D was artesian.

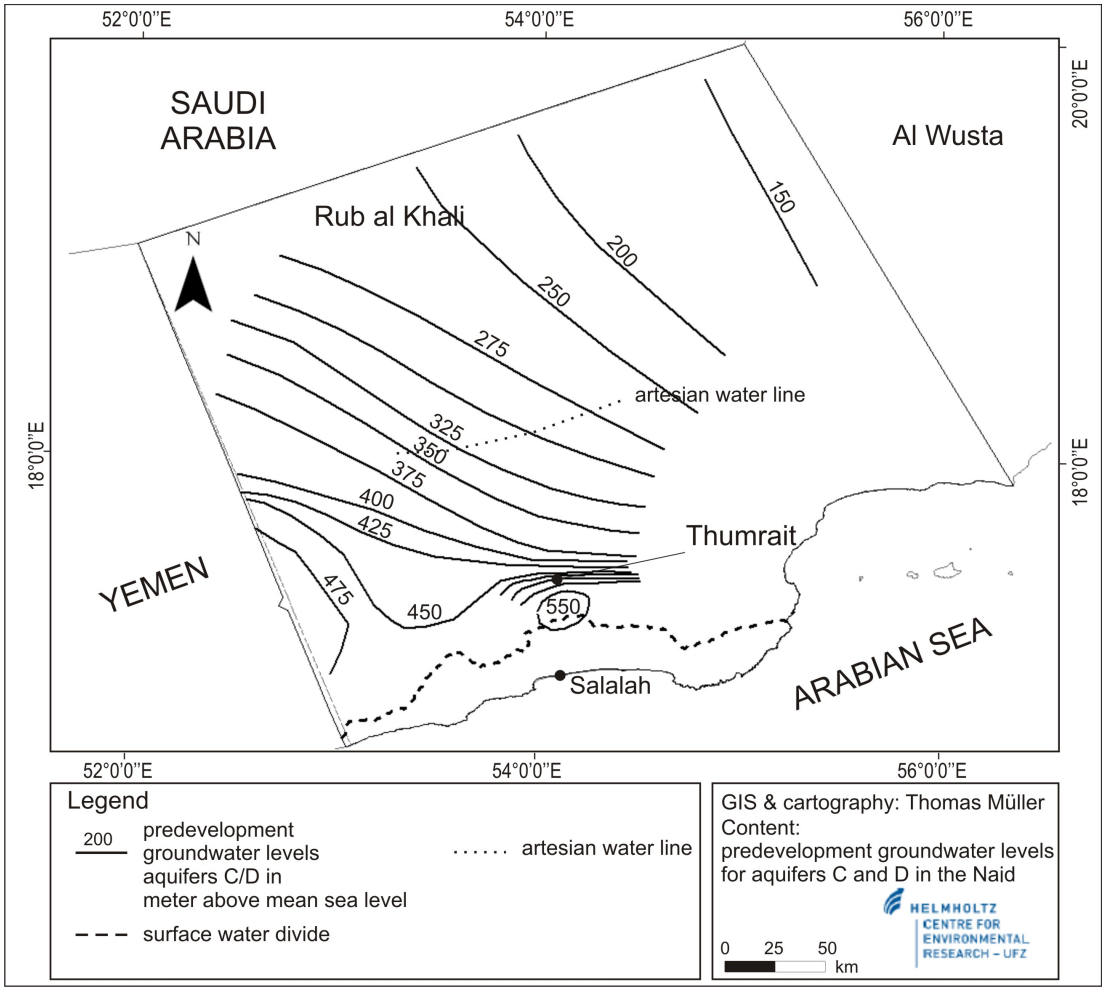

Figure 4.5: Predevelopment hydraulic heads (around 1970) in the Najd area for aquifers C and D represented by the solid lines. Highest groundwater levels were located in the Dhofar Mountains and at the border to Yemen. Main groundwater flow direction was from the high elevations in direction north-east.

For most of the area the constructed groundwater levels should relatively accurately represent the situation before development, and should not lie above a tolerance of ± 10 meters. Some uncertainties exist about the maximum water level in the Dhofar Mountains. Tolerance up to ± 20 meters should be reasonable here.

Today, water levels in the central Najd, the centre of abstraction, are down to 40 to 50 meters lower than before development. As previously mentioned, the reason for this decline remains unknown in terms of numbers because the abstraction is not monitored and the effect of the leaking boreholes cannot be quantified. The

artesian water line is now approximately 35 to 45 km further to the north. The regional groundwater still flows in a northeasterly direction.

Monitoring of groundwater levels in the Najd started in the 1980s. The number and the location of the observation wells (status 2011) are shown in Figure 4.1. It can be seen that the majority of the wells are located in the central Najd, around the farm areas of Jica and Hanfeet. The monitoring interval is dependent on the location of the well and varies from 2 weeks to six months. From 2006 to 2009 the monitoring of groundwater levels in the Najd was stopped.

4.1.4 Aquifer characteristics

Transmissivity

The aquifers are zones with high water yield, encountered during drilling and engineering of the wells. These zones are described as a series of fractures and fissures. Aquifer C has karstic features (GRC, 2008). Groundwater flow can take place in the fractures but also in the matrix. For the main aquifers C and D the mean thickness is 28 and 79 m, respectively. However, this thickness is quite variable ranging from 1 to 69 m for aquifer C and 1 to 133 m for aquifer D (GRC, 2008). The mean transmissivity for aquifer C is 556 m^2 d^{-1}. It is therefore much higher than the value for aquifer D at 13 m^2 d^{-1}. For the central and western areas of the Najd, transmissivities of 100 to 450 m^2 per day are cited, while the values for the Thumrait area (part of the modeled cross-section) range from 30 to 100 m^2 per day (N.N., 2007).

The collected data show that there is a wide range for the transmissivities in aquifer C, with values spanning from 1 m^2 d^{-1} to beyond 10 000 m^2 d^{-1} at some places, indicating heterogeneities and discontinuities of the fissures. The values for transmissivity and the storage coefficient were based on short term pumping tests of less then one day, in most cases. They were performed for well development following well drilling and installation. Zones of higher transmissivity most likely represent fractures. Furthermore, the numbers for the thicknesses of the producing zones vary between 1 and 50 m. How these zones are connected to each other or to the matrix surrounding them, or how areas of better permeability are developed and connected in the horizontal direction is not known. It might be that discrete karstified channels, and not the given thickness of the aquifers or

the screen length, provide the main yield at the wells. Thus, for structures like this, converting transmissivity at wells to hydraulic conductivities for the entire thickness of the formation may not be appropriate. It seems unlikely that the mentioned high tranmissivity values are of regional significance. Only long time pumping tests could provide more detailed information on the parameter range in these cases.

Porosity

An important aquifer parameter when evaluating groundwater resources or estimating groundwater travel times is the porosity. Generally speaking, the porosity is the ratio of volume of voids and total volume of the soil or rock material. This porosity is called the total porosity. The volume where water transport can take place - the effecitve porosity - is below this total porosity, because of connate water or dead end pores. The dead end pores or disconnected pores or voids are of no interest for the flow in the system, but can be important for the water chemistry or the concentration of a solvent in the system. For flow systems with quite long residence times where the concentration of a tracer is in focus, the total porosity has to be considered.

Aquifer systems with karst features are known to exhibit dual porosity characteristics. One is provided by the matrix and the other provided by the fissures and fractures. Here the matrix forms most of the storage of the system whereas the fractures and fissures represent the part of the system where high-velocity flow can take place.

The co-existence of matrix and fracture porosity influences the flow in the system, with the mentioned high-velocity flow in the fractures and in contrast slow flow in the connected pore system of the matrix. But dual porosity systems can have also impacts on the concentration and evolution of chemicals and isotopes solved in the water, for example due to diffusion transport into secondary pores, micropores or microfractures. This will be of less influence when the solvent is a conservative tracer and the system is in steady state, which will result in a uniform concentration over time.

When using radioactive tracers in contrast, diffusion into micropores with ongoing decay at the same time can result in a concentration gradient between fractures and matrix. The interpretation of tracer concentrations in such systems in terms

of groundwater residence times can lead, for example, to quite different residence times compared to residence times based on advective flow only. Among others, the size of the fissures, the residence time or the water volume in the micropores play a significant role for the fracture-matrix interactions. For the influence on the role of porosity in combination with groundwater age, the interested reader is refered to Clark and Fritz (1997); Neretnieks (1981) or Cook et al. (2005).

For the Umm Er Radhuma aquifers large variances exist for the aquifer porosity. GRC (2005b), for example, give values between 20 and 28 % for the LUER, based on geophysical measurements of three wells in the northern Najd. Al-Mashaikhi (2011) cited estimates of 0.5 %, and 0.4 to 10 %, respectively, from two studies (1989 and 1993) for the central Najd.

Values of 30 % for the total porosity are desribed for the umm Er Radhuma in Saudi Arabia (Bakiewicz et al., 1982). This value agrees with the range of 0-20 % for limestone (dolomite) and 5 to 50 % for Karst limestone, given by Freeze and Cherry (1977).

Bakiewicz et al. (1982) and Freeze and Cherry (1977) refer to the total porosity, for the other cited works above it is not clear if these values refer to total or effective porosity.

Storage and specific yield

Recent studies on the hydrogeology of the Umm Er Radhuma aquifers give values for the specific yield (S_y) of 0.01 for the aquifers A to C and values for the storage coefficient (S_s) of 1.0×10^{-6} for the aquifers A and B and 1.5×10^{-4} for aquifer C (GRC, 2008).

4.1.5 Discussion of available data

A first glance at the location and distribution of the monitoring sites in Figure 4.1 already reveals the major gaps in our understanding of the regional groundwater hydraulics: No observation wells exist in the west of the Najd, which makes it impossible to evaluate the groundwater inflow from Yemen. Starting from the Dhofar Mountains, the first monitoring well is 50 km away from the (assumed) subsurface water divide and more than 35 km away from the outcrop areas of the Umm Er Radhuma. There is no chance to observe groundwater fluctuations in the

area where recharge most likely would occur. No monitoring devices have been installed so far in the north and north-east where the groundwater is artesian. With that, neither the inflow to, nor the outflow out of the Umm Er Radhuma aquifers can be estimated with the necessary accuracy.

The location of the monitoring wells within the reach of the abstraction wells, together with the monitoring interval that proves insufficient for this purpose, makes an observation of groundwater level changes as result of an freshwater input nearly impossible. The limitations due to the location of the monitoring wells and the monitoring interval on one hand, and the lack of a monitoring for the abstraction rates on the other hand, are the major drawbacks when assessing and evaluating the groundwater resources in the Najd.

The same holds true for the southern area. We can be certain that groundwater recharge takes place at the south side of the mountains (see subsection 2.5.3). But even here interpretation is limited. The lack of monitoring wells in the mountains (see Figure 4.1) and an insufficient monitoring interval make it impossible to evaluate input to the system (Monsoon, Cyclones) or to observe manmade influence (increased population, improved infrastructure in the mountains, overgrazing). Statements on response times of the underground system, influence on groundwater levels by varying monsoon intensity (years, decades), or thresholds for rain causing groundwater level fluctuation cannot be made.

It was also not possible to correlate data from the rain stations with wadi flow data, which is only partly due to the quality of the data. Much more this is due to logistic reasons. Figure 4.1 reveals that most rain stations are outside the monitored wadi catchments. Or, like in the most western catchment Gharah and the most eastern catchment Andour, the rain stations lie close to the outlet of catchments. Monitored wadiflow is most likely not caused by rainfall nearby, but by rainfall occurring further upstream in the wadi.

The data sometimes register a wadi flow without a monitored rain event, or the other way around, rain occurred but no wadi flow was measured. Therefore, the available data on precipitation and surface flow make it impossible to correlate the flow data with rainfall events or the catchment size. Furthermore, it is impossible to draw conclusions what rainfall amount is necessary to produce surface water flow.

4.2 Status of the system and conceptual model

A conceptual model for the groundwater flow along a flow path from the Dhofar Mountains in the south to the Sabkha Umm as Sammim in the far north-east was developed and will be the basis for the work presented in subsequent chapters. The system status that is presented here incorporates hard data (heads, flows, water chemistry, isotopes) and interpretations, as well as assumptions based on the information given in the previous sections . The main facts and assumptions the conceptual model is based on, are listed below. In addition, the main unknowns of the system are stated. Following this summary, the developed conceptual model is presented.

The main facts are:

- today's groundwater flow runs from the Dhofar Mountains in a northeasterly direction to the Sabkha Umm as Sammim
- today's climatic conditions are different from the conditions when the majority of the groundwater reservoir was filled
- the relevant timescale for the groundwater flow system is over 10,000 years

The main assumptions are:

- the groundwater in the aquifers is continuous; even though geological faults exist (see Figure 4.6) there is no evidence for major aquifer compartments separated by faults, changing facies or the like
- there exist no large influx from underlying aquifers to the Umm Er Radhuma aquifers
- today's weather systems (Monsoon, Cyclone) are similar to the conditions when the aquifers were filled
- groundwater flow occurred from the Dhofar Mountains in north easterly direction in the past as it does today

The main gaps are:

- the distribution and effect of karstic structures in the aquifers remains unknown

- parameters and influence of the thick unsaturated zones, which possible recharge must pass through, remain unknown
- the effect of (i) leaking boreholes, (ii) extensive pumping and (iii) long screen depths of the sampled wells on the groundwater dynamics and water levels (i and ii) and the analyzed groundwater samples, used for the calculation of residence times and water origin (i to iii), cannot be qualified

Figure 4.6 presents a simplified version of the generalized conceptual model for today's hydrology of the Najd. The major components are: (1) infiltration to the deep aquifers generally varies in space and time but is limited to the outcrop areas adjacent to the Dhofar Mountains and the upstream areas of the wadi channels. (2) infiltration to the shallow aquifers also varies in space and time but is limited to the central area in the Najd. (3) flow occurs vertically in the assumed recharge area at the beginning of the flowpath. (4) at the southern mountain face we find a highly fractured system. (5) there is lateral flow downstream in the aquifers. (6) there is upward flow from aquifer D to the upper aquifers. (7) there are fast pathways in the fissures and fractures. (8) matrix and fracture system mix. (9) natural leakage occurs. (10) leakage also was induced by drilling or at geological faults. (11) there is manmade discharge, and (12) natural discharge at the Sabkha Umm as Sammim.

The main physical processes of the conceptual model are depicted. Not presented are numbers on infiltration rates, leakage or discharge, since these numbers are not known and can also not be estimated at this stage from the available data (see subsection 4.1.5).

Besides the above mentioned gaps in understanding, the model is simplified in that for example no perched aquifers, upward (vapour) flow in the unsaturated zone or varying matrix saturation was taken in account. This is because the objective was to start with a simple approach that fits the observed situation. Components (1) to (12) highlight that already enough uncertainties or degrees of freedom exist which are hardly to evaluate. Another reason is, that omitted components are believed to be of minor importance to the regional aquifer system.

The presented conceptual model is the basis for the numerical groundwater model presented in Chapter 5 and for the calculation of the residence times in Chapter 6.

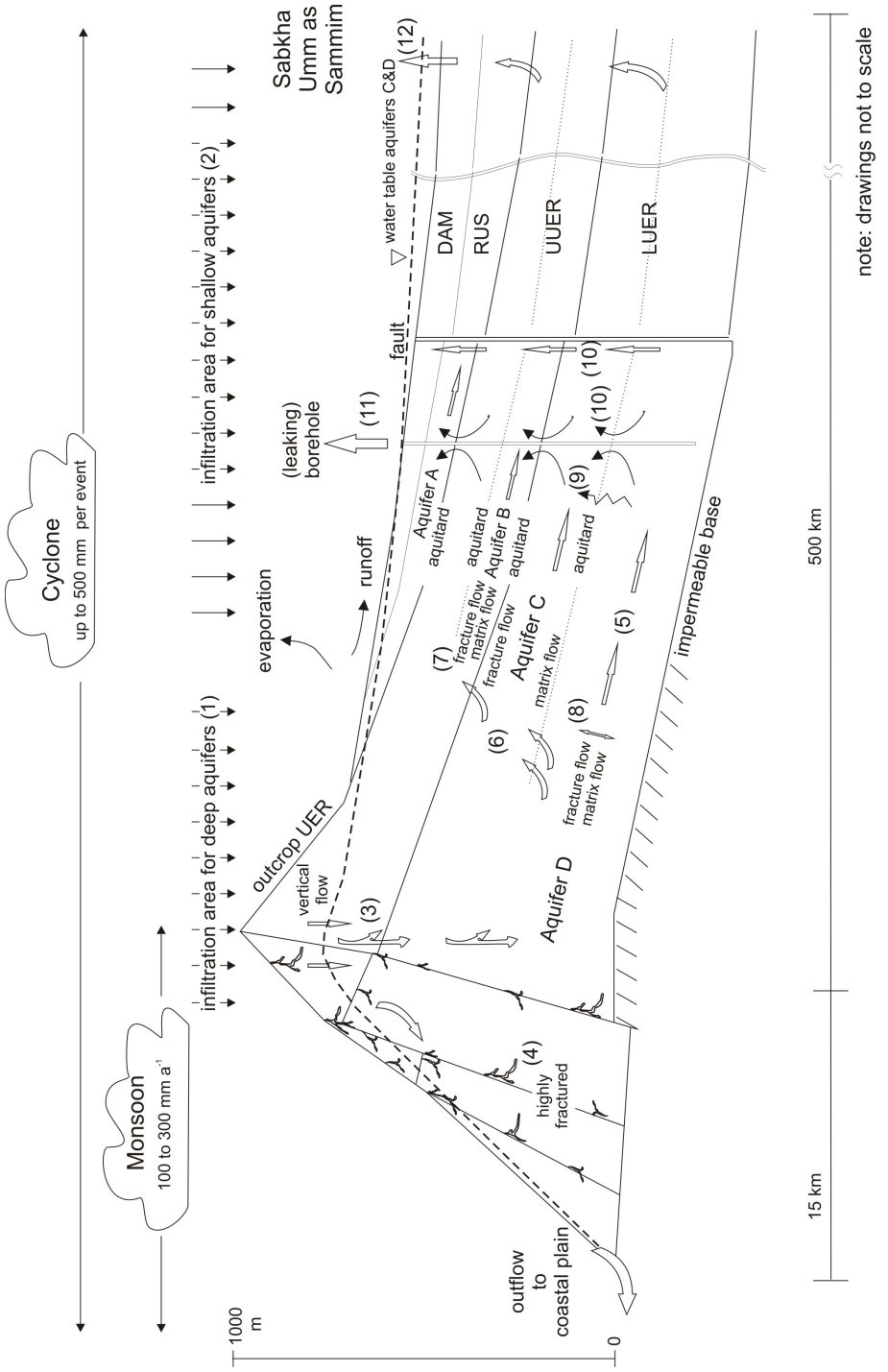

Figure 4.6: Generalized conceptual model of todays Najd hydrology.

Chapter 5

Groundwater model

One of the main issues regarding the Najd groundwaters, is the question of whether or not there is any recent groundwater recharge to the deep aquifer system. The previous chapter concluded that this question cannot be answered by the available monitoring data. In response, one could try to improve the overall monitoring procedures, for example, by installing additional monitoring devices or by increasing the monitoring frequency. Although such measures might provide important information and should therefore parallel any other efforts, they are time consuming and will not necessarily lead to meaningful results. Another possibility is groundwater flow modelling, allowing for an evaluation of groundwater flow on a theoretical basis.

For this purpose, the conceptual model develped in chapter 4 was transformed into a flow model. The aim of the flow modelling is (i) to qualitatively simulate the groundwater flow and evaluate possible recharge scenarios and (ii) to quantitatively estimate the flow parameters, such as hydraulic conductivity, recharge and aquifer porosity.

Today, groundwater flow modelling is a state-of-the-art method. Numerous applications for groundwater flow and groundwater transport can be found in the literature. This section starts with an introduction to numerical modeling with a focus on the parameter estimation process, followed by the description of the creation of the Dhofar 2D-model. The model results, a model application and the result of the field observations are also presented in this chapter.

5.1 Theoretical background numerical modelling

5.1.1 The groundwater flow

The groundwater flow can be described by Darcy's Law and the principles of mass balance. The movement of groundwater can be described as a derivation from these basic principles in a partial differential equation:

$$\frac{\partial}{\partial x}\left(K_x\frac{\partial h}{\partial x}\right)+\frac{\partial}{\partial y}\left(K_y\frac{\partial h}{\partial y}\right)+\frac{\partial}{\delta z}\left(K_z\frac{\partial h}{\partial z}\right)=S_s\frac{\partial h}{\partial t}-Q(x,y,z,t) \qquad (5.1)$$

In (5.1), h is the potentiometric head, K is the hydraulic conductivity in the directions x, y and z, S_s is the specific storage, Q is a volumetric flux representing a source or a sink of water, and t is time. The groundwater flow equation (5.1) can be solved when the hydraulic properties K and S_s are known and the initial and boundary conditions are described. Initial conditions and S_s are not required for steady-state conditions. The solution of equation 5.1 is the head distribution in the aquifer system.

Equation 5.1 can be solved analytically when geometry and boundary conditions are simple and the aquifer is homogeneous. For complex systems there normally is no analytical solution and Equation 5.1 is solved numerically. Finite differences and finite elements are two numerical solution techniques which are often used for solving the flow equation. MODFLOW-2005 (Harbaugh, 2005) which uses finite differences, or FEFLOW (Diersch, 2009) which uses finite elements are numerical codes that are widely used for modelling groundwater systems, for example. Observed values, for example the observed groundwater heads, and the simulated (head) values from the numerical model are compared, in order to evaluate the numerical flow model. The match between these two indicates how well the real world system is represented by the numerical model. The process to minimize the differences between observed and simulated values is called calibration. The calibration process has one important goal: it gives an estimate of the parameter values that result in the best possible fit between observed and simulated values. Parameters can be adjusted manually by trial-and error, or with the use of automated parameter estimation codes.

5.1.2 Automated parameter estimation

There are several advantages to using automated parameter estimation codes to calibrate the model rather than a manual trial-and-error method. One important advantage is that these codes can provide useful information that helps understand the flow system. The associated statistics allow for several analyses, such as sensitivity and parameter correlation, which can be of great use when evaluating how the model performs under changing parameters. The codes also often save time, for example in determining which parameters have less impact on the simulated results and whether it is worthwhile to estimate values for them. As calibrating a groundwater model can be quite time consuming, it is important to understand the system well enough to be able to generally predict what will happen to the simulated values when one or more parameters are changed. However, it is not necessarily useful to estimate this for every single step. The difficulty during the calibration process is that, unless the system is very simple, there is no guarantee that the parameters producing the best fit to given observations can be clearly determined. Automated parameter estimation can help to verify whether a better fit is possible, and, if so, can assist in finding the corresponding unique solution. The automated process can reveal model weaknesses or insensitivities. It is important for the modeler to be able to qualify the calibration and the uncertainties of parameter estimates in classifying model results. Ultimately, this makes the modeling process more transparent for community stakeholders as well.

Automated parameter estimation also has some disadvantages. One disadvantage is that it cannot find the global minimum for the model if multiple minima occur. However the trial-and-error hand calibration method has the same problem. Thus, model optimization can result in finding local optima instead of global ones. This is particularly likely to happen in complex systems with many parameters. One way to test for this issue is to run the model with different initial values for the parameters, before checking if the final estimated parameter values are the same. Another potential problem is that uncertainties, which result in differences between observed and simulated values, can have various origins, for example random or systematic errors in the input or the observation data. An automated routine cannot distinguish between these sources of error and could return unrealistic parameter estimations as a result. This can be avoided by defining upper and

lower boundaries for the parameter values. Such a definition requires prior knowledge and a comprehensive understanding of the system, including the structure of the model, its expected parameter ranges, and a notion of potential sources of uncertainty. With this background information automated parameter estimation can be used effectively. Thus, a combination of manual fitting and automated parameter estimation is a valuable tool; initial manual adjustment establishes reasonable parameter limits for defining upper and lower boundaries, while the fine adjustment is completed by the automated routine and leads to final results and a best possible fit. This study combined manual and automated approaches in order to reap the advantages of both methods in calibration.

Objective function

How well the simulated values fit the observed values, and how well the model in turn represents the actual system is measured by the objective function, which compares simulated and observed values. The minimum value returned by the objective function indicates the parameters which produce the best fit between observed and simulated data.

The nonlinear regression method employed by UCODE (Poeter et al., 2005), which was used in the present study, minimizes the squared weighted differences between the observed and simulated values of the objective function by estimating optimal parameter values. The weighted least-squares objective function can be expressed as follows (Hill and Tiedeman, 2007):

$$S(b) = \sum_{i=1}^{n} w_i \times e_i^2 \tag{5.2}$$

Where b is the vector of parameters to be estimated, n is the number of measurements, w_i is the weight on difference e_i, e_i is the residual for measurement i with $\mathrm{e}_i = [\gamma_i\text{-}\hat{\gamma}_i(\mathrm{b})]$, γ_i is the observed quantity and $\hat{\gamma}_i(\mathrm{b})$ is the simulated quantity. The quantities which are normally used are head and sometimes flow.

The residuals for both types of data, the head differences in [m] and the flux differences in [m s^{-1}] have to be converted into the same unit to use them in the objective function. This is one reason why the observations are assigned weights. Multiplying the residual e_i with the weight w_i gives a dimensionless number. Hence, the squared weighted differences for the heads and the flow can

be summed up in one objective function. Furthermore, the weight reflects the relative importance of the observation. Observations with a high measurement precision are assigned greater weights relative to observations with less precise measurements.

Different statistical methods are available to calculate the weight w_i. The method to choose depends, *inter alia*, on the type of observation. UCODE offers statistical methods including variance, standard deviation or coefficient of variation. This study uses standard deviation to assign weights for the head and the flow observations.

Sensitivity analysis

Sensitivity analysis explores the relationship between observation input and parameters in the model. Whether and how much the simulated values at an observation location change as a result of changes made to model parameters (for example hydraulic conductivity or recharge), is calculated by using statistics. Sensitivities are expressed mathematically as follows (Hill and Tiedeman, 2007):

$$\left(\frac{\delta\gamma_i^{'}}{\delta b_j}\right)\Bigg|_b \tag{5.3}$$

where $\gamma_i^{'}$ is the simulated value corresponding to an observation and b_j is the jth parameter. The sensitivities are calculated for the parameter values in vector b which is indicated by the notation.

The sensitivities of the model are computed during the optimization process. These sensitivity values indicate how much information a specific observation contributes to the estimation of a specific parameter. The composite scaled sensitivity (CSS) formula is used to summarize the information all observations provide in the estimation of a single parameter j (Hill and Tiedeman, 2007):

$$CSS_j = \left\{ \frac{\sum_{i=1}^{n} w_i \left(\frac{\delta\gamma_i^{'}}{\delta b_j} b_j\right)^2}{n} \right\}^{\frac{1}{2}} \tag{5.4}$$

The values for different model parameters can be compared since b_j scales them so that the parameter sensitivities are dimensionless. Large values for the CSS

indicate that the parameter has a greater impact on the simulated observations and that those parameters would likely better be estimated by regression. Smaller values of CSS indicates that a parameter has less impact.

Parameter correlation coefficients (PCC) are another useful statistical tool to combine with CSS. These coefficients are calculated for all possible parameter combinations and can vary between -1.00 and +1.00, where -1.00 is a perfect neagtiv correlation and +1.00 is a perfect positive correlation. Parameter pairs showing these values indicate that they are nonunique. In other words, various parameters can have the same or similar influence on the model, and different values can lead to the same result for the regression. Such nonunique parameters represent uncertainty in the model.

5.1.3 Software and processing

In the present study, MODFLOW-2005 (Harbaugh, 2005), which is free for scientific use, was used for the simulation of the groundwater flow. MODFLOW-2005 is a finite-difference ground-water model with a modular structure composed of a main program and several independent packages. This structure allows the user to define and examine special hydrologic features independently. There are four package categories, the hydrologic internal packages - simulating the flow between adjacent cells, the hydrologic stress packages - simulating individual kinds of stress (recharge, for example) the solver packages - implementing the solutions for the algorithm of the finite-difference equations, and the program control package - controlling and organizing the process.

MODFLOW-2005 software does not include parameter estimation. For this reason, the automated parameter estimation code UCODE (Poeter et al., 2005) was used to evaluate the sensitivity of the parameters and to establish optimal parameter values. UCODE is an indirect inverse model, meaning that observation data (for example hydraulic head values) and optimization techniques (regression) are used to estimate model input values (for example hydraulic conductivity). UCODE employs the nonlinear least-squares regression method.

After reading the input-files, UCODE connects with MODFLOW-2005 during the parameter simulation process. The simulated process model output values are then compared to observed values. In each iteration, the input parameters are

automatically adjusted until the best possible fit between simulated and observed data is reached. The Dhofar model required UCODE to implement additional code after each MODFLOW run in order to extract the simulated heads from the result file and write them to the initial head file. Thus with each new MODFLOW run, the starting heads were rewritten to be the simulated final heads from the previous run. This was done to increase the model's stability for the Newton-Raphson solver. The nonlinearity introduced by solving for the water-table surface required an estimate of the initial heads that was not greatly different from the final head solution.

5.2 Creation of the 2-D Najd groundwater flow model

The conceptual model (see section 4.2) shows the direction of the groundwater flow as running from the Dhofar Mountains into the Najd and from there to the Sabkha Umm as Sammim. Recharge areas are in the Dhofar Mountains and the adjacent area to the north; the discharge area is the Sabkha at the end of the flowpath. This section explains the design and construction of the two-dimensional groundwater flow model representing the characteristics of the aquifer system.

The essential characteristics of the Najd aquifer system that should be represented in any model are: first, the steep topographical gradient; second, the main geologic formations and their formation elevations; and finally the hydraulic disconnect between the upper and lower aquifer system.

Spatial discretization

The vertical structure of the model spans the distance between the land surface and the bottom of the lower Umm Er Radhuma, indicating a vertical thickness of up to 685 m. The four hydrogeologic units DAM, RUS, UUER and LUER form the main aquifers A, B, C and D (see section 2.5.1). The aquifer thickness is small compared to the thickness of the geologic formations (see sections 2.5.1 and 4.1.4), which was taken into account in defining the number and thickness of the 10 layers in the model. This relatively small thickness was also the reason for defining each hydrogeologic unit as being comprised of 1 to 4 layers.

All layers span the whole model domain, with the minimum thickness (5 m) occurring in the southern part of the Dhofar Mountains, where the geologic formations were thin or had disappeared. In the north, a uniform thickness was assumed for layers 5, 8 and 10, representing the aquifers B, C and D in the 2-D model. Layer 2 represents aquifer A, which becomes thinner with increasing elevation. All other layers vary in thickness. Table 5.1 shows the vertical structure of the model and the thickness of the layers.

Table 5.1: Model layers, geologic formation, aquifer and thickness.

model layer	geol. formation	aquifer	thickness [m]	model unit
1	DAM, Rus		5-45	
2	RUS	A	5-20	aquifer
3	RUS		5-205	top
4	UUER		5-65	
5	UUER	B	15	
6	UUER		5-55	
7	LUER		5-50	conf
8	LUER	C	25	
9	LUER		5-100	aquifer
10	LUER	D	75	bot

Defining ten layers made it possible to use different parameters to define each layer. Horizontally, the model spans 560 km, with an equally spaced grid size of 1-kilometer, resulting in a total of 5,600 (560 $\times$ 10) elements in the model.

Boundary and initial conditions

Boundary conditions were set for areas in which inflow to or outflow from the modelled domain could occur. Such locations include: 1) the natural spring discharge near the southern end out of the model; 2) the recharge areas in the Dhofar Mountains and in the interior Najd; 3) the discharge area at the Sabkha Umm as Sammim. The lower and east-west boundaries of the model domain were assigned no-flow conditions.

The spring outflow was represented by defining a general head boundary for the lowest layer (layer 10) in the first row of the model using the General Head Boundary Package. The general head boundary condition (GHB) was chosen because a spring flow value was calculated and used as an observation later on in the calibration process. For the general head boundary, a head value of 140 m was assigned, which is the approximate elevation of the springs. The boundary conductivity, or the proportional constant, was defined with a high value of 1.0E+06 m s^{-1} to assure that the flow out of the cell would be unlimited. With such a high conductivity value, the boundary acts like a typ I boundary condition, yet it also allows the model to calculate the outflow implicitly.

The discharge area at the southern end of the model section, which represents the Sabkha Umm as Sammim, was defined as a constant head boundary (CHB) with a head value of 85 m, equivalent to land surface, i.e. at the topmost layer in the last row of the model, see Fig 5.1. Although the spring and Sabkha both behave as type I boundaries, they were assigned different boundary types so that their calculated flow rates could be observed separately in the model's budget output.

Two recharge zones were defined for the model. The monsoon-affected area of the region stretches at maximum only 1 km north of the surface water divide. In the model, column 16 represents the surface water divide. Recharge zone 1 (RCH1), which represents recharge generated by the monsoons, was therefore allocated to columns 1 to 17.

Zone 2 represents the recharge zone in the interior area. Recharge zone 2 (RCH2) has no clear boundaries, and cannot be defined in a straightforward manner. This is due to rainfall data showing that cyclonic events can occur in the mountains north and south of the topographic divide, as well as in the Najd (see section 4.1.1). Depending on their intensity, these events may cause a runoff that moves downstream in the wadis and is sometimes observed far off in the Najd (see section 4.1.2). The extent of the area through which these flows and direct rainfall filter into the aquifers, remains unclear. For the LUER (aquifers C and D) no infiltration should be possible in the central and northern Najd because the pressure heads in these aquifers is above the pressure heads in the aquifers above them (where the groundwater is artesian). Thus the potential recharge area for the deep confined aquifers can be approximately limited to the area near Thumrait, circa

40 km north of the topographic divide. The upper aquifers A and B, in contrast, can receive input from above in the interior area. This holds for the entire extent of aquifer A, but is limited to the artesian water line for aquifer B. However under the assumption that recharge to the deep aquifers would be in the south, recharge zone 2 was defined to span columns 18 to 60.

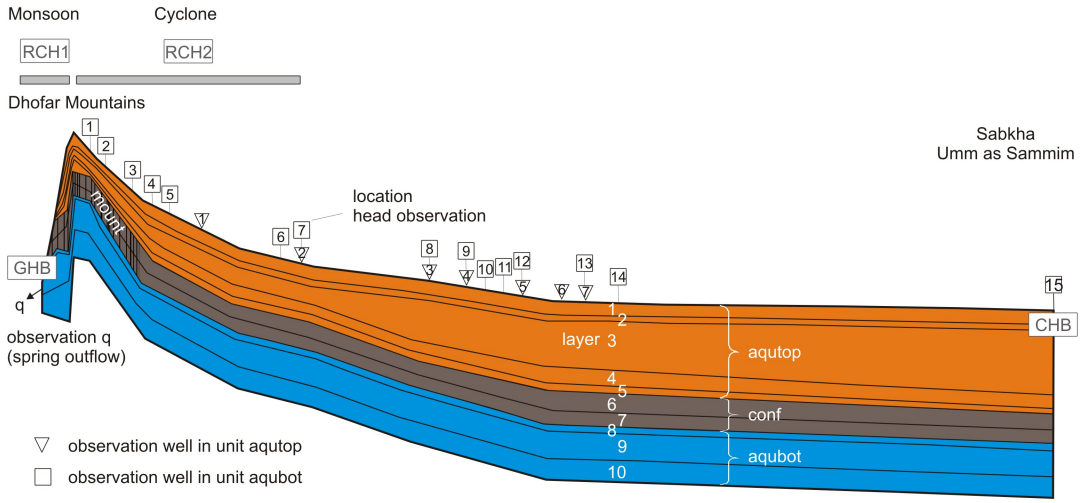

Figure 5.1: Schematic structure of the 2D-model with location of observations and boundary conditions. Ten layers and the aquifer units are shown. The monsoon recharge is represented by *Rch1*, cyclone recharge in the Najd by *Rch2*. The natural spring outflow at the southern end of the model is represented by a General Head Boundary (GHB), the Sabkha at the northern end by a Constant Head Boundary (CHB). Vertical exaggeration: 80x

The initial conditions, or the heads at the beginning of the simulation, represent the pre-development waterlevels (see section 4.1.3 and Figure 4.5), with one value set for every cell in the model.

The initial parameter values for the hydraulic conductivity were specified in the parameter input file. Investigation in the study area yielded these values (see section 4.1.4). The final values used in the model will be discussed later on during the description of the calibration process.

Using the Newton Solver requires the upstream weighting package, which specifies properties that control flow between cells such as whether the layers are confined (i.e. saturated thickness equals cell thickness) or convertible (i.e. cells can have variable saturated thickness). For the Dhofar model, layers 1 to 7 were de-

fined as convertible and the layers 8 to 10 as confined. Convertible layers can switch back and forth between either saturated or unsaturated conditions.

For the Dhofar model both head and flow observations were used for the calibration of the model. Observation data were water levels in wells along the cross section which are believed to represent the water level in the aquifers. The flow observation (natural spring) was associated with the general head boundary condition.

Steady state simulation

In a steady state, flow conditions do not change over time. Creating a groundwater model often begins with the simulation of a steady state condition, which is represented by a single stress period with a single time step and a storage term of zero in the model (see also equation 5.1).

5.3 Calibration of the Dhofar model

A prudent approach to modelling is to begin with a simple model containing a low number of essential parameters (Hill and Tiedeman, 2007). Therefore for the Dhofar model, the 10 layers of the model were partitioned into 2 aquifer units, *aqutop* and *aqubot*, separated by a confining unit. The confining unit was also subdivided in two units. One zone represented the confining unit in the Dhofar Mountians (*mount*), while the other represented the confining unit in the rest of the cross-section (*conf*). Drilling results supported this subdivision for the confining layer (see section 2.5.1). It was assumed for all four units that the hydraulic conductivity was isotropic and constant throughout each entire unit.

Calibration data

The main data sources for the hydraulic-head values along the modelled cross-section come from wells administered by the MWRWM and include well monitoring and drilling records. For the calibration 21 observation wells were used. In aquifers A and B, seven wells had open intervals, while in aquifers C and D, 14 wells had open intervals. The observation well furthest north (well B14, location shown in Figure 5.1), is at a distance of 330 km from the surface water divide. Between

well B14 and the well in the Sabkha Umm as Sammim, no monitoring data are available. Because there are no known major geologic fault zones or anthropogenic interferences in this region, the model design assumes that the water level between well B14 (136 m amsl) and the Sabkha (85 m amsl) declines approximately linearly between the wells. The model cannot be expected to provide an exact simulation of the observed heads, especially because the measured heads are estimates based on long open intervals. The observed heads were defined using available information, but the predevelopment head values remain subject to a degree of uncertainty. In the UCODE main input file, values of 10 m were assigned for all the wells as the expected measurement error in the hydraulic heads. These were assigned as standard deviations and used to weight the head observations.

Modelling the flow (q) at the foot of the Dhofar Mountains was the other calibration objective. The outflow is the sum of the spring outflow and the subsurface flow into the plain. Only the outflow from the springs is a directly measurable quantity, and is measured as 10 Mm^3 per year (GRC, 2005a). This value represents the minimum outflow. A value corresponding to a 1 km-wide cross-sectional width in the model was defined as flow observation. The expected measurement error was also assigned as a standard deviation with a value of 10 % of the calculated outflow.

The initial calibration does not include ages, because there was additional uncertainty associated with the age values (see section 1.2) as well as with the values for porosity (see section 4.1.4), which would have to be assigned or estimated in order to simulate age. Model and UCODE run that include the simulation of the ages will be explained later in the section 6.4.

5.4 Modelling Results

The goal of the calibration was to estimate the set of parameter values that would provide the best fit between the simulated and observed head and outflow values, and therefore the best representation of the natural system and its predevelopment conditions. Those conditions include the head gradient in the lower Umm Er Radhuma (Aqu C and D), the steep head gradient in the Dhofar Mountains, the upward vertical gradient in the interior Najd, and the rate of spring outflow at the Dhofar Mountains.

Table 5.2: Observed heads (WL obs) and simulated heads (WL sim) of the final model run for the wells along the cross-section.

aqutop				aqubot			
Well	WL obs [m amsl]	WL sim [m amsl]	residual [m]	Well	WL obs [m amsl]	WL sim [m amsl]	residual [m]
T1	320	330	10	B1	550	532	18
T2	275	274	1	B2	500	476	24
T3	260	227	33	B3	370	376	6
T4	220	209	11	B4	340	355	15
T5	143	134	9	B5	325	322	3
T6	110	115	5	B6	310	321	11
T7	108	106	2	B7	300	309	9
				B8	280	280	0
				B9	265	262	3
				B10	239	218	21
				B11	200	205	5
				B12	175	182	7
				B13	150	153	3
				B14	136	133	3

Heads and outflow

The simulation yields the highest water levels for the Dhofar Mountain region with water levels up to 550 m amsl. The heads in all layers decrease from the high elevations (Dhofar Mountains) to the lowest elevation at the Sabkha.

Table 5.2 displays the head values of the wells, with the the wells in aqutop on the left side, and the wells in aqubot, as the primary goal in calibration, on the right side. The wells in the Dhofar Mountains, B1 and B2 have the largest differences between simulated and observed water-levels, with differences of up to 24 m. In the interior area well B10 has the greatest difference between simulated and observed levels at 21 m.

The model successfully represents the high groundwater levels in the Dhofar Mountains, as well as the upward gradient in the interior area, where the observed

Table 5.3: Observed and simulated water levels representing the upward gradient for three locations in the Najd.

location 1			location 2			location 3		
Well	WL obs [m]	WL sim [m]	Well	WL obs [m]	WL sim [m]	Well	WL obs [m]	WL sim [m]
T4(B)[a]	220	210	T5(B)	143	134	T7(A)	108	106
B9(D)	265	262	B12(D)	175	182	B13(D)	150	153

[a] B - aquifer B, C and D respectively

values in the LUER are higher than the water levels in the UUER. This is also shown in Table 5.3, where the simulated and observed water levels for 3 locations in the interior Najd are listed. The differences in head values between the upper aquifers A and B and the lower aquifers C and D are evident in Table 5.3.

The spring outflow at the south side of the Dhofar Mountains was simulated using MODFLOW's general head boundary package, which calculates the flow into or out of a general head boundary cell. For the steady state simulation, an outflow of 0.01 m s^{-1} was calculated as being equal to around 16 Mm^3 a^{-1}. The output value for the discharge point at the Sabkha Umm as Sammim, represented by the constant head boundary at the northern end of the model, is 0.0024 m^3 s^{-1} or 210 m^3 d^{-1}.

5.4.1 Parameter Estimates

Hydraulic conductivity

The calibration process combined simulations using automated nonlinear regression and manual parameter adjustments. During calibration it became evident that the hydraulic conductivity of the confined unit (*conf*) had to be below 1×10^{-11} m s^{-1} to obtain an upward gradient between lower and upper aquifers. After this became apparent, the value for the confining unit was no longer estimated, but was instead assigned a value of 1×10^{-11} m s^{-1}.

Another value that was eventually assigned was the confined unit (*mount*) in the Dhofar Mountains. Here the value assigned was the estimated parameter

Table 5.4: Parameters of the groundwater flow model and optimised values.

Parameter name	parameter description	parameter location	unit	optimized parameter value
aqutop	hydraulic conductivity RUS, UUER	area up to border Dhofar	m s^{-1}	1.7×10^{-5}
aqutso	hydraulic conductivity RUS, UUER	area north to border Dhofar	m s^{-1}	1.0×10^{-3}
confin	hydraulic conductivity UUER, LUER	area north to Dhofar Mountains	m s^{-1}	1.0×10^{-11}
mount	hydraulic conductivity UUER, LUER	Dhofar Mountains and adjacent area	m s^{-1}	6.6×10^{-7}
aqubot	hydraulic conductivity LUER	whole area	m s^{-1}	6.6×10^{-7}
Rch1	recharge	southside Dhofar Mountains	m s^{-1}	4.4×10^{-10}
Rch2	recharge	area north to Dhofar Mountains	m s^{-1}	1.0×10^{-10}

value of *aqubot*. This assigned value was already found to be consistent with the hydrogeological characteristics in this area, as mentioned earlier. The parameter combination shown in Table 5.4 was used to obtain the model which best fit the heads and the spring outflow.

On the one hand the CSS showed that the definition of the parameter *mount* has almost no influence on the other parameters. Therefore, the parameter was excluded from the sensitivity analysis. On the other hand it became evident that the inclusion of *mount* changed the relative importance of the other parameters.

For the 5 parameters in the automated parameter estimation, UCODE was used to evaluate the parameter correlation. A correlation value of 0.99 was calculated for the parameters *aqutop* and *Rch2*. The value indicates that these parameters are nonunique. This behaviour was somewhat expected for the Najd model, which

is dominated by head observations. Also this model behaviour is well documented in the literature (Hill and Tiedeman, 2007).

In a relatively simple model dominated by head observations, like the present Najd model, it is not uncommon to encounter a strong parameter correlation. In this case, the head distribution depends on both the flow and the hydraulic conductivity. Since these two factors are directly related through Darcy's law, it is not possible to distinguish them. On the other hand, from a hydrologic point of view, the recharge rate is limited; a maximum value would be the average annual rainfall rate (extremly unlikely to be the case). This prior knowledge of the expected recharge rates can be used to constrain the recharge values assigned, and thus, in turn, to constrain the estimated values for the hydraulic conductivity. No other parameter pairs show a correlation value greater than 0.9 or less than -0.9, which suggest that no other parameters are strongly correlated.

Recharge

Two recharge zones are defined in the groundwater flow model. *Rch1* represents the input from the monsoon and Rch2 the recharge in the interior area. The calibrated model gives a value of 17 mm a^{-1} for *Rch1*. This recharge occurs in the monsoon-influenced southern side of the mountains and can be observed every year on the basis of increased groundwater levels and spring discharge in the foothills.

In the model, the estimated value for *Rch2* is 4.3 mm a^{-1}, calculated as the recharge value to maintain the steady state predevelopment heads. This number says nothing about real recharge occurring today. The model's estimated value indicates that a modern recharge north of the Dhofar Mountains is possible. Its quantity would be dependent on the amount and spread of rainfall events. A value of 4.3 mm a^{-1} was used as an estimate for a possible cyclone recharge.

One important question is whether some of the monsoon recharge (*Rch1*) also reaches beyond the hills into the interior area in the north. The post-processing program MODPATH can be used to check this in the groundwater flow model (Pollock, 1994). MODPATH was used to track the path of a parcel of water from the uppermost active cell (where recharge is applied) to the discharge area. Figure 5.2(a) shows the path lines for this scenario (here only shown up to cell 45) for the calibrated model. The blue lines represent path lines from those cells where *Rch1* is applied; the red lines are the path lines for *Rch2*.

These pathlines indicate an absence of flow from the southern side into the north. Instead, the first 5 cells of Rch2 drain southward. In the steady state model, no time-dependent boundary conditions were applied. Therefore the model applies *Rch1* and *Rch2* simultaneously. In nature it is possible that both events occur at the same time, but in most years only *Rch1* will occur. Therefore it may be possible that the direction of flow changes when only *Rch1* is applied. For this reason, only *Rch1* was applied in the model, and examined in another MODPATH forward particle tracking analysis. Under these conditions, the northernmost cell drains into the interior area (Figure 5.2(b)).

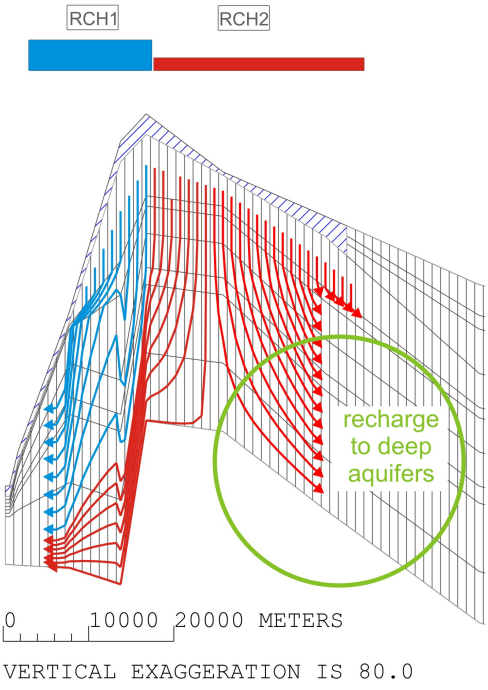

(a) Particle path Rch1 and Rch2

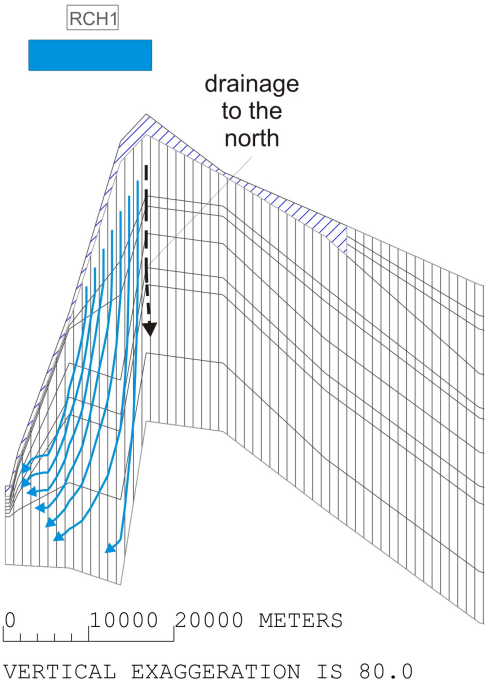

(b) Particle path Rch1.

Figure 5.2: Pathlines in the recharge area derived by particle tracking with the groundwater flow model. (a) represents the calibrated model when *Rch1* and *Rch2* are applied. (b) represents the calculated pathlines when only *Rch1* was applied.

5.4.2 Model fit

Several features of the UCODE 2005 package were used to evaluate the fit of the model to observational data. One of the simplest ways to assess the model fit is to plot the observed values against the simulated values. In the event of a perfect fit, the simulated values would be equal to the observed values, and therefore all points of the plot would fall on the 1:1 line. Figure 5.3 shows the head observations for the Dhofar model. When plotted, the values for *aqutop* (triangle) and *aqubot* (square) are close to the 1:1 diagonal line, indicating a good fit between observed and simulated values.

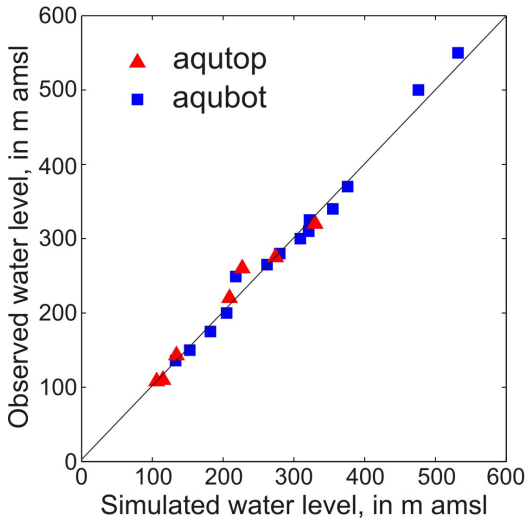

Figure 5.3: Observed water levels plotted against simulated water levels.

The optimized parameter values and 95% linear confidence interval for the parameters hydraulic conductivity and recharge are shown in Figure 5.4. The parameters *aqubot* and *Rch1* both have small confidence intervals, indicating that the model estimates them with a high degree of precision. *aqutop* and *Rch2*, in contrast, show larger confidence intervals (two orders of magnitude), indicating that they could not be estimated with a high degree of precision. This was not unexpected, due to these parameters' higher correlation values, which yield greater uncertainty. The values for *aqutop* (1.05×10^{-6} to 2.52×10^{-4} m s^{-1}) fall within a reasonable range, whereas the upper value for *Rch2* (2.3×10^{-9} m s^{-1}, equivalent to 72 mm recharge per year) seems rather unlikely.

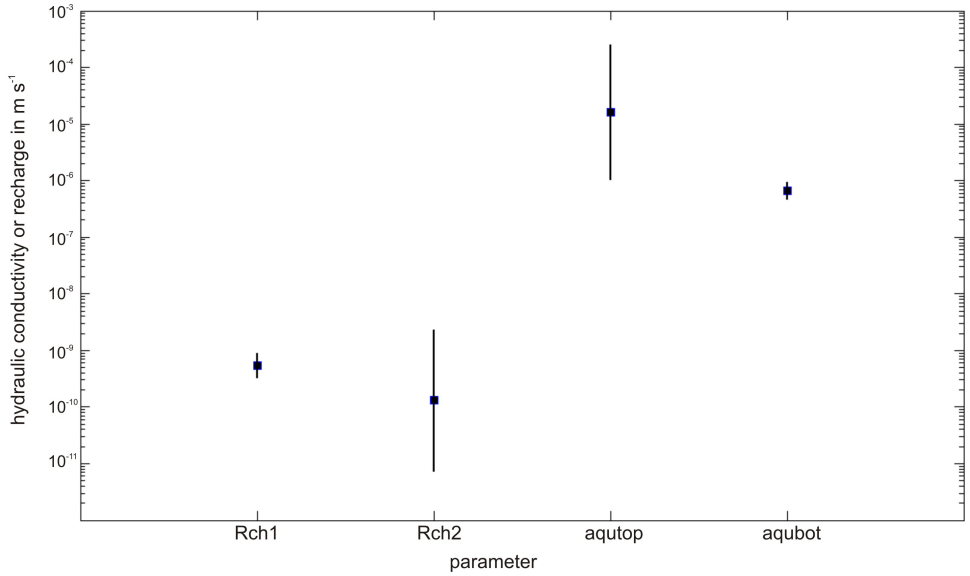

Figure 5.4: The estimated parameter values and their 95% confidence intervals for the parameters recharge and hydraulic conductivity.

Because this value is almost twice the annual mean rainfall rate for the Najd, it is likely much too high.

As a measure of the overall fit of the model to the calibration data, the standard error of regressions can be calculated by using S as the sum of the squared weighted residuals (UCODE output), the number of parameters p and the number of observations n, where smaller values (close to 1) indicate a better fit (Hill and Tiedeman, 2007).

$$s = \left\{ \frac{S}{n-p} \right\}^{\frac{1}{2}} \tag{5.5}$$

For the calibrated model with S=28.2, p=8, n=21, the standard error of regression is 1.47.

In summary, the overall fit of the model is good. This can be confirmed quickly and easily by examining the residuals (Table 5.2) or graphically looking at the 1:1 plot (Figure 5.3). The latter is the preferred presentation of model fit for relatively simple models dominated by a relatively small number of head parameters such as this one. Nevertheless, the additional analysis of residuals offered some valuable insights into the model behaviour and the influence of its various parameters.

5.5 Discussion model concept and model results

Conceptual model

The usefulness and power of any model depends on the accuracy and correctness of the corresponding conceptual model. Some of the assumptions made when conceptualizing the hydrogeology and hydrology of a region are less susceptible to error than others. For example, it is relatively easy to arrive at a certainty that the modern monsoon impacts the Dhofar Mountains mainly on their southern side and no further than 1 km north of the surface water divide; this can be observed every year during the monsoon season. In contrast, subsurface conditions are more difficult to observe and conceptualize, because in their case only limited point information is available.

In the groundwater model this affects, for example, the modelled thickness of the layers, their interconnection and their parameterization, with each factor having an impact on the model's results. In the current model, considerable uncertainities exist for the subsurface structure in the Dhofar Mountains. As mentioned earlier, it has not been possible to date to clearly define the boundaries between the RUS and upper UER as well as between the upper and lower UER formations. Furthermore some of the drillings indicate the presence of karst structures. Therefore not only the locations of contact between the different geological layers, but also the lateral thickness and extent of some of the relevant formations in this boundary region are unknown. Hence these factors have been idealized in the model and included in the layered structure. The recharge process is one of the major issues this study attempts to resolve. Here the key questions are where and when recharge occurs and what its sources are. If the southern monsoon contributes to recharge to the north, the water would have to flow in a northerly direction, where, in addition to an appropriate hydraulic gradient, geological structures and connections would have to exist, which could facilitate the downward seepage of water into the deeper aquifer system. Thus a considerable amount of geologic uncertainty remains in this primary area of interest.

Observations and results

Another goal of the model calibration was to reflect the head values representing water levels before groundwater abstraction from the aquifers began in the 1970s. Only a limited number of monitored water levels reflect this predevelopment situation. This necessitated the use of a combination of monitored data and hydrogeological observation as a basis for observation values as well as the constructed map of equipotential lines for the aquifers. Here uncertainties of up to ± 20 m with regard to these observations exist. Such uncertainty in the input and calibration data will inevitably affect the model results. However, the general hydrologic features, like flow direction, the steep gradient in the Dhofar Mountains and the upward gradient from the deeper to the upper aquifers are well supported by the data. The model simulates not only the head distribution in the given range, but also the outflows. Therefore the overall model with its estimated parameter values successfully reproduces the general hydrologic features of the region.

The outflow at the south side of the Dhofar Mountains is composed of spring outflow, as well as the subsurface flow into the plain. The simulated value of 16 $Mm^3\ a^{-1}$ (for a 50 km wide section) corresponds well to the value of 10 $Mm^3\ a^{-1}$ as minimum outflow given by GRC (2005a).

According to the groundwater flow model, the discharge at the Sabkha Umm as Sammim is 0.207 mm d^{-1}. Since today no open surface water exists at the Sabkha, this discharge is lost to evaporation from the soil. Sanford and Wood found the evaporation of coastal Sabkhas in in the UAE in 1997 and 1998 at two different sites to be 0.14 mm d^{-1} and 0.24 mm d^{-1} respectively (Sanford and Wood, 2001). The simulated value of 0.21 mm d^{-1} falls well within this range. The upward leakage and the evaporation at the Sabkha surface are the dominant sources of outflow under current conditions.

Hydraulic conductivity

For the upper aquifer unit, the estimated hydraulic conductivity values are within a reasonable range, with values of $1.7\times\ 10^{-5}$ m s^{-1} (*aqutop*) and $1.0\times\ 10^{-3}$ m s^{-1} (*aqutso*). The monitored water levels in the upper aquifers in the far northeast necessitated relatively high value for *aqutso*. The large difference between these values is striking, but since detailed modelling of the upper aquifer unit (especially

in the north) was not the primary goal of the calibration, and since it is uncertain whether wells in the upper aquifer in the central mountains are tapping the same aquifers as wells in the far northeast, no further effort was made to calibrate the parameters for the upper unit.

The estimated value for the hydraulic conductivities for *aqubot*, representing aquifers C and D, is 6.6×10^{-7} m s^{-1}. This is below the range given in section 4.1.4, where the transmissivity of the high yielding zones in aquifer C were given with 556 m^2 per day and for aquifer D with 13 m^2 per day. For comparison, however, calculating the transmissivity for the model with 6.6×10^{-7} m s^{-1} and a thickness of 200 m (layers 8, 9, 10) gives a transmissivity of about 10 to 12 m^2 per day. This value estimated by the current model is close to the cited value for aquifer D but not close to the cited values for aquifer C. Nevertheless, values higher than 12 m^2 per day were expected for the hydraulic parameters of the lower aquifer unit.

Modelling two aquifers with drastically different values of transmissivity in one system raises the question if this simplification was justified. The following reasoning supports the strategy pursued in the model's design. The monitored water levels do not indicate a head difference between aquifers C and D. This is in part due the quality of the data - the horizon of the measurement is not always clear - but also due to the distribution of the monitoring wells across the area. For the Najd area, a unified map could only be constructed for the water levels in C and D. Finally, the lack of head difference may also be due to the fact that there are no wells that measure the heads in the different aquifers at the same place. In spite of these limitations, the data indicate that the head differences between the aquifers, if existent, are likely to be small. This would support the assumption that aquifers C and D have a significant hydraulic connection. Furthermore, it may be that inappropriate drilling and installation of deep wells has created hydraulic shortcuts between the aquifers, which, in turn, makes it difficult to obtain information related to specific aquifers.

Finally, the above-mentioned model simplifications are also justified for the following reason: Especially in the case of deeper wells, measurements or sampling activities which involved tapping into the wells were not always clearly associated with a specific aquifer. So in terms of model calibration, the data available may not adequately distinguish between the aquifers.

Furthermore, in applying the "Rule of Parsimony" (Hill and Tiedeman, 2007) the model was developed with the goal of adding complexity only when necessary. As mentioned above, the thickness of the water bearing zones (aquifers) in the formation varies from 1 to 73 m (D). When the model was developed, the mean thicknesses of layers 8 (representing C) and 10 (D) was assigned such that the model would generally offer the possibility to define different values for the layers representing the aquifers. However the model still needed to be parameterized so that some water could flow to aquifer C by way of aquifer D. While it would be possible to find a parameter combination that would fulfill all these requirements, its additional parameters and structures would not be based on observed data. Thus although this adjustability could potentially improve the model, the elaboration necessary was not found to be feasible with the rule of parsimony in mind.

The same is true for the issue of the anisotropic behaviour of the hydraulic conductivities. Most likely the vertical hydraulic conductivity in sedimented layers is lower than horizontal conductivity, but there are no data that support the ratio being 1:2, 1:1.5, 1:3 or any other specific value. Therefore, in the model the aquifers of the lower UER were ultimately represented as one unit with one isotropic value of hydraulic conductivity.

In order to simulate the monitored head distribution, the conductivity value for layers 6 and 7, representing the confining units between the upper and lower UER, had to be at least 1.0×10^{-11} m s^{-1}. Values lower than this were not reasonable for the types of formations present. In one run of the model, all of the parameters (hydraulic conductivities, recharge) and the conductance value for the general head boundary were doubled, and, as expected, the model simulated the same head distributions for the layers. This demonstrated that the absolute values for hydraulic conductivities of the confining layers were not constrained, but rather that the ratio of hydraulic conductivities between the aquifer and the confining units, as well as the ratio of the recharge to the hydraulic conductivities were under constraint. Thus the magnitude of the hydraulic conductivities could be estimated with the same certainty as that which was assumed for the recharge values. Being able to constrain the recharge values was a key component of the model calibration.

Boundary conditions

The boundary conditions defined for the model were *Rch1* and *Rch2*; a general head boundary represented the outflow in the south, and a constant head boundary represented the discharge area in the north. Present day aerial extension of the monsoon rainfall was observed and applied in the model (*Rch1*). The area for *Rch2* could not be easily defined, since the rain events that result in recharge are intermittent and variable in their regional extent. One objective of the modelling process was to determine whether groundwater recharge to the deep aquifer is possible. Because of the observed hydraulics, this should only be possible in an area close to the Dhofar Mountains. The shallow aquifer A can receive recharge throughout the region, but for aquifer B, recharge should not occur where the aquifer is artesian in relation to aquifer A. It is therefore possible that recharge zone 2 extends into the central area. Furthermore the model shows that the observed head difference between aqutop and aqubot requires a difference in recharge elevation, which is reasonable, because recharge occurring at the same elevation for both aquifer units would not result in such head value differences.

If the water level in the model declined below the defined value of the constant head boundary at the northern end, the boundary condition would switch to act as an input for flow, in order to maintain the constant head. Such low water levels are not conceivable, because they would require low water levels throughout the entire model including the high elevation cells representing the Dhofar Mountains in the south. A more critical question is whether the calculated outflow at the constant head boundary could be too low in relation to real conditions. However, information about the real output could only be obtained via observations of the water levels, measurements of the vertical gradients, and from information about the climate variables that have a bearing on evaporation. Such observational data are not available, so further calculations would not be meaningful at this point.

5.6 Applying the groundwater model

Initial applications were undertaken to demonstrate how the calibrated model could improve understanding of the hydrogeologic system. In addition, some simple plausibility checks were used to demonstrate the utility of the model.

5.6.1 Cyclone Recharge (*Rch2*) = 0

The model showed that the application of around 4 mm a^{-1} for the cyclone recharge (*Rch2*) would be sufficient for a steady-state simulation using today's measured water levels to stabilize the system and to replicate present conditions. This long-term recharge rate, however, does not provide information on the transient nature of the water levels in response to recharge rates. Therefore it is important to determine what transient changes were observable in the last 20 to 40 years, since the exploration and monitoring of groundwater resources began.

To explore transient changes with the model, a transient groundwater-flow simulation was performed. The simulation was run using eight five-year time steps, preceded by a 10-million-year stress period, which should yield a preceding steady-state condition. For the long initial time step, the calibrated values for Rch1 and Rch2 were applied. For the eight five-year time steps, Rch1 was still defined with the calibrated value, but Rch2 was set to zero. In order to observe the simulated groundwater levels at different locations in the model, HYYDROGRAPH (Software USGS, no citation available), a tool which reports the simulated groundwater level for each time step and each defined location, was used in conjunction with the location of the wells used for the calibration. Transient model runs with time-dependent boundary conditions require the specification of the specific yield (S_y) and the confined storage coefficient or specific storage (S_s). For the Umm Er Radhuma aquifers values for (S_y) of 0.01 for the aquifers A to C and values for the storage coefficient (S_s) of 1.0×10^{-6} m^{-1} (A and B) and 1.5×10^{-4} m^{-1} (C) are given (see section 4.1.4). The simulation was run with the different values for S_y and S_s to simulate both a more conservative projection of conditions (S_y=0.01; S_s=1E-6 m^{-1}) and a best case scenario (S_y=0.05; S_s=1.0E-4 m^{-1}).

The conservative conditions produce lower groundwater levels at the end of the eight five-year time steps in the model. The decline in the simulated transient period of 40 years is, at maximum, about 15m. The best-case conditions show a decrease of only 2 to 3 m over the same time period. Therefore the changes in the head are quite small relative to regional values. Given the mentioned uncertainties in the observations, especially concerning the predevelopment groundwater levels, it is assumed that a steady depletion in the last 40 years due to no recharge in the interior area, would be unlikely to have been observed. The more difficult

problem is that exploitation of the groundwater resource in the last 40 years has seriously disturbed the natural system. So even with sufficient monitoring of the groundwater levels over this period, it is still difficult to determine what part of the decline in groundwater level can be attributed to groundwater abstraction and what part can be attributed to steady depletion as a result of changing climatic conditions in the area.

Given that the groundwater in the study area is quite old (tens of thousand years), and that climatic conditions have changed over the last geological epochs, and given the potential for the existence of fossil groundwater gradients, a number of applications and scenarios on the long time scale are possible using the model that have potential to provide valuable information on groundwater hydraulics and the impact of the paleoclimate. This will be the focus in the next section, starting with an examination of potential fossil gradients.

5.6.2 Maximum recharge

First, some theoretical considerations: today's relatively low water levels in the Dhofar Mountains are around 550 m amsl, but another constraint would be the maximum water levels in the mountains. For a rough calculation, the surface elevation could be taken as the maximum water level during humid times, which would be 1,000 m amsl. But this highest value is unlikely because groundwater levels reaching up to the surface in a high elevation area would lead to significant outflow and drainage at the slopes and areas of lower elevation. It is not likely that recharge was high enough to maintain such high groundwater levels and outflows. By using numerical model with drains, as will be explained later on in detail, it can be concluded that groundwater levels much above 600 m amsl in the Dhofar Mountains would be unlikely. Nevertheless, taking 1,000 m amsl as the maximum and 600 m amsl as the plausible value for a high groundwater level and therefore as the initial heads, would make the difference from today's water levels 450 m and 50 m, respectively. Considering that the last humid period ended around 6,000 years before the present day, the mean decline in water level per year would be 7.5 cm and 0.8 cm, respectively. For the last 40 years, this would correspond to a decline between 0.3 and 3.0 m. Given the recording length and accuracy for the monitored groundwater wells, such a relatively small change could not or would

not have been observed. This rough calculation does not consider changing head gradients in space or time, and is only presented as a first estimate of the possible head decline.

Groundwater Model and maximum recharge

Evaluation of whether there is an ongoing long-term water decline requires knowledge of the initial water levels in the aquifers at the time when depletion began. As no water-level observations exist prior to the current observation period (or prior to the 1970s), this initial groundwater level remains unknown. Instead, one scenario for examining this would be to use current water levels to run the model with *Rch2*=0, and then observe the time required for the groundwater levels to decline to a certain level, for example to the bottom elevation of the layers. Taking into account that in previous times more humid conditions existed in the study area, and that groundwater levels observed now are from the recent drier period, one must assume that the water levels were higher during the past humid periods. The exact levels are not known, but what can be constrained is the maximum water level, where the maximum level can be assumed to be the surface elevation. This scenario can then be evaluated with the Dhofar groundwater model, the results of which are shown below.

To begin with the maximum water levels, the model must first be filled. This was accomplished through a stepwise increase of the recharge values for the interior area of the basin, while at the same time observing the groundwater levels and the outflow at the surface in order to avoid the water level reaching above the surface. This was done by using the drain-package of MODFLOW to define drain elevations as the top elevations of the uppermost active layer, and then by allowing the model to calculate the outflow.

The extent to which recharge occurred in the interior (*Rch2*) during previous times is not the major focus for this scenario, although the source of the water is a topic of interest. As explained in the model calibration, it is assumed that the area where groundwater recharge can occur is limited because of the upward gradient and the observed hydraulics within the artesian conditions. For this reason, the aerial extent for *Rch2* was not changed from the calibrated version. Observation points were established at the locations of the wells used in the model calibration, as well as some ”virtual” observation points at locations on the

constant head boundary of the discharge area. A *Rch2* value of around 10 mm a^{-1} resulted in maximum groundwater levels. This value is two to three times modern day recharge, the recharge rate which would be sufficient to maintain today's groundwater levels. The 10 mm a^{-1} rate is sufficient to fill the system and, more importantly, indicates the long term maximum recharge rate during humid periods (with the constraint that today's discharge conditions at the sabkha are also valid for this period). These maximum groundwater levels also represent the conditions for maximum flow, since they give the highest gradient caused by the highest recharge value.

Scenario

The focus here will be on what has happened since the last humid period (6,000 to 8,000 years before present, see section 2.3.2) and the low or zero recharge in the interior that followed, assuming that the latter conditions are similar to today's observed climate. Therefore, the boundary conditions implemented were as follows: south of the Dhofar Mountians recharge, meaning *Rch1*, was stable, and only *Rch2* changed. In addition, the previous humid period was assumed to be long and "wet" enough that the groundwater levels could reach their maximum. The procedure followed was first, to run the model under steady-state conditions with the high recharge value, followed by a transient model run (100,000 years) with 1,000-year time step, assuming no recharge in the interior area. Figure 5.5 schematically represents this scenario.

In addition, the scenario was simulated for the conservative condition variant (S_s=1.0E-6 m^{-1}, S_y=0.01) and the best case variant (S_s=1.0E-4 m^{-1}, S_y=0.05). The main purpose here is to examine the decline in water level in the area where recharge to the deep aquifer can occur, that is, in the area where the confining layer between the upper and lower aquifer units is non-existent, represented by column 1 to 50 in the model. The greatest decline in head is expected in this location.

Rch2=0, conservative variant

During the simulations it was observed that gradient and duration of the decline varies for the two aquifer units and depends on their location along the cross

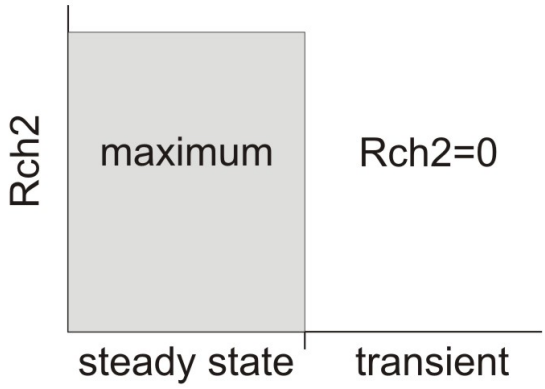

Figure 5.5: Schematic representation of a wet-dry scenario, assuming previous humid conditions with a maximum value for *Rch2* followed by a period where *Rch2*=0.

section. This is constrained in part by the boundary condition, *Rch1* in the south, which applies for the whole simulation, as well as by the constant head boundary as the discharge area in the far north. For the conservative variant, the major decline, defined as a change of more than 10 m $(\text{ka})^{-1}$, in the lower aquifer unit (*aqubot*), takes place in the first four thousand years, with the steepest decline (up to 35%) occurring in the first 2,000 years. After 8,000 years, the decline in the calculated groundwater levels was less then 1 m $(\text{ka})^{-1}$. Nearly steady-state conditions, fluctuations of less then 0.1 m $(\text{ka})^{-1}$, were reached after 13,000 years. Compared to the initial water levels, the simulated water levels at the end of the simulation were between 57 and 80 % of the starting values, with the greatest decline occurring in the central area of the aquifer. Figure 5.6 shows the simulated heads for the lower aquifer unit (*aqubot*) along the cross section. Water levels are shown for the beginning (blue line), after one (green), four (red) and seven (black) thousand years and finally for the end of the simulation (light blue). The dashed green line shows today's observed water levels. The graphs show that already after 1,000 years the groundwater levels in the unconfined zone should be below today's measured water levels. The black line, showing the water levels after the assumed length of the dry period (7,000 years) is close to the water levels at the end of the simulation (20,000 years) where near steady-state conditions are reached.

For the upper aquifer unit (*aqutop*) the major decline is complete after 5,000

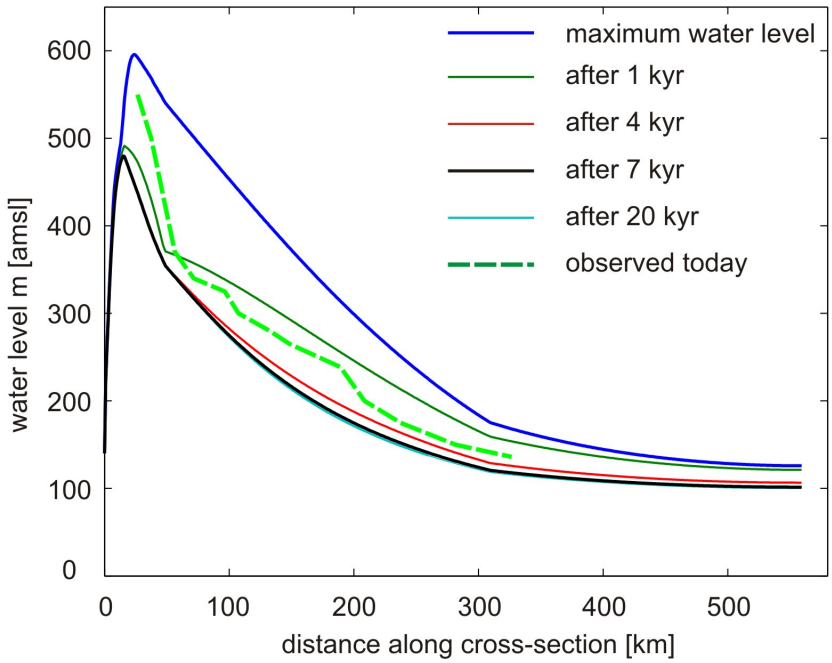

Figure 5.6: Simulated water levels for the conservative sceanrio for the lower aquifer unit. Groundwater level decrease over time can be observed for different time steps. After 1,000 years the water levels in the unconfined zone are below today's measured water levels.

years, a slower decline of 1 m $(\text{ka})^{-1}$ occurs after 10,000 years, and after 15,000 years, near steady-state conditions are attained. Analogous to *aqubot*, the steepest decline of up to 45% takes place in the first 2,000 years.

Rch2=0, best case variant

For the best case scenario, the situation is different in that the decline takes more time. For the confined aquifer, most of the decline has occurred by 7,000 years (up to 28%). Even after 100,000 years, however, the change in simulated water levels is at some places still more than 0.30 m. Compared to the initial water levels, the projected water levels at the end of the simulation are between 61 and 92% of the starting values. The nearly steady-state water levels of the conservative variant are not reached in the best case scenario within the simulation period of 100,000 years. Figure 5.7 shows the simulated heads for the lower aquifer unit and the line

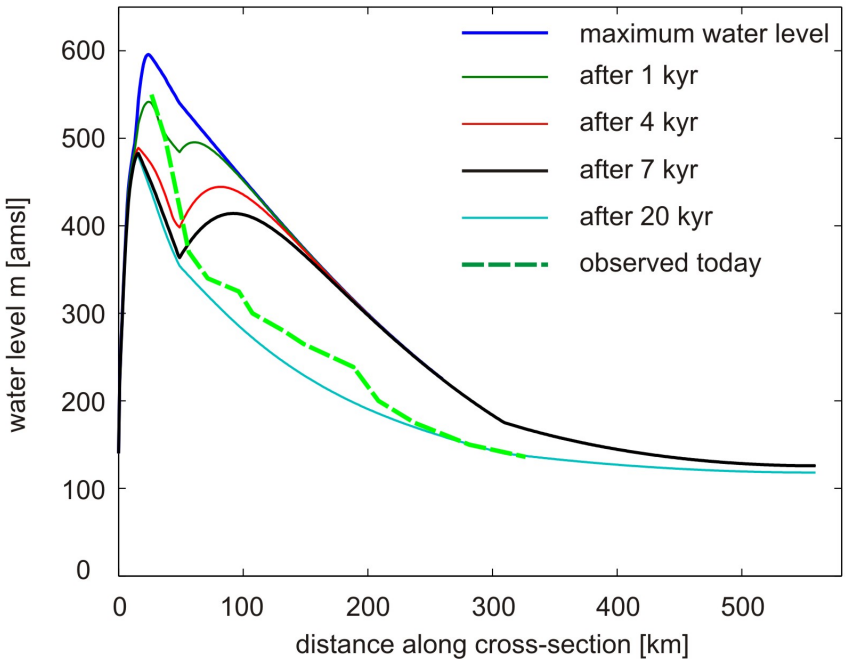

Figure 5.7: Simulated water levels for the best case scenario for the lower aquifer unit. Groundwater levels decrease over time, but the decline takes more time than in the conservative scenario (see Figure 5.6). Simulated water levels in the unconfined zone after 4,000 years are below today's measured water levels.

of observed water levels. But what is also evident is that after 4,000 years, the water levels in the unconfined zone are below today's observed water levels, and that the difference in water levels after 7,000 years and at the end of the simulation is small. Here too, near steady-state conditions in the unconfined area are already reached after 7,000 years. For the confined aquifer, changes up to 10 m $(\text{ka})^{-1}$ were calculated for the first nine thousand years, changes less then 0.10 m after 83,000 years. The final water levels are between 33 and 95% of the initial values.

Figure 5.7 shows peaks and a through of the simulated water levels after 1,000, 4,000 and 7,000 years. This spatial and timevarying behaviour of the simulated water levels will be investigated in further studies.

Results and discussion

Taking both variants as the upper and lower boundaries for possible head decline leads to the conclusion that today's observed heads cannot be remnants of the past, because in both cases the simulated heads (after a time period of 1,000 or 4,000 respectively - in both cases less time than since the last humid period) are below today's observed levels. Furthermore, this can be interpreted as evidence that modern recharge to the aquifers in the interior exists. The model results indicate also that monsoon recharge, which can contribute to the system in the north (as seen from the pathlines in the model calibration), is not sufficient for maintaining the observed groundwater levels.

In addition to the assumptions made in development of the conceptual model, further assumptions were also required to run the model for a time period for which no hard data were available. Thus, in the case of the transient simulation, the boundary condition recharge was variable, but the discharge conditions in the Sabkha, represented in the model by a constant head boundary, was constant throughout the simulation. This could represent an uncertainty, because higher or lower outflows at the sabkha are possible and could therefore change the flow through the system. For example, it is not known whether the groundwater system at the sabkha was ever connected to the sea. If that were the case, then lower sea levels may have resulted in different hydrogeologic conditions at the sabkha, which in turn would have changed the flow system. For the time period under investigation here, steady conditions were assumed for the sabkha.

In the model, zero recharge was assumed in the interior area. This simplification was made in order to evaluate how the system would behave without recharge in its interior. Several heavy rain events have been observed during the last 40 years within the study area, showing that even in dry periods, rain events take place and recharge might occur. So, many thousands of years without any recharge is unlikely, and the transient model results are consistent with this.

5.7 Validation by field data

All field activities that contributed to the present study were listed in section 3.2. As stated above, a primary aim of the measures was to observe possible fluctuation of the groundwater level as a result of influences by the monsoon or cyclonic events. The location of the wells where automated pressure transducers were installed is displayed in Figure 4.1 in chapter 4.

Cyclone Keila (see for example NASA (2011)) made it possible to observe the impacts of an cyclonic storm event on the deep groundwater aquifers in the Najd. Although up to date (November 2012) no hard data on rainfall or wadi flow are available for this event, it is ensured that in the time frame end of October/ beginning of November 2011 heavy rainfall, in some areas lasting up to 5 days, hit large parts of Oman and Yemen, including the Dhofar region with the Najd. As a result surface flow occurred in the wadi channels and much of the land was light green. Some of the remnants could be still observed during the field trip in January 2012: for example, open water bodies in the interior area approximately 200 km north to the Dhofar Mountains, or settled sludge in the wadi channels.

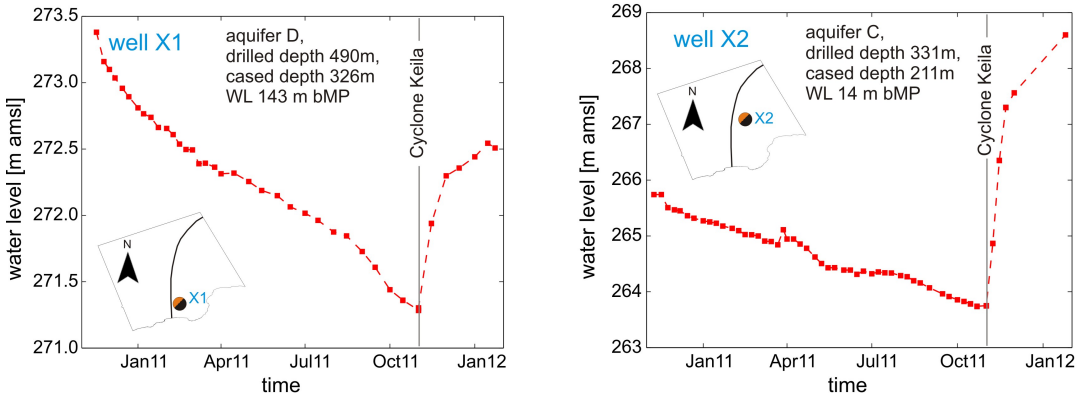

(a) Groundwater level vs time well X1

(b) Groundwater level vs time well X2

Figure 5.8: Increase in groundwater levels in two wells in the Najd as a result of the extrem rain event in November 2011 (Cyclone Keila).

The monitoring records of some of the installed pressure transducers also indicated that the deep groundwater had been impacted. Figure 5.8 shows this for two wells tapping into aquifer D (Figure 5.8(a)) and C (Figure 5.8(b)) in the Najd. The

groundwater monitoring records from November 2010 (installation) until January 2012 are plotted. Both records show an increase in the groundwater level with the beginning of November 2011. Well X1 (Figure 5.8(a)) is located approximately 50 km north to the surface water divide in the eastern Najd. Here the increase lasts until January 2012, and the total groundwater level rise over this period is 1.2 metres. Well X2 displayed in Figure 5.8(b) is located farther to the north, approximately 120 km away from the surface water divide. The increase in the groundwater level here amounts to more than 4 meters and was still ongoing when the wells were measured in January 2012.

These observation results confirm the modelling results of the 2D-groundwater flow model: modern recharge to the deep aquifers can take place under today's arid conditions in the Najd.

However, most of the other wells in aquifers C and D equipped with automated pressure transducers exhibit either no increase in groundwater levels, or they reflect pressure responses without significant rises in the groundwater levels. This can have different reasons: for example, regional rainfall could be limited or parallel pumping activities could have an influence. Another explanation could be that the wadi catchments show different characteristics. Some of them are vulnerable to an input to the deep groundwaters while others are not. A more detailed analysis of the impact of Cyclone Keila on the Najd groundwaters should be possible with data on rainfall and wadi flow.

An impact of the Monsoon on the groundwater levels in the Najd should be observable first at the monitoring wells in the Dhofar Mountains. Unfortunately, only one of the three wells equipped with pressure transducers in the Dhofar Mountains (see Figure 4.1) provides data, whereas the other two monitoring devices were out of function. The monitoring record for well X3, which is located on the surface water divide in the Dhofar Mountains, indicates that the Monsoon could also have an impact on the deep groundwater. Figure 5.9 shows an increase of the groundwater levels approximately 7 weeks after the beginning of the Monsoon. The increase is around 0.8 m and lasts for approximately 5 weeks. So far only monitoring data for the period 02/2011 until 01/2012 are available, covering only one Monsoon season. The observed groundwater level increase in well X3 should therefore be taken as a first indication. A longer monitoring record is necessary to provide a more meaningful analysis for a Monsoon impact on the deep groundwater.

Figure 5.9 also reveals that Cyclone Keila had no impact on the deep groundwater in the Dhofar Mountains.

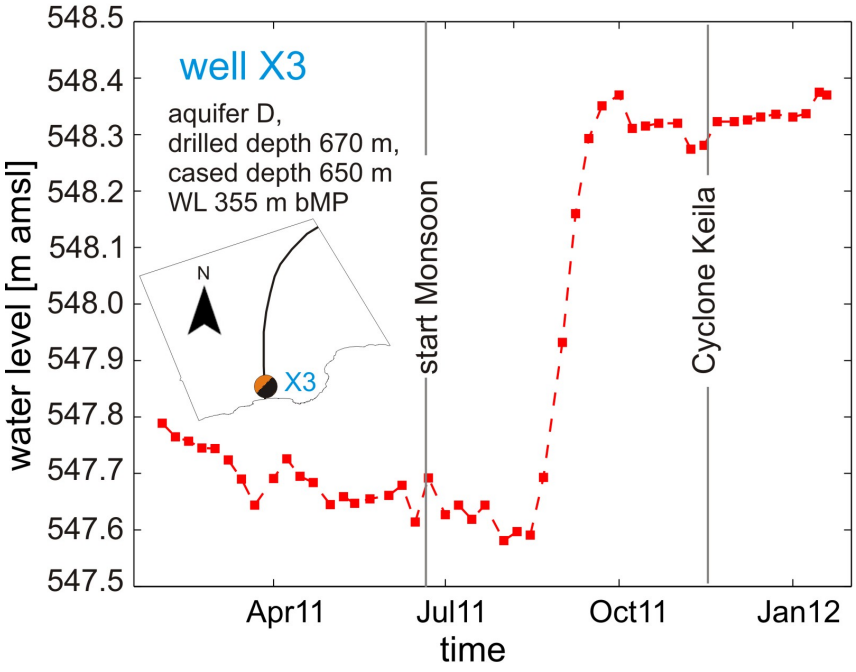

Figure 5.9: Increase in groundwater level in a well in the Dhofar Mountains.

5.8 Conclusions Groundwater model

The primary aims of the flow modelling were the evaluation of possible recharge scenarios and the estimation of the flow parameters. The developed groundwater flow model allows the study of these processes on a theoretical basis.

The model shows that recharge to the deep aquifers is possible. In the model both defined recharge areas, *Rch1* and *Rch2* contribute to groundwater recharge in the deep layers in the north.

The values for *Rch1* with 18 mm a^{-1} and *Rch2* with 4 mm a^{-1} lie in a reasonable range, given the climatic conditions in the study area.

The value of 4 mm a^{-1} for *Rch2* is sufficient to maintain today's groundwater levels.

The maximum recharge of 10 mm a^{-1} for *Rch2* obtained with the flow model is two to three times today's reacharge.

There is no definite answer to the question if a natural depletion of the groundwater levels is ongoing, neither by observations in the field nor by modelling. The model shows that changes in wet and dry periods, meaning more recharge or less recharge, can cause transient responses in heads and head gradients lasting for several thousand years.

What the model can provide is that the current water levels cannot be fossil gradients from past recharge, because the model simulations show that the water levels fall too quickly without modern recharge. In order to maintain the observed groundwater levels, groundwater recharge in the interior area must be assumed. This model application on fossil gradients illustrates how the model can be used in gaining a better understanding of the regional groundwater flow system in the Najd.

Groundwater level rises in the deep aquifers after cyclone Keila (November 2011) confirm the modelling result: modern recharge to the deep aquifers in the Najd takes place.

Chapter 6

Dating Dhofar groundwater

The evaluation of groundwater resources and management decisions concerning their exploitation strongly require an estimation of the time the groundwater has been in the system. This applies to the Dhofar groundwaters, where ages were estimated to evaluate whether the deep aquifer system is connected to an active flow system, which would allow for modern recharge (even at minor rate).

But what exactly is the age of the groundwater? In order to prevent misunderstandings, some theoretical background on the concept of groundwater age, and established common terminology[1] is provided first.

6.1 Theoretical background

6.1.1 The concept of groundwater age

In simple terms, the age of the groundwater is the timespan the water has spent in the groundwater system. Figure 6.1 i) schematically illustrates the trajectory of a single water particle in the ground. Water infiltrates the recharge area, moves downward until it reaches the saturated zone (a) and then moves with the groundwater flow (driven by the head difference). The water molecule leaves the system through the discharge well (b). Groundwater age is then defined by the time it takes for the water molecule to get from (a) to (b). This concept of groundwater age was, for instance, described by Goode (1996) and Glynn and Plummer (2005).

[1] Common terminology is bolded.

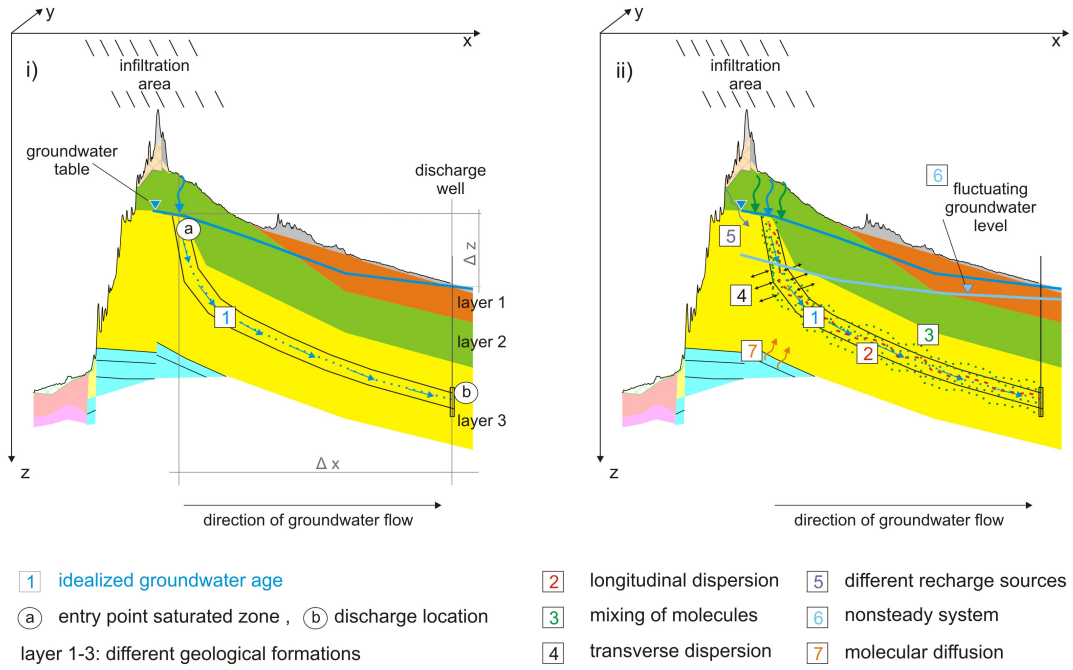

Figure 6.1: Concept of groundwater age, i) Idealized groundwater age for a single water molecule equals the travel time along an idealized flowpath (1) from (a) to (b). ii) General factors (2)-(7) affecting groundwater age, in most cases result in higher ages.

When assuming piston flow, i.e. that flow occurs strictly along an ideal single flowpath, no mixing occurs and flow is driven by a constant head gradient, the result would be an **idealized groundwater age**.

The term "age" seems to express a single value. Obviously, this understanding would only be an adequate characterization of the idealized groundwater age of a single water molecule. In nature, the amount of traveling water molecules is usually far greater, and, processes are exceedingly complex. This can be seen in Figure 6.1 ii). The main influences on groundwater ages are schematically depicted and marked by numbers. Most of them lead to higher groundwater ages (Torgersen et al. (2012, in preparation)). Longitudinal dispersion (2), different pathways (3), transverse dispersion with adjacent layers (4), different recharge sources - i.e. the monsoon and the cyclonic events that can impact the Dhofar groundwaters - (5), transient flow conditions (6) or molecular diffusion from aquitards (7) can affect the actual time each single water molecule spends in the system.

The water sampled at the well consists of many single molecules, which all have been affected by one, multiple or all of these processes. Since each water molecule has its own age, the groundwater sample represents a **frequency distribution of groundwater ages**.

Because the timespan during which the water has been in the system cannot be measured directly, different ways to calculate the groundwater age exist. In Chapter 5 it was shown that the groundwater flow can be described by the physics of fluid mass transport, which is one way to calculate the age of the groundwater. By knowing the differences in head (Δz), distance (Δx) and the aquifer parameters (hydraulic conductivity, porosity) a unique age for each location can be calculated. The so calculated ages are called **hydraulic ages**. If the groundwater model is used to calculate groundwater ages, the so calculated ages are **flow-model ages**.

Another way to estimate groundwater ages is to use environmental tracers, such as isotopes, i.e. the radioactive isotopes of carbon (^{14}C) and chlorine (^{36}Cl). Their abundance in the water is measured and interpreted in relation to the system's behaviour and to their radioactive decay characteristic. Age estimated using this method is generally referred to as **tracer-model age**, and, in case of ^{14}C, **^{14}C-model age**.

The age, for example for ^{14}C or ^{36}Cl calculated by the decay equation, gives an **apparent age**. This notion is used because the analysed water sample contains a mixture of water molecules with different origins, and the extent of mixing in the wells remains unknown.

6.1.2 Environmental tracer for groundwater dating

Dating groundwater via the use of environmental tracers can be done in two ways, referred to as "clock" and "signal" approach respectively (Glynn and Plummer, 2005). The "clock" approach requires knowledge or assumptions about the initial concentration, the tracer behaviour, e.g. its decay rate, and the processes, which control the transport. With these data and a measure of the tracer concentration, the ages can be calculated. In the present study, the "clocks" ^{14}C and ^{36}Cl[1] and ^{4}He, were used.

The "signal" approach relies on the assumption that an event occurred and left

[1] strictly speaking both have both characteristics.

a signal. Such signals can be anthropogenic in nature, e.g. caused by radionuclide signals from nuclear testing in the 1960's, or, as in Dhofar, they can stem from various sources of precipitation (e.g. monsoons, cyclones) with different isotopic concentrations of ^{18}O and ^{2}H due to isotope fractionation. The interpretation of recent signals, like the bomb tests or the Chernobyl accident, is easier because their point in time is known and their signal discrete. Interpreting signals over a longer stretch of time can be more difficult, because assumptions about previous conditions are required. For example, for the mentioned ^{18}O and ^{2}H signatures of the monsoon and cyclone, one has to consider, whether their past signatures were similarly distinguishable as today's. Here a combination with other information, e.g. the interpretation of stalagmite growth in caves from the same region and period, can reduce the uncertainty of one's assumptions.

As can be seen in Figure 6.2, in isotope hydrology a variety of tracers are at our disposal that allow for dating groundwater. The timescale represented by the X-axis shows that dating groundwater as old as a million years is possible.

The combination of different tracers can be particularly valuable. All tracers have their limitations. For instance, they might require initial values or they rely on previously detected sinks and sources in the subsurface.

These may again be based on other assumptions, since they were used to interpret measured concentrations. The use of multiple tracers can overcome some of these limitations. On the other hand, it also allows for cross-checking the estimates that other tracers use. Hence, multiple tracers enable us to assess the reliability of each single tracer. This procedure of reassurance was used in the present study.

The tracers scrutinized in the Dhofar groundwater study (2008-2012) were the isotopes ^{2}H, ^{18}O, ^{3}H, ^{14}C, ^{4}He and ^{36}Cl. Initially it was planned to use ^{3}H and ^{14}C for the estimation of the groundwater ages. However, ^{4}He was mainly used in a noble gas study, which focussed on the estimation of the temperature of noble gases. To overcome the partially contradicting results of the ^{14}C and ^{4}He interpretations, ^{36}Cl was sampled and analysed. This allowed us to cover almost the entire timescale presented in Figure 6.2.

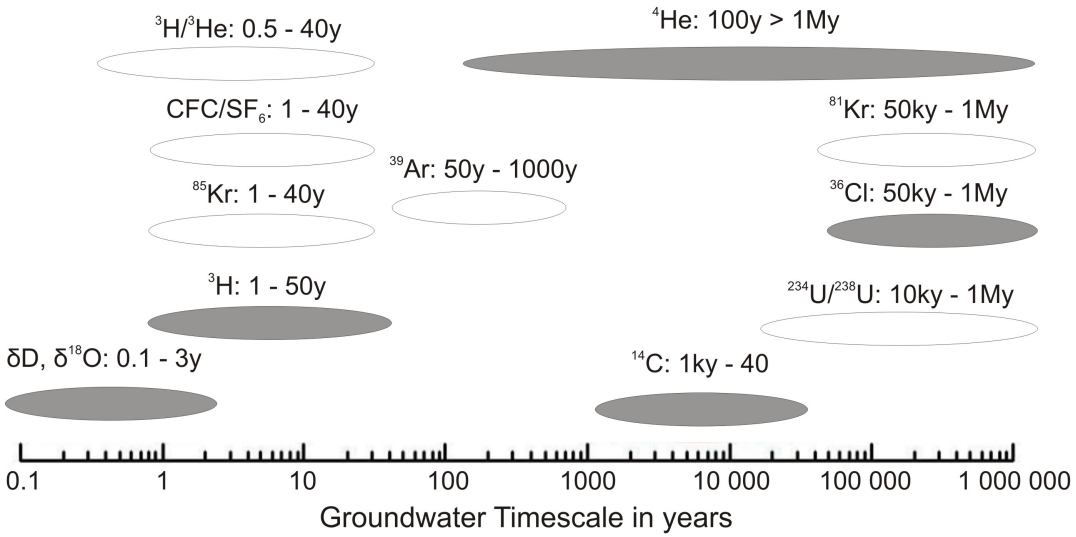

Figure 6.2: Tracers in Isotope Hydrology and their timescales (modified from Yokochi et al. (2012, in preparation)). Filled symbols mark the tracers used in the Dhofar Groundwater Study (2008-2012).

Radiocarbon dating

Radiocarbon dating of groundwater was introduced by Muennich (1957). Since then, numerous investigations, accompanied by advances in the analysis of ^{14}C, have taken place. Applications of ^{14}C dating, as well as conceptual ideas and problems in interpreting measured concentrations, are described in a great number of publications e.g. Fontes and Garnier (1979); Geyh (2005); Plummer and Glynn (2012, in preparation).

^{14}C is the heaviest of the three natural carbon isotopes (^{12}C, ^{13}C, ^{14}C), and the one with the least relative abundance. ^{12}C and ^{13}C, in contrast, comprise more than 99.9% of the relative abundance of carbon. Cosmogenic ^{14}C is produced in the upper atmosphere, when cosmic ray neutrons collide with the most abundant light nitrogen isotope ^{14}N:

$$^{14}_{7}N +^{1}_{0} n = \ ^{14}_{6}C +^{1}_{1} p \tag{6.1}$$

where n=neutron and p=proton.

Due to oxidation, $^{14}CO_2$ is formed, mixes with other atmospheric gases, and

becomes part of the biological cycle of the Earth through photosynthesis, and the hydrological cycle (through CO_2 exchange reactions). CO_2 dissolves into the groundwater by infiltrating rainwater. During this process, water, although containing some atmospheric $^{14}CO_2$ itself, gets the radiocarbon signal from the soil (where the CO_2 partial pressure is significantly higher, compared to the atmosphere). The soil is a huge reservoir for ^{14}C, because of degradation of dead biomass and respiration from roots. Along the flow through the soil and the aquifer to the discharge location, various chemical and physical processes alter the concentration of ^{14}C. The challenge in radiocarbon dating is to find out the input signal that the water got during the infiltration process, or, in other words, what the initial concentration was, and how to specify and quantify the impact of the main geochemical reactions, as well as physical processes that occurred along the flowpath.

While cosmogenic production is the source of the $^{14}CO_2$, the Earth's carbon reservoirs (oceans and plants), are the sinks for $^{14}CO_2$. Furthermore, ^{14}C is subject to radioactive decay, during which ^{14}C is reduced by beta decay, with a half-life of 5.730±40 years (Godwin, 1962). This decay rate serves as the base for radiocarbon dating and can be represented by the decay equation:

$$a_t = a_0 \cdot e^{-\lambda \cdot t} \tag{6.2}$$

Here, a_0 is the initial activity of the parent nuclide, a_t the activity after time t and λ is the decay constant.

While a_t is measurable, uncertainties remain about the initial concentration for the parent nuclide and its behaviour in the past and at the time of the infiltration of the water particle. On top of natural variation in ^{14}C concentration of the atmosphere, caused by geophysical effects, there is additional variation as a result of anthropogenic impacts, such as the testing of nuclear weapons. In calculating the time (a_t-a_0), these anthropogenic impacts are negligible, when it comes to groundwater which was recharged several thousand years ago. Natural variations, such as atmospheric ^{14}C concentrations having been up to 40 % higher during the last glacial maximum (Clark and Fritz, 1997), can distort radiocarbon dating. Other uncertainties regarding the initial ^{14}C values are, for example, plant-specific processes influencing the concentration of CO_2 in the soil, and climatic variations

resulting in changes of vegetation.

Dating based on the decay equation is only valid if one assumes a "closed" system. This means that no other processes than decay are affecting the concentration of ^{14}C. Unfortunately, in most cases, other processes (e.g. mixing of young and old water through hydrodynamic dispersion) and geochemical reactions (e.g. dissolution of limestone) in the soil and along the flowpath affect ^{14}C. This must be factored in when interpreting radiocarbon data.

The initial concentration of ^{14}C can be estimated by measuring the radiocarbon content of the groundwater in recharge areas, or via geochemical adjustment models e.g. (Fontes and Garnier, 1979; Ingerson and Pearson, 1964; Tamers, 1967; Vogel, 1967). Each of these models has its advantages and disadvantages, but none of them factors in redox reactions and mixing. This limits their application when dealing with geochemically evolved waters.

Today, the widely-used software NETPATH (Plummer et al., 1994) offers a way to account for mixing and geochemical reactions. It uses an inverse model that is able to define possible geochemical reactions of water along a flowpath.

Conventionally, the abbreviation pmC (percent modern carbon) describes the activity of modern carbon in groundwater samples, where pmC=$(A/A_{Ox})\times 100$ (Mook, 1980), with A as the measured activity and the standard activity A_{Ox}.

Groundwater dating with Helium

Helium (He) is one of the five noble gases (He, Ne, Ar, Kr, Xe) that has stable isotopes and occurs in the Earth's atmosphere. The unique properties of the noble gases namely that they are chemically inert, high volatile, and rare - have increasingly been the subject of research in the last 100 years. Due to their geochemical characteristics, noble gases are particularly qualified to act as trace elements, e.g. in the hydrogeosphere. Ozima and Podosek (2002) as well as Porcelli et al. (2002) give a comprehensive overview of noble gases, their characteristics, and their application in different subfields of geochemistry and cosmochemistry.

The equilibration of noble gases in water depends on the solubility of each element, and hence on the temperature, salinity and pressure of both, and the solvent. Henry's law (Henry, 1803) describes their solubility. Because it is temperature-dependent, one can derive its temperature at the time of equilibration from the

elemental ratios of the atmosphere-derived noble gases.

Among the noble gases, helium stands out, because it is the only gas that escapes from the terrestrial atmosphere (Mamyrin and Tolstikhin, 1984). It forms a flux from the Earth's interior, through the atmosphere and into space. In nature, it can be found everywhere: in natural gases (from which it is extracted for commercial use), geochemical fluids and solid materials. If not in direct contact with the atmosphere, as, for example, in groundwater, helium accumulates in fluid phases (Kipfer et al., 2002). Because of that, the concentration of stable helium isotopes ^{3}He and ^{4}He in the groundwater can be used to qualitatively date the water. ^{3}He in combination with ^{3}H allows for dating waters younger then 50 years, while ^{4}He, and the radiogenic helium $^4He_{rad}$ in particular, can be used for more ancient groundwaters up to the millenium time scale (Kipfer et al., 2002). The ^{3}He/^{4}He ratios can furthermore be used for the interpetation of the sources of the Helium, but also for the interpretation of the groundwater movement and ongoing mixing processes.

^{3}He and ^{4}He are decay products. ^{3}He is produced by β-decay. ^{4}He is produced by neutralisation of α-particles during the U and Th decay series. The reaction for ^{3}He is:

$$^6Li(n,\alpha)\ ^3H \longrightarrow\ ^3He \tag{6.3}$$

The number of ^{3}He atoms can be calculated according to Pearson et al. (1991):

$$N_3 = \rho \times [Li] \times \Phi \times t \times 6.12 \tag{6.4}$$

whereby N_3 is the number of ^{3}He atoms, ρ is the density of the aquifer matrix [g cm^{-3}], [Li] the decimal fraction of Lithium in rock, Φ the neutron flux in the rock matrix [n (cm^2 s)$^{-1}$] and t is the accumulation time [s]. According to Andrews et al. (1986) the neutron flux Φ (in n (cm^2 s)$^{-1}$)can be calculated with:

$$\Phi = 10^{-5}(a[U] + b[Th]) \tag{6.5}$$

where a and b are coefficients for the respective rock material.

^{4}He in groundwater can originate from:

- equilibration with soil air during infiltration - $^4He_{eq}$
- excess air - $^4He_{ex}$

- terrigenic $^4He_{ter}$, consisting of radiogenic helium produced in the aquifer and the Earth's crust $^4He_{rad}$ and a helium flux from the earth mantle ^4He_m

The concentration of ^{4}He in the atmosphere is constant up to an altitude of 100 km at a value of 5.239 ± 0.005 ppmv (Mamyrin and Tolstikhin, 1984). When, e.g. after a rain event, water infiltrates in the ground and passes the unsaturated zone, it equilibrates with soil air, and is replenished with atmospheric helium ($^4He_{eq}$). Because of the above-mentioned temperature dependency, $^4He_{eq}$ can be determined as long as the recharge temperature is known.

The amount of noble gases that equilibrates mainly depends on their temperature during infiltration, and on processes which produce a surplus of noble gases ('excess air') in groundwater. Excess air is produced from air bubbles entrapped in the unsaturated zone and fluctuating groundwater levels. As a result of high infiltration rates, the groundwater level can fluctuate (rise) and the increasing hydrostatic pressure can force entrapped air bubbles to dissolve. If the fluctuating groundwater levels are a result of the amount of infiltration (precipitation) and a good characterization of the excess air component ($^4He_{ex}$) is possible, it can be used as an indicator of past environmental conditions (Aeschbach-Hertig et al., 2001). The calculation of $^4He_{ex}$ is possible via different models, i.e. the unfractionated excess air model (Andrews and Lee, 1979) and the closed-system equilibration model (Aeschbach-Hertig et al., 2000).

Reaching the saturated zone, water is isolated from the atmosphere and can accumulate ^{4}He. Helium is produced in the aquifer sediments themselves ('in-situ'), by the α-decay of the $^{235.238}$U and ^{232}Th decay chains. In shallow aquifers, this could be the helium released by weathering of sediments (Solomon et al., 1996). Its production is directly proportional to the concentration of the radioelements U and Th in the sediments of the aquifer. From the sediments of the aquifer, the produced helium is delivered to the pores, and thereupon captured by the water. Helium is also produced in-situ in aquitards above and below the aquifers. From there it leaks into and mixes with the aquifer and thus changes its helium concentration.

A large 'external' helium reservoir is constituted by the $^4He_{rad}$ found in the earth crust and the ^4He_m, found in the earth mantle. From there, helium can transfer to the aquifer by diffusion, advection and dispersion. In most cases, helium

quantities gained from these outside sources, which accumulate in the aquifer, exceed those expected from in-situ production.

Different helium reservoirs can be distinguished by their $^3He/^4He$ ratio. When plotted in the so-called isotope plot ($^3He/^4He$ over the Ne/He ratio), the different components can be separated. Benson and Krause (1980) stated that the $^3He/^4He$ ratio is 1.36×10^{-6} for helium dissolved from the atmosphere, while a typical value for the $^3He/^4He$ ratio of crustal helium is 2×10^{-8} (Mamyrin and Tolstikhin, 1984). For the mantle component on the other hand, the $^3He/^4He$ ratio is around 10^{-5} (Ozima and Podosek, 2002).

In-situ ^{4}He production (P_4)

The simplest approach for using helium for dating would be to assume that all the helium in the aquifer originates from in-situ production. In a closed system where the only source of ^4He is the decay of ^{238}U, ^{235}U and ^{232}Th the in-situ production can be calculated as stated by Andrews (1985):

$$N_4 = t \times \rho \times N\{8[U]\times \\ [^{238}U](\lambda_{238}/M_{238}) + 7[U] \times [^{235}U](\lambda_{235}/M_{235}) + 6[Th] \times [^{232}Th](\lambda_{232}/M_{232})\} \tag{6.6}$$

whereby N_4 is the in-situ production of ^4He per matrix volume [atoms cm^{-3}], t the accumulation time [s], ρ the density of the aquifer matrix [g cm^{-3}], N Avogadro's Constant [6.022×10^{23} atoms mol^{-1}], 8,7,6 the number of α-particles released in the corresponding decay chain, $\lambda_{238,235,232}$ the decay constants for ^{238}U, ^{235}U and ^{232}Th ($4.92\times10^{-18}s^{-1}$, $3.12\times10^{-17}s^{-1}$ and $1.57\times10^{-18}s^{-1}$), $M_{238,235,232}$ the molecular weights [g mol^{-1}], [U] and [Th] the decimal fraction in the rock [g g^{-1}] and [^{238}U], [^{235}U] as well as [^{232}Th] the decimal fraction of the isotope in the entire uran and thorium concentration.

Via the conversion factor c (1.17×10^{-12}) the in-situ production N_4 [atoms cm^{-3}] is converted to the production rate P_4 [cm^3 STP cm^{-3} rock a^{-1}]:

$$P_4 = c \times \rho \times (0.103 \times [U] + 0.1245 \times [Th]) \tag{6.7}$$

If the production rate in the host rock equals the release rate of ^4He in the

groundwater (release factor $\Delta = 1$), the ^{4}He release R_4 can be calculated via

$$R_4 = \Delta \times c \times \rho \times (0.103 \times [U] + 0.1245 \times [Th]) \tag{6.8}$$

We measure the accumulation of helium in the groundwater, therefore the ^{4}He accumulation rate A_4 [cm^3 STP $g_{H_2O}^{-1}$ s^{-1}] has to be calculated, taking into account aquifer porosity (ϕ) and density of the water (ρ_{H_2O}). This can be achieved by using the following equation (Torgersen, 1980):

$$A_4 = R_4 \frac{(1-\phi)}{\phi} \frac{1}{\rho_{H_2O}} \tag{6.9}$$

Under the assumption that ^{4}He is only produced in-situ in the aquifer and the accumulation rate is known the groundwater age (τ) is calculated as follows:

$$\tau = \frac{[^4He]}{A_4} \tag{6.10}$$

Previous studies showed that groundwater ages calculated solely on in-situ production, overestimate the mean residence times of the groundwater. Hence sources outside the aquifer should be taken into account when assessing measured concentrations of non-atmospheric helium (Solomon et al., 1996; Torgersen and Clarke, 1985). Furthermore these studies reveal that the influence of the various sources changes along the groundwater flow path, with dominating in-situ production close to or in the recharge area, and dominating external sources in the more distant areas (Blaser, 2007; Torgersen and Clarke, 1985; Torgersen and Ivey, 1985).

Crustal ^{4}He flux F'

Torgersen and Clarke (1985) calculated the production in the earth crust by using equations 6.7 and 6.8, multiplied by the thickness of the upper crust.

Torgersen and Ivey (1985) show that, when the main components for $^4He_{rad}$ are in situ production (short distances) and crustal $^4He_{rad}$ degassing flux (long distances), the $^4He_{rad}$ distribution in the aquifer is calculated as follows: Under the assumptions that:

- there are steady state conditions in the aquifer
- the initial concentration of ^{4}He for all depths is zero

- ^{4}He flux out of the top of the aquifer is zero
- ^{4}He flux across the bottom of the aquifer is constant
- the vertical diffusion coefficient for ^{4}He in the aquifer is constant

the ^{4}He-concentrations, as a function of distance (x) and depth (z), can be derived with:

$$^4He_{x,z} = \left(\frac{P_4}{V}\right) x + \left(\frac{F'}{V}\right) \left[\frac{x}{h} + \left(\frac{hV}{K_a}\right)\left\{\frac{3z^2 - h^2}{6h^2} - \frac{2}{\pi^2}\sum_{n=1}^{\infty}\frac{(-1)^n}{n^2}\exp^{-K_a n^2\pi^2 x/hV}\cos\frac{n\pi z}{h}\right\}\right] \tag{6.11}$$

where V represents flow velocity, F' (=F/ϕ) the ^{4}He flux into the aquifer water, h aquifer thickness, z vertical position in the aquifer (measured from the top of the aquifer) and K_a the effective diffusive coefficient for ^{4}He. Since the external source, the ^{4}He crustal flux, is entering the aquifer from below, the highest concentration will occur at the bottom of the aquifer, with decreasing concentrations towards the top.

Figure 6.3 shows the general evolution of $^4He_{rad}$ over time and for different depths. Parameters were taken from Torgersen and Clarke (1985). We observe that the accumulation of $^4He_{rad}$ increases with time across all depths. In-situ production alone (first term in Equation 6.11) will result in the lowest values for the accumulation of $^4He_{rad}$. Since in-situ production is independent from the vertical location in the aquifer, the evolution curves for all depths plot on the same line.

Chlorine-36 Dating

The radioactive isotope ^{36}Cl is used for dating very old groundwater, because of its long half life of 301 000 $\pm$ 4000 years. ^{36}Cl is produced in the upper stratosphere when argon interacts with cosmic radiation. The atmospheric production of ^{36}Cl depends on the geomagnetic latitude. High production rates occur near the poles, while low rates occur near the equator. The fallout on Earth depends on the stratosphere-troposphere mixing and is highest at around 40° latitude.

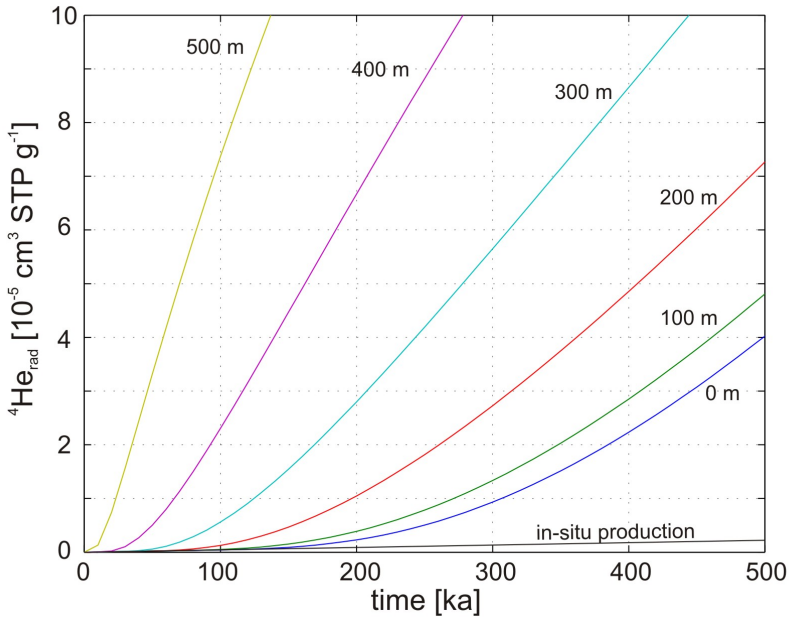

Figure 6.3: $^4He_{rad}$ accumulation over time for different depths in the aquifer (0 to 500 m) according to Torgersen and Ivey (1985). $^4He_{rad}$ increases with time.

The cosmic radiation has varied with time due to geomagnetic field intensity - and so has the cosmogenic production of ^{36}Cl. Although the impacts of these fluctuations on the initial ^{36}Cl concentration have not been verified yet (Phillips, 2012, in preparation), one has to be aware that these fluctuations may have led to different input signals of ^{36}Cl over time.

The main decay cycle (98%) leads to ^{36}Ar. ^{36}Cl is transported from the stratosphere into the troposphere, where the residence time is short - usually within few weeks. The meteoric ^{36}Cl mixes with the atmospheric chloride Cl^- (from the ocean) and reaches the surface on the Earth via rain and snow, or as dry deposit. Near the coast the ratio of ^{36}Cl and Cl^- is low, but, with increasing distance to the oceans, this ratio increases.

Through infiltrating water, ^{36}Cl and Cl^- is carried into the ground. With the water, the atoms move through the soil and the unsaturated zone and, when reaching the saturated zone, are transported by the flowing groundwater. The structure and thickness of the sediments in the vadose zone can be of importance, especially in sediments with high permeability fractures, but a low permeability

matrix. While in the matrix solutes can be retained for hundreds or even thousands of years, the fractures permit the water to be rapidly transmitted to the saturated zone (Phillips, 2012, in preparation). The input signal at the land surface is therefore not necessarily equal to the signal which reaches the groundwater.

The decay of ^{36}Cl takes place with increasing distance from the infiltration area, or, in other words, increasing age. When no other ^{36}Cl sources and sinks exist, the time the water has been in the system can be calculated from the difference between initial and sampled concentration, and the use of the radiometric decay equation. Similar to equation 6.2 where the activity a_t was calculated, N_t the number of nuclei after time t is calculated as:

$$N_t = N_o \cdot e^{-\lambda \cdot t} \tag{6.12}$$

Here, N_o is the initial number of nuclei in the sample and λ is the decay constant for the nuclei (here ^{36}Cl).

In nature, the situation is much more complicated. Uncertainties exist, for example, with respect to the input signal of ^{36}Cl and Cl^- in space and time, including the cosmogenic production and deposition on the land surface. Davis et al. (1998) discuss six methods which are commonly used to determine initial ^{36}Cl values: (i) the calculation of the theoretical cosmogenic production and fallout according to latitude, (ii) the measurement of ^{36}Cl in precipitation and assuming that anthropogenic influences are of minor importance, (iii) assuming that shallow groundwater represents pre-anthropogenic ^{36}Cl concentrations, (iv) the abstraction and sampling from vertical depth profil's in desert soils, (v) the analysis of ^{36}Cl in glacial ice cores and (vi), the subsurface production of ^{36}Cl.

More uncertainties arise from the transport into and through the unsaturated zone. The residence times in the unsaturated zone can be quite long, depending, for example, on the rock matrix and the amount of the infiltrating water (intensity of the rain event).

Furthermore, ^{36}Cl can be produced in the ground in the upper meters of the Earth's crust, under the impact of cosmic radiation (epigene production), or in the deep ground, as the result of the reaction of ^{35}Cl with thermal neutrons (hypogene production).

A man-made source of ^{36}Cl are nuclear weapons tests with fallouts 2 to 3 times

above the natural production rate (Bentley et al., 1982).

^{36}Cl/Cl ratios are measured by accelerator mass spectrometry (AMS). Information on the tandem accelerator, the sample preparation, background levels and the measurement itself are described by Akhmadaliev et al. (2012).

Atmospheric deposition and ^{36}Cl in recharge

The annual deposition (dep) of Cl onto the land surface can be calculated with:

$$dep = P \times C_p \tag{6.13}$$

Here, P is the annual precipitation and C_p is the average chloride concentration in precipitation. Multiplying the deposition of Cl (in atoms m^{-2} s^{-1}) with the initial ^{36}Cl/Cl ratio, the ^{36}Cl flux (in atoms m^{-2} s^{-1}) to the land surface can be calculated.

Today's global atmospheric production rate of ^{36}Cl is between 20 to 30 atoms m^{-2} s^{-1}. Beer et al. (1999), for example, give 24 m^{-2} s^{-1}. Figure 6.4 shows the relation between latitude and ^{36}Cl deposition. Three curves are displayed: Curve *a*) represents the results of first calculations by Lal and Peters (1968). Curve *b*) shows normalized deposition rates calculated via the mean latitudinal precipitation - see, for example, Parrat et al. (1996). Curve *c*) is closest to the observed ^{36}Cl deposition rates of 26 monitoring stations in Australia and the United States. Curve *c*) is approximately 1.47 times Curve *b*), indicating that theoretical predictions underestimate actual ^{36}Cl deposition (Phillips, 2000).

Pearson et al. (1991), for example, showed how to calculate ^{36}Cl produced by cosmic ray in shallow groundwaters:

$$N_{36} = 3.2 \times 10^7 \times \frac{F \times 100}{P \times (100 - E)} \tag{6.14}$$

Here, N_{36} is the number of ^{36}Cl atoms l^{-1}, F is the fallout rate in atoms $m^{-2}s^{-1}$, P is the annual precipitation in mm a^{-1} and E is the evapotranspiration in %.

Subsurface processes

^{36}Cl is also produced in the upper meters of the earth crust (epigene production), when ^{35}Cl, ^{39}K and ^{40}Ca are activated by cosmic radiation. Other processes that

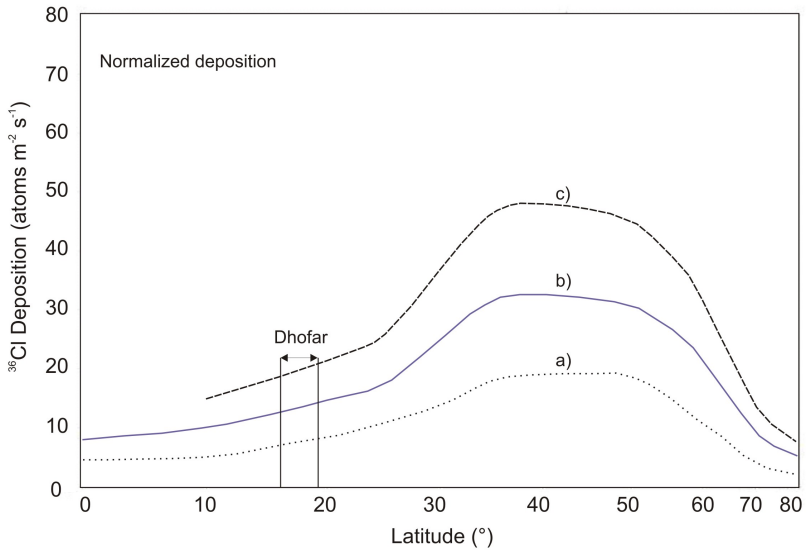

Figure 6.4: ^{36}Cl Deposition as a function of latitude. Curve *a*) ^{36}Cl deposition according to Lal and Peters (1968). Curve *b*) normalised deposition corrected for annual precipitation according to Parrat et al. (1996). Curve *c*) deposition curve closest to the observed values; it is approximately 1.47 times Curve *b*). The Dhofar area lies between 17° and 20° latitude. Figure adopted and modified from Phillips (2000).

induce the production of ^{36}Cl are the alpha decay of ^{40}Ca and the neutron activation of ^{35}Cl. The so produced ^{36}Cl can be released to the aquifer by weathering of the host rock. Although exceptions can exist, many studies agree that the near subsurface production of ^{36}Cl is probably minor compared to the atmospheric ^{36}Cl input (Bentley et al., 1986; Davis et al., 1998; Pearson et al., 1991; Phillips, 2000).

However, the effects of weathering can be significant when, for example, the host rock is limestone. This material has a high concentration of Calcium and weathers rapidly. Weathering also has significant impact when the area under investigation is located at higher elevations. At sea level the contribution of weathering of ^{36}Cl can be $\sim$ 10% of the atmospheric flux. At high elevations (above 2000 m) and close to the equator, where atmospheric deposition rates are low, the release of weathering ^{36}Cl can be above the atmospheric flux. Phillips (2012, in preparation), for example, states that amounts above 200 % (compared to the atmospheric deposition) are possible.

Deep subsurface production (hypogene production) of ^{36}Cl is mainly the result of the thermal-neutron absorption reaction of ^{35}Cl(n,γ)^{36}Cl. Groundwater containing Cl^- and undergoing a neutron flux will produce ^{36}Cl. Neutrons are produced in the subsurface by the spontaneous fission of uranium atoms. Furthermore light elements produce neutrons when they absorb α particles which are released during the decay of uranium-series nuclides. The production of neutrons depends on the concentration of uranium and thorium and light elements in the rock matrix.

The subsurface production is usually expressed as a ratio of ^{36}Cl to stable chlorine. This ratio at equilibrium with the subsurface neutron flux, is called the secular equilibrium (R_{36}) and increases with time. According to Pearson et al. (1991) it can be calculated with:

$$R_{36}(t) = 4.55 \cdot 10^{-10} \cdot \Phi \cdot (1 - e^{-\tau t}) \tag{6.15}$$

Here, Φ is the neutron flux in the rock matrix [n $(cm^2\ s)^{-1}$] (see equation 6.5) and τ is the ^{36}Cl decay constant ($7.3 \times 10^{-14} s^{-1}$). Pearson et al. (1991) gives about 1.5 My for the time until equilibrum is established.

Dating of groundwater by ^{36}Cl decay

Bentley et al. (1986) and Phillips et al. (1986) were the first who demonstrated how to calculate groundwater ages by the use of ^{36}Cl decay dating. Based on the mass balance of ^{36}Cl in the subsurface, the concentrations of ^{36}Cl, Cl and ^{36}Cl/Cl and their variations are interpreted.

Assuming meteoric input as the only source for ^{36}Cl, decay as the only sink, and no sinks and sources for chlorine in the subsurface, the residence time of the groundwater can be calculated with (Bentley et al., 1986):

$$t = \frac{-1}{\lambda_{36}} \ln \frac{R - R_{se}}{R_o - R_{se}} \tag{6.16}$$

Here, R is the measured ^{36}Cl/Cl ratio, R_o the initial ^{36}Cl/Cl ratio, and R_{se} the above-mentioned secular equilibrum ^{36}Cl/Cl ratio due to hypogene production.

Quite often sources for the addition of chloride in the subsurface exist. This could be, for example pore water from adjacent aquitards or inputs from neighbouring leaking aquifers. Assuming that the "extra" chloride is in equilibrum with

the aquifer, the second term of Equation 6.16 is extended by the ratio of C - as the sampled concentration of chloride, and C_o - as the concentration of chloride in recharge (see Equation 6.17).

$$t = \frac{-1}{\lambda_{36}} \ln \frac{C(R - R_{se})}{C_o(R_o - R_{se})} \tag{6.17}$$

Further evolutions for Equation 6.16 were developed for different scenarios, e.g. the additional chloride being a result of the dissolution of evaporites, or chloride coming from a brine source with a different secular equilibrum than the aquifer water. For more information see the works cited above or Phillips (2012, in preparation) for example.

6.1.3 Dating of groundwater and numerical modeling

Groundwater residence times or groundwater ages are not a measurable quantity. As previously explained the estimated ages are interpretations of the measured concentrations. There are two ways to include them in the modeling process: by using the measured tracer concentrations or by including apparent ages (interpretations of the measured tracer concentrations). Using tracer concentration makes it possible to include tracer specific processes, using apparent ages can be useful when time dependent processes (e.g. decay rates) are under investigation (Newman et al., 2010).

Three methods are common when groundwater ages are incorporated in the groundwater flow modeling process: direct simulation of groundwater age (Goode, 1996) where advection and dispersion are included and the groundwater age is simulated as the concentration of a solute age; models taking advection, diffusion, dispersion and radioactive decay in account (called breakthrough of a block-front model in Visser (2009)) or reactive transport models (for example Bethke et al. (2000)); and particle tracking where advective flow along a flow path is used (for example Izbicki et al. (2004)). The literature offers quite a few studies on groundwater residence times in combination with groundwater flow modeling, and the interested reader is referred to Castro et al. (2005); Sanford et al. (2004); Zhu (2000).

In the present study particle tracking was used. The reasons were (i) to start with a simple approach and (ii) the available data. (i) was explained before (see

chapter 5. Once the "simple" approach of advective flow is understood, processes influencing the tracer concentration, like diffusion or dispersion, could still be incorporated and their effect for the Dhofar groundwaters could be evaluated. (ii) The available data are, however, inappropriate for interpreting them beyond advective transport. The sections below will clarify this point. Nevertheless, Sanford and Pope (2010) showed that advective age simulation can still be quite valuable when interpreting groundwater flow.

In the present study the apparent groundwater ages were incorporated in the modeling process by using MODPATH (Pollock, 1994), which is a pathline post-processing program. Using pathlines for the age calculation is an extension of the above-mentioned hydraulic age estimation, where the distance (Δx) between two points was a straight line, and was divided by the interstitial velocity (Δh, k_f, n). MODPATH calculates pathlines that a fictional water particle would travel across the aquifer, therefore the distance between two points is no longer a straight line.

MODPATH was designed to work with MODFLOW (Harbaugh, 2005) which is a finite difference groundwater model with rectangular model cells. Velocities at the cell boundaries can be calculated at the cell nodes using Darcy's law. With help of the velocities at the cell boundaries the travel time (Δt) of a particle of water across a finite-difference cell is calculated for the x- and in the y-direction. The shorter time (Δt_x or Δt_y) is the time the particle travels to the cell wall and exits the cell. The exit point is then calculated and equals the entrance point of the neighbouring cell. More details on the assumptions and theory are reported by (Pollock, 1994). The advantage of particle tracking is that it is quick. However, the disadvantage is that only advective path lines can be calculated. Weak sink cells could be another drawback of particle tracking. Sink cells in the groundwater flow model are the cells where abstraction wells or drainage features are defined, they are specified as "weak" when they do not capture all the water flowing within the cell. The resulting problem is that it is undefined whether the particle entering the cell is passing the cell, or is discharged. In the model used in the present study no sink cells are defined, so this drawback can be neglected. The calculation of the travel time of a particle can be forward, where the particle starts from the water table and travels to the discharge cell, or backward, where the particle starts at the well location and travels to the recharge location. The latter calculation was used in the present study.

6.2 Data base of Dhofar groundwaters

The data used in the present study consist of two sampling campaigns. In November of 2009, 34 wells were sampled for ^{14}C, and 25 wells for noble gases, including helium. In January of 2012, 10 wells were sampled for the analysis of Chlorine-36. The locations of the sampled wells are shown in Figure 6.5. The present study focuses on the wells that are located close to the modeled cross-section (Chapter 5).

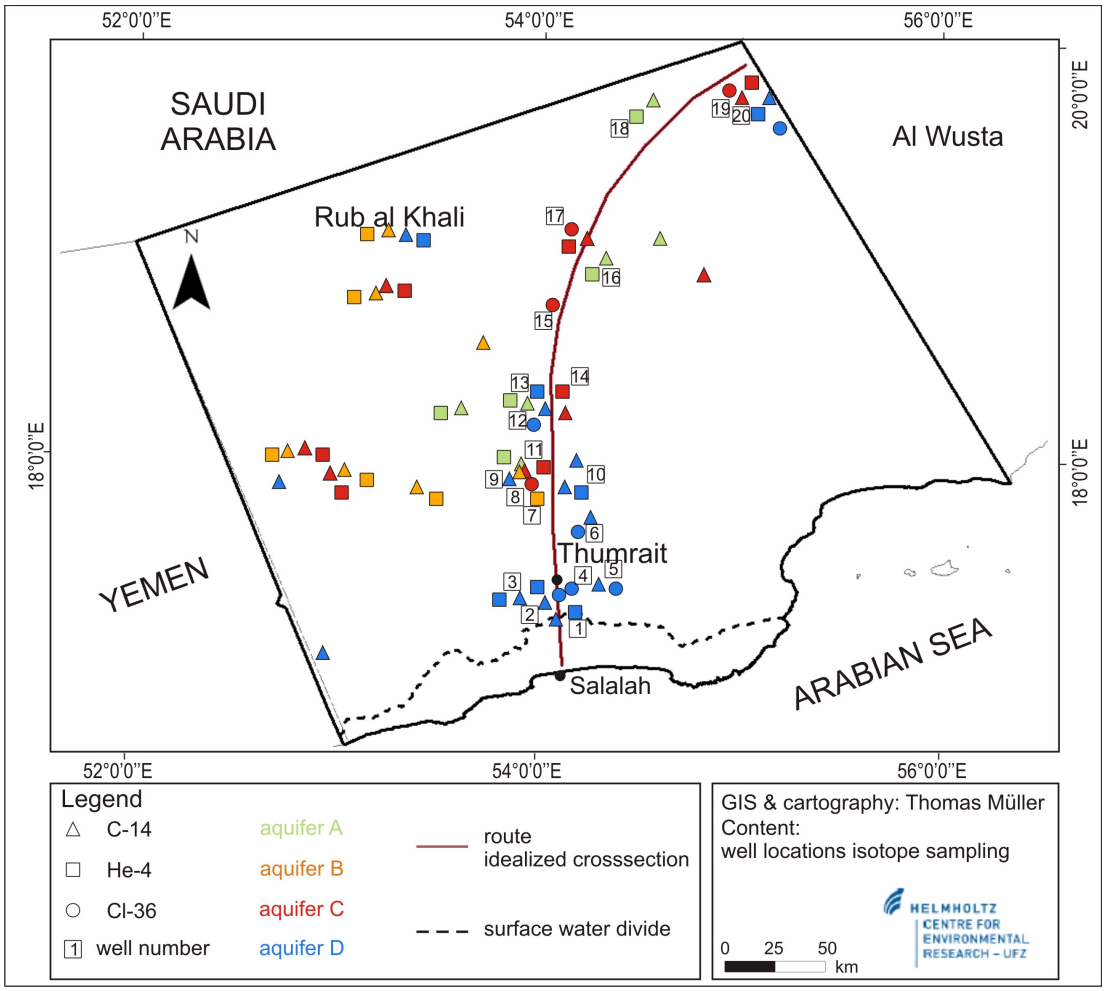

Figure 6.5: Well locations for isotope sampling in the Dhofar area. Different colors indicate the aquifers from which the water was sampled.

In total 20 wells were used in the analysis. Four wells in aquifer A, one in aquifer B, 5 in aquifer C and 10 wells in aquifer D. The main interest lies on the

deep aquifers C and D. The distribution of the wells along the cross-section is shown in Figure 6.6. Location, drilled depth and length of the casing are shown schematically. For some wells data on their construction were unavailable. For example, we neither have information on drilled depth and casing of well 11 and 14, nor on cased depth of well 1 and well 10.

Table 6.1 summarizes the main facts about the sampled wells. The column named "well type" specifies whether the well is pumped regularly (p), is used for observation only (o), or is artesian (a). Data for drilled and cased depth were obtained from the drilling logs. The column called "distance" indicates the distance of the well from the surface water divide in the Dhofar Mountains. Today's recharge area for aquifers C and D stretches form the surface water divide approximately 50 km in northern direction. No distances are given for the wells in aquifers A and B. This is partly due to their local distribution, but also due to the fact that the recharge area for A and B could potentially be located anywhere in the distribution area of the aquifers.

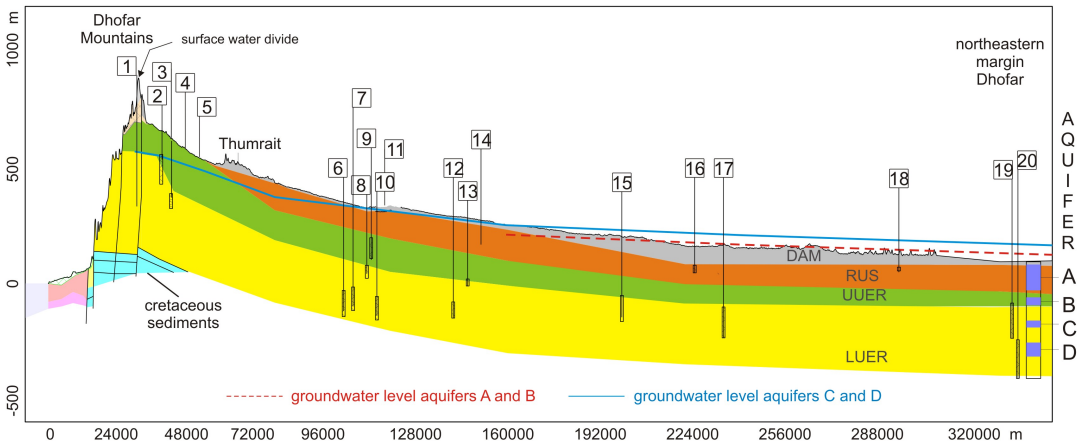

Figure 6.6: Schematic cross-section including the location of the sampled wells during campaigns 2009 and 2012. Numbers assigned to the wells used in the present study (see also Table 6.1). Drilled and cased depth are schematically shown. Vertical exaggeration: 80x

Table 6.1: Information on the sampled wells: number, aquifer, well type and data on the well development for the sampled wells along the principal cross-section (see Figure 6.6 including measured concentrations for ^{14}C, He and Ne (sampling campaign 2009), and for $^{36}Cl/^{35}Cl$ (sampling campaign 2012).

Well	Aqu.	well type[a]	drilled depth [m]	cased depth [m]	distance [km][b]	sampl. date	^{14}C[c] pmC (%)	±err pmC (%)	He[d] ×10E-6 [ccSTP/g]	err He ×10E-9 [ccSTP/g]	Ne ×10E-7 [ccSTP/g]	err Ne ×10E-9 [ccSTP/g]	$^{36}Cl/^{35}Cl$ ×10E-15 [at at^{-1}]	err $^{36}Cl/^{35}Cl$ (%)	Cl [mg l^{-1}]
1	D	p	500	(-)[e]	0	17.11.2009	22.8	0.5	0.122	1.22	2.76	1.38			
2	D	p	229	106	10	17.11.2009	18.0	0.3	0.129	1.29	2.17	1.08			
2	D	p	229	106	10	28.01.2012							29.6	31.74	426
3	D	p	300	220	17	17.11.2009	3.2	0.5	0.179	1.79	2.01	1.01			
4	D	o	260	139	18	23.01.2012							15.7	40.1	1073
5	D	o	330	150	20	24.01.2012							33.1	31.38	394
6	D	p	550	372	67	16.11.2009	5.7	0.8	5.66	56.66	2.93	1.47			
6	D	p	550	372	67	25.01.2012							6.8	68.13	447
7	D	o	550	280	80	16.11.2009	14.4	0.3							
8	C	o	286	230	83	17.11.2009	7.7	0.3	2.59	25.90	2.13	1.06			
8	C	o	286	230	83	25.01.2012							28.0	31.15	536
9	B	p	200	116	( )[f]	18.11.2009	3.3	0.3	2.04	20.40	2.15	1.08			
10	D	o	553	(-)	81	02.05.2009	52.8	(-)[g]							
11	A	p	(-)	(-)	( )	16.11.2009	28.1	0.8	0.0758	0.758	1.96	0.98			
12	D	o	430	360	110	13.11.2009	44.7	0.3	2.37	37.4	1.93	0.966			
12	D	p	430	360	110	13.11.2009							8.5	54.32	296
13	C	p	291	260	110	18.11.2009	5.2	0.5	4.00	40.00	2.39	1.20			
14	A	p	(-)	(-)	( )	13.11.2009	45.6	1.6	0.0623	0.623	1.86	0.929			
15	C	a	360	300	180	24.01.2012							17.3	41.30	273
16	A	o	163	115	( )	14.11.2009	15.8	0.3	0.046	0.468	1.74	0.86			
17	C	a	378	244	210	14.11.2009	10.4	0.3	14.5	318.00	2.46	1.23			
17	C	a	378	244	210	24.01.2012							9.8	50.91	307
18	A	o	118	63	( )	14.11.2009	9.9	0.3	0.0504	0.504	1.81	0.907			
19	C	a	332	179	330	15.11.2009	5.6	0.3	29.00	290.00	1.88	0.939			
19	C	a	332	179	330	24.01.2012							1.2	104.65	2489
20	D	a	506	338	330	15.11.2009	5.3	0.3	25.80	258.00	1.79	0.896			
20	D	a	506	338	330	24.01.2012							6.2	60.11	5245

[a] o - observation, p - pumped, a -artesian; [b] distance to recharge area; [c] sampling and analysis see Al-Mashaikhi (2011); [d] sampling and analysis noble gases see (Herb, 2011); [e] well construction unknown; [f] no recharge area given because of local distribution of aquifer A and B; [g] no error given by Al-Mashaikhi

In the following, more details on the sampled wells are provided. In general the pumped wells are running regularly. Since no monitoring for pumped water takes place, their different use might give an impression of the discharged quantities.

Well 1 and **3** are water supply wells for nearby villages. They are regularly used to fill tanks from where water is distributed.

Well 2 is situated on an agricultural farm and runs daily, although the hours of operation are unknown. In spite of the well being fully functional and the farm still running, the well has been idle since November 2011. Hence other wells must exist nearby.

Well 6 is installed on a chicken farm. According to the responsible personnel, its discharge lies between 28 and 35 m^3 h^{-1} when the well runs for 8 to 10 hours per day. At least two other wells (39 m^3 h^{-1}, 45 m^3 h^{-1}) that also run daily 8 to 10 hours have been operated since about 2004. With 9000 m^3 per month, an overall abstraction of circa 230 000 m^3 for the time span from November 2009 (sampling 1) to January 2012 (sampling 2) was calculated. Adding the two other known wells on the farm (with approximately the same production), results in an overall abstraction of 700,000 to 800,000 m^3 for the time span between the two samplings.

Wells 7, 8, 9 and **10** are observation wells. Even though they are not being pumped, they are located in close vicinity of large farm areas and thus within the reach of the cone of depression.

Well 11 and **14** are shallow wells located on intensively used agricultural farm areas. These wells are run daily, but their hours of operation are unknown.

Well 12 was drilled in 2008, but its pump was not installed until 2011. **Well 13** was a supply well for two houses and a small garden area. It has been operated daily for many years. In 2011 well 13 was replaced by well 12.

Well 15 is an artesian well, used only for filling tanks and to supply passing Bedouins. When the well was sampled in January 2012, it was open and apparently had been running for several weeks as indicated by the greening and flooding of larger parts of the surrounding area.

Well 17 is located on an agricultural farm which was running in 11/2009. When the well was sampled in January 2012, the farm was deserted and the well was broken. Hence, water could flow out of the well unhampered.

The artesian **wells 19** and **20** are far out in the dunes of the Rub Al-Khali

desert. Most likely they are open from time to time, when Bedouins pass by.

In summary, most of the wells have a rather complex history, which means that it cannot be said with certainty that the sampled water really originates from the approximate location of the respective well.

For ^{14}C and ^{4}He we used data that were already available. Sample preparation, analysis and results are described in Herb (2011) and Al-Mashaikhi (2011). The measurements for ^{14}C were gained by using accelerator mass spectrometry (AMS). For more detailed information I refer the reader to the works cited above.

Another source of information was the PhD-thesis by Clark on ^{14}C and stable isotopes (^{2}H, ^{18}O) (Clark, 1987).

In Section 6.1.2, the procedure to calculate the $^{4}He_{rad}$ component in the aquifer was introduced. The values for uranium and thorium were analysed for three locations in Dhofar, the analysed materials were drilling cuttings from three different wells (drilling campaigns 2005 and 2006). All samples were taken from the LUER. Table 6.2 shows the wells, the depth the samples were taken from, and the analyzed values of U and Th. The values in Table 6.2 fall within the range of cited values for limestone, which are 2 (alternatively 1.3) ppm for U and 2.4 (alternatively 0.5) ppm for Th (Dinh Chau et al., 2011).

Table 6.2: Information on the wells with sampling depth and lithology encountered during drilling. Th- and U-values analysed by ICP-MS.

Well	Aqu.	Lithology description	Depth [m]	Th [ppm]	U [ppm]
A	LUER	biomicritic and fossiliferous limestone interbedded with thin laminae of marl	280	0.04	1.41
B	LUER	pale brown and grey limestone interbeded with clay, shale and siltstone (same description for intervall 270 to 490 m)	332	0.21	1.31
B	LUER		453	0.01	0.71
B	LUER		482	0.01	1.24
C		no detailed lithology given, base LUER 620m?	632	0.28	1.64

6.3 Dating Dhofar groundwaters based on environmental tracers

Figure 6.7 gives an overview about the results obtained. It contains the aforementioned cross-section, and the locations of the wells. Further, the measured concentration / activity of all three tracers (Y-axis) is plotted against distance along the flow path (X-axis), where 0 km represents the surface water divide in the Dhofar Mountains. At first glance one can see that ^{4}He and ^{36}Cl, in general, display the expected behaviour. For ^{4}He increasing concentrations can be observed, indicating an accumulation of Helium (plot C). For the ^{36}Cl/^{35}Cl ratio a decreasing trend, indicating decay over time, is presented in plot D. Both plots support the assumption of a continuous flow path from the high, elevated mountains to the northeastern margin of Dhofar.

For ^{14}C activities (plot B) one would expect high activities at the beginning of the flow path and a decrease as distance increases. The groundwaters of aquifers C and D in the Najd do not display such behaviour.

6.3.1 Dating using ^{14}C-data

The wells 1 and 2 at the beginning of the flowpath in aquifer D show higher pmC-values, indicating younger water in this area. Apart from well 12, all other wells in aquifer C and D are below a pmC of 10 (Figure 6.7 plot B). Looking at all wells sampled in 2009 an irregular distribution of the pmC values can be detected. In aquifer C for example, high pmC-values were measured - both in the far northwest and the far northeast (see Figure 6.8(b) for all sampled wells in aquifer C and D in the Najd).

For further classification and evaluation, these data were compared to existing data. As mentioned in chapter 1, the first study on the Dhofar groundwaters using radiocarbon data was undertaken by Clark in the 1980's (Clark, 1987). Then, the most distant well (in aquifers C and D) was north of the centre of the Najd, approximately at the location of well 15 in the present study. The location of the wells and the activities measured in Clark's study are shown in Figure 6.8(a). The maximum value for aquifer C was obtained at 19.4 pmC, all other wells had values below 5 pmC.

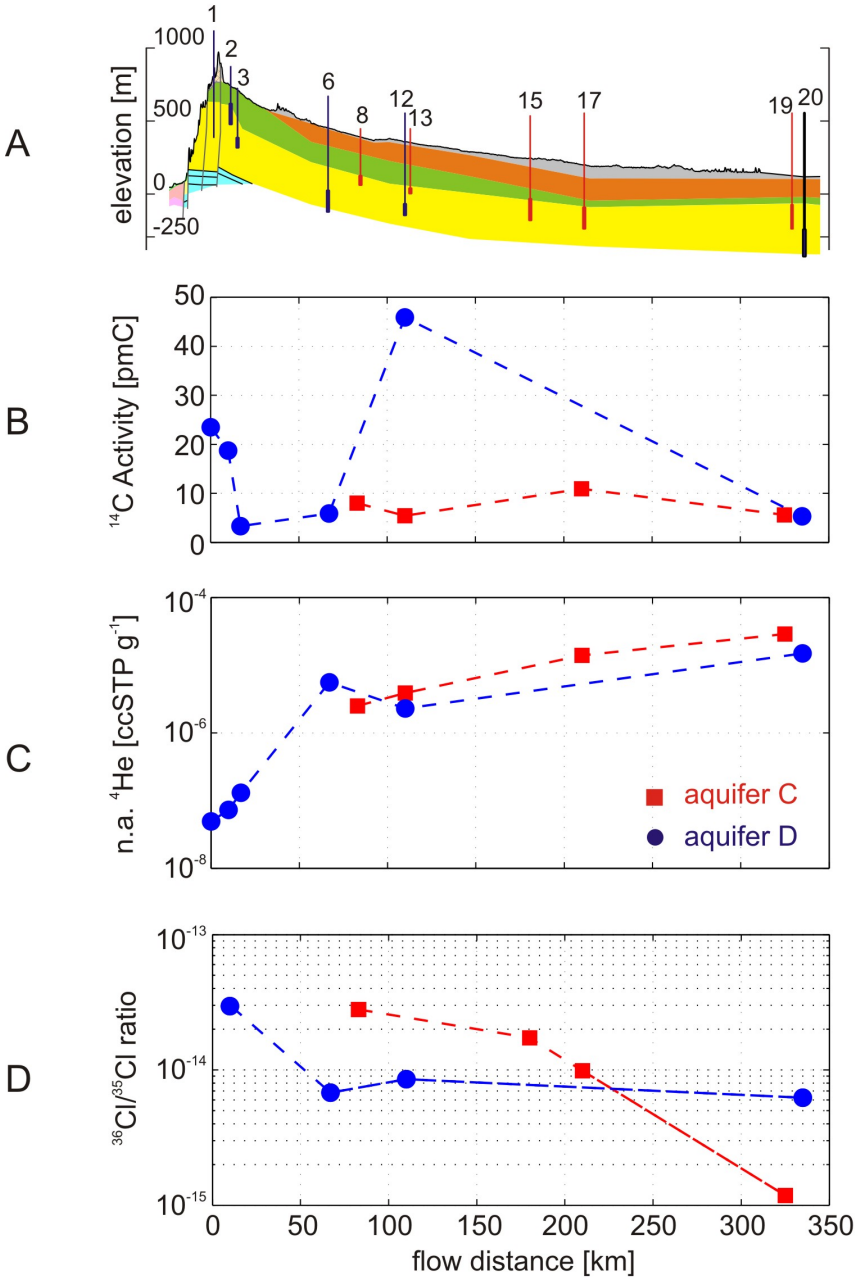

Figure 6.7: All tracers along the cross-section from the Dhofar Mountains to north-eastern margin of Dhofar. Plot A: cross-section with location of the wells. Plots B, C and D give the measured concentrations for the wells represented in plot A, with square symbol for aquifer C and circle symbol for aquifer D.

For aquifer D the maximum value was 7.5 pmC, and three of the other four wells fall below 2.5 pmC. In some cases, the activities measured by Clark exhibit slightly higher pmC-values in direction of the groundwater flow. However, these differences are small, and, taking in account the indicated error limits, do not result in contradictory groundwater ages (i.e. older ages at the beginning of the flowpath).

In contrast to Clark (1987), the 2009 sampling campaign found pmC-values clearly above 5 pmC for the majority of the measured wells, with the highest value in aquifer C being 77 pmC in the far northeast. For three of the eight wells in aquifer C, a pmC-value greater than 10 was determined. It is particularly striking that these three wells are all in the far north of Dhofar, and thus far away from the beginning of the flow path. In aquifer D, pmC-values for twelve wells were determined, and nine of them turned out to have pmC-values above 10. Observed can be a rough trend of pmC-values being higher at the beginning of the flow path in the west of the study area, whereas in the central area the highest values (between 35 and 52 pmC) occur mostly in the interior area. Well 10 in aquifer D delivers the most striking results: the same well was sampled by Clark and showed a pmC-value of 2.8 in 1985. In 2009, the pmC-value was at 52.8.

Al-Mashaikhi (2011) and Herb (2011) suggest that mixing or infrequent activation of wadis could be responsible for the activities measured. In summary, their work confirms that the direction of groundwater flow goes from south to northeast. In the end, they come up with almost the same age range as Clark, that is, up to 23.000 years (Al-Mashaikhi, 2011) and 32.000 years (Herb, 2011), respectively. Since different correction models were used in each of the three studies, this comparison might not be adequate. However, it should be noted that all studies agree that the groundwater was recharged during more humid times in the last 30 ka BP.

However, the simplest explanation for these higher activities would be an addition of more recent water. Unfortunately, this would not explain the high values from inside the Najd. It would also raise the question of how the water could reach these depths (see Table 6.1), especially under the given circumstances, i.e. with an upward hydraulic gradient.

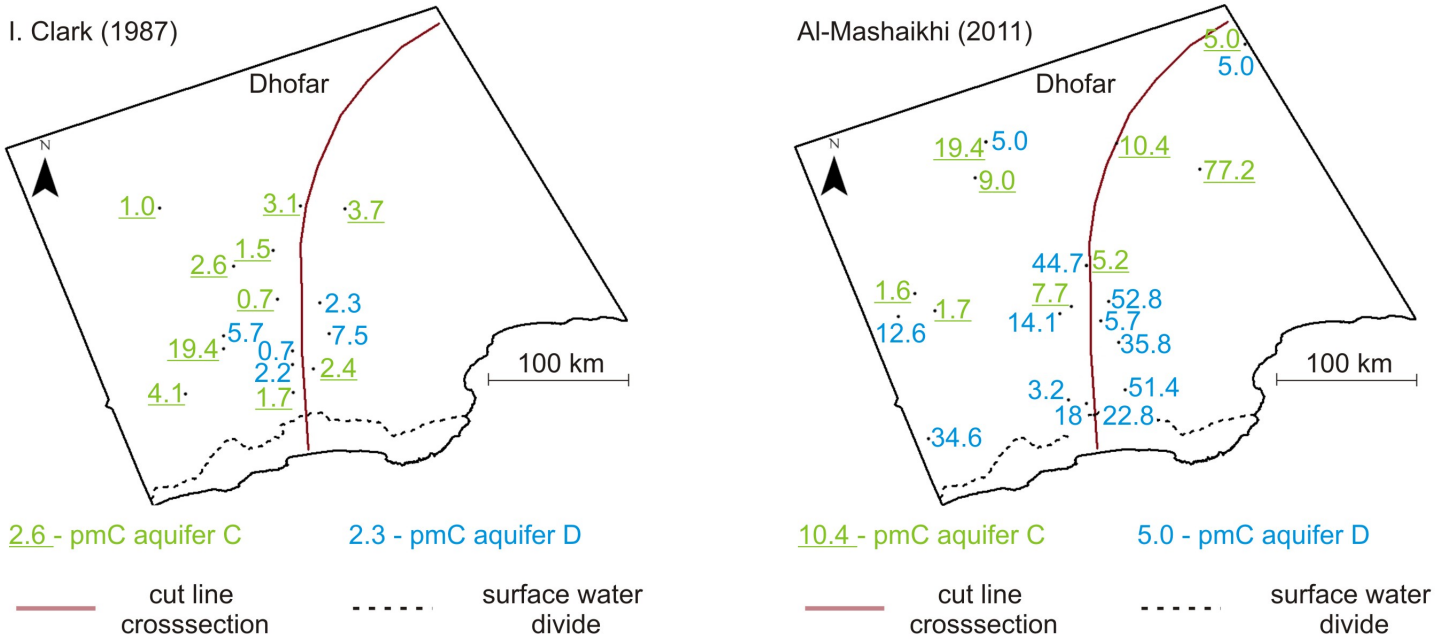

(a) C^{14}-activities for aquifers C and D in Dhofar 1987

(b) C^{14}-activities for aquifers C and D in Dhofar 2011

Figure 6.8: C^{14}-activities aquifers C (underlined) and D in Dhofar 1987 and 2011. (a) Analysed pmC-values from the study of Clark (1987). Majority of the wells shows pmC below 5. (b) Analysed pmC-values from the study of Al-Mashaikhi (2011). High pmC in the interior area can be observed. In general the values are much above the values of 1987.

An explanation through local infiltration, due to rippled surface, however, can almost certainly be excluded because there are no large moulds or similar structures, that would permit the accumulation of water on the surface before infiltrating into the deeper ground.

Despite the insights gained from recent ^{14}C-data, it is still widely held that assuming a north-easterly flow direction with a starting point in the Dhofar Mountains produces good representations of reality. Currently, the concentrations measured in 2009 have not yet been satisfactorily interpreted. Moreover, one can assume that the data sampled by Clark are more reliable, since in 1985, agricultural development of the area had just begun, and with fewer wells drilled and lower abstraction rates anthropogenic influences on the aquifer system were much more limited.

Nevertheless, the ^{14}C-activities measured in the 2008/2009 campaign should not be ignored. However, dating and interpreting the Najd groundwaters based on this ^{14}C-data seems unreasonable at this stage.

6.3.2 Dating using ^{4}He-data

15 wells along the principal cross-section were sampled for noble gases in 2009 by Herb (2011). Table 6.3 presents the noble gas data, the well locations are according to Figure 6.5 and Figure 6.6.

Table 6.3: Neon and Helium for the wells along the principal cross-section in the Najd as analyzed by Herb (2011).

Well	Aqu.	Ne/He [-]	err Ne/He [-]	^{3}He [ccSTP/g]	err ^{3}He [ccSTP/g]	^{3}He/^{4}He	err ^{3}He/^{4}He	^{4}He$_{rad}$ [ccSTP/g]	err ^{4}He$_{rad}$ [ccSTP/g]
1	D	2.27E+00	2.54E-02	9.77E-14	4.87E-15	8.03E-07	4.02E-08	4.91E-08	1.36E-09
2	D	1.68E+00	1.88E-02	7.42E-14	3.63E-15	5.76E-07	2.83E-08	7.34E-08	1.40E-09
3	D	1.12E+00	1.26E-02	5.84E-14	2.84E-15	3.26E-07	1.59E-08	1.29E-07	1.89E-09
6	D	5.18E-02	5.79E-04	1.00E-13	4.57E-15	1.77E-08	8.12E-10	5.58E-06	5.66E-08
8	C	8.12E-02	9.17E-04	6.89E-14	4.10E-15	2.66E-08	1.59E-09	2.54E-06	2.59E-08
9	B	1.06E-01	1.18E-03	5.45E-14	3.08E-15	2.68E-08	1.52E-09	1.98E-06	2.04E-08
11	A	2.59E+00	2.90E-02	7.03E-14	2.58E-15	9.28E-07	3.44E-08	2.45E-08	8.80E-10
12	D	8.14E-02	1.35E-03	6.95E-14	5.39E-15	2.93E-08	2.32E-09	2.32E-06	3.74E-08
13	C	5.99E-02	6.70E-04	9.99E-14	5.99E-15	2.50E-08	1.50E-09	3.93E-06	4.00E-08
14	A	2.98E-02	3.34E-02	6.81E-14	7.15E-16	1.09E-06	1.49E-08	1.47E-08	8.86E-10
16	A	3.71E+00	4.15E-02	5.93E-14	2.91E-15	1.27E-06	6.24E-08	2.42E-09	4.68E-10
17	C	1.7E-02	3.83E-04	2.02E-13	2.96E-14	1.40E-08	2.07E-09	1.44E-05	3.18E-07
18	A	3.60E+00	4.03E-02	6.02E-14	2.95E-15	1.20E-06	5.89E-08	3.66E-09	5.82E-10
19	C	6.49E-03	7.25E-05	2.48E-13	1.88E-14	8.55E-09	6.49E-10	2.89E-05	2.90E-07
20	D	6.94E-03	7.76E-05	3.26E-13	1.45E-14	1.26E-08	5.67E-10	2.58E-05	2.58E-07

The observation that ^{4}He increases with distance (Figure 6.7) matches the overall concept of the nature of the Najd groundwater system. The crucial question is what the sources of ^{4}He are. For the endmembers this can be examined by the use of the isotope plot. For a comprehensive overview, data for all of the wells were plotted in a ^{3}He/^{4}He - Ne/He diagram (Figure 6.9). The wells along the principal cross-section are marked by their number. Almost all wells plot along the mixing line from the atmospheric endmember (atm) to the radiogenic endmember (rad). However, mantle ^{4}He cannot be observed. The wells in aquifer A plot close to the atmospheric endmember, indicating atmospheric influence. Apart from the wells in the recharge area (1, 2, 3), the wells in aquifers C and D plot close to the radiogenic endmember.

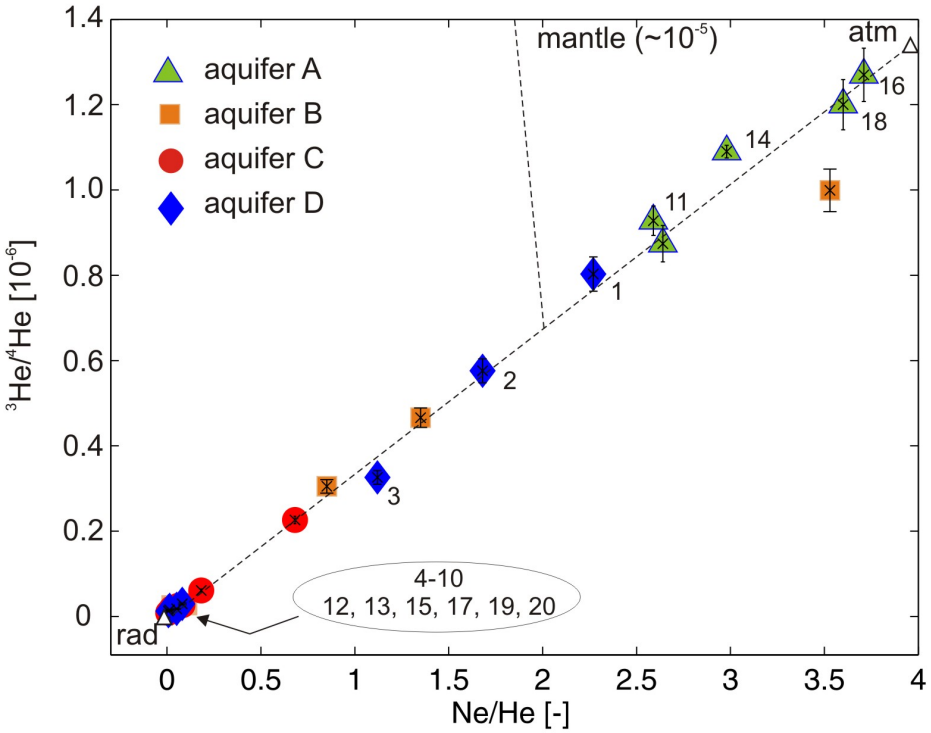

Figure 6.9: ^{3}He/^{4}He ratio versus Ne/He ratio to distinguish the different helium endmembers. The dashed, grey line represents the mixing line between radiogenic endmember (rad) with ^{3}He/^{4}He = 2×10^{-8} and the atmospheric solubility endmember (atm) with ^{3}He/^{4}He = 1.36×10^{-6} and Ne/He = 4.13. (modified from Herb (2011))

Figure 6.10(a) reveals that the increase in $^4He_{rad}$ is not a linear function. The $^4He_{rad}$ curve shows exponential characteristics, which potentially indicates that in-situ production cannot be the only source of the accumulation of $^4He_{rad}$.

Figure 6.10(b) shows radiogenic helium concentration over drilled depth. The long, open hole-sections are schematically indicated by the dashed grey lines. $^4He_{rad}$ can be found at the drilled depth of the borehole. Comparing Figure 6.10(a) and Figure 6.10(b) reveals that - apart from well 6 and well 12 - the order of the wells is the same. This suggests that distance (and, in turn, residence time) seems to have a greater influence on the concentrations than depth. The distribution in both plots indicates that no major sources of different types influence the helium concentrations. Such sources could, for example, be local high concentrations of Uranium leading to higher helium concentrations, and probably a more random distribution of the values along the flow path.

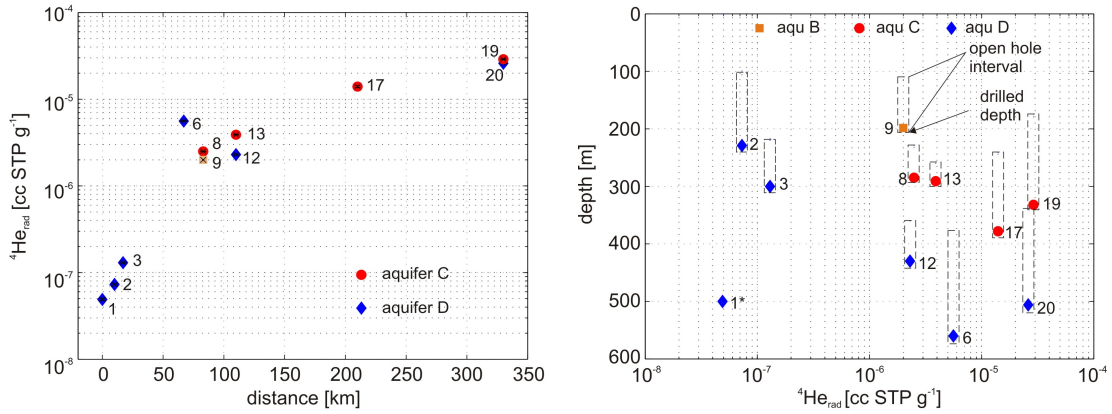

(a) $^4He_{rad}$ plotted against distance

(b) $^4He_{rad}$ plotted against depth

Figure 6.10: Radiogenic ^4He component plotted against distance (a) and depth (b). $^4He_{rad}$ ranges over three orders of magnitude and is therefore plotted on a logarithmic scale. Distance seems to be of greater influence than depth. (a) The increase in $^4He_{rad}$ is not a linear function. Dashed grey lines in (b) represent open-hole sections of the wells. (1* - no borehole data available).

The observed trend of concentrations being higher in aquifer C than in D could be due to: (i) the residence time of the water in C being longer compared to D (which would support the hypothesis that aquifer C is fed by aquifer D), or (ii)

greater amounts of U and Th in the matrix of aquifer C causing greater production of $^4He_{rad}$.

Previous studies have shown that a comparison of measured and analysed ^3He and ^4He concentrations can be used to identify the sources of $^4He_{rad}$ (Lehmann et al., 2003; Pearson et al., 1991). This method was applied in the present study. In Figure 6.11(a) the measured ^3He-values are plotted against the measured $^4He_{rad}$. Furthermore the figure shows the calculated ^3He and ^4He production lines for shale and limestone with lithium concentrations of 5 ppm and 28 ppm. ^3He was calculated by using equations 6.4 and 6.5 with the parameters shown in Table 6.4. ^4He was calculated by using equation 6.7, and U and Th were taken from Table 6.2.

The resulting $^3He/^4He$ ratios are $3.2\times\ 10^{-9}$ for Li = 5 ppm and $1.8\ \times\ 10^{-8}$ for Li = 28 ppm. Consequently, they are in the range of values we find in the literature, namely 0.1 to $1.14\ \times\ 10^{-8}$ (i.e. Andrews (1985)). For shale a $^3He/^4He$ ratio of $1.99\ \times\ 10^{-8}$ was taken for the plot, according to Torgersen and Stute (2012, in preparation).

Table 6.4: Parameters limestone for ^3He production

Parameter	Value
Li	5; 28 ppm [1]
ρ	2.6 g cm^{-3}
a	1.07 [2]
b	0.28 [2]

[1] Ahrens (1965) [2] Pearson et al. (1991)

The calculated $^3He/\ ^4He$ production line for limestone with a lithium content of 5 ppm shows only a slight increase in ^3He. Shale and limestone with a lithium content of 28 ppm have much higher ^3He values and plot close to each other, as Figure 6.11(a) shows. The measured values for wells 6, 8, 12, and 13 in the interior are in the range of the $^3He/^4He$ production lines of shale and limestone with higher lithium content. For the distant wells ^3He and ^4He values lie between the calculated production lines for the two different limestone values.

The lithium concentration in the rock is unknown in most cases. The two values taken from the literature cover the measured range for ^3He and ^4He. A

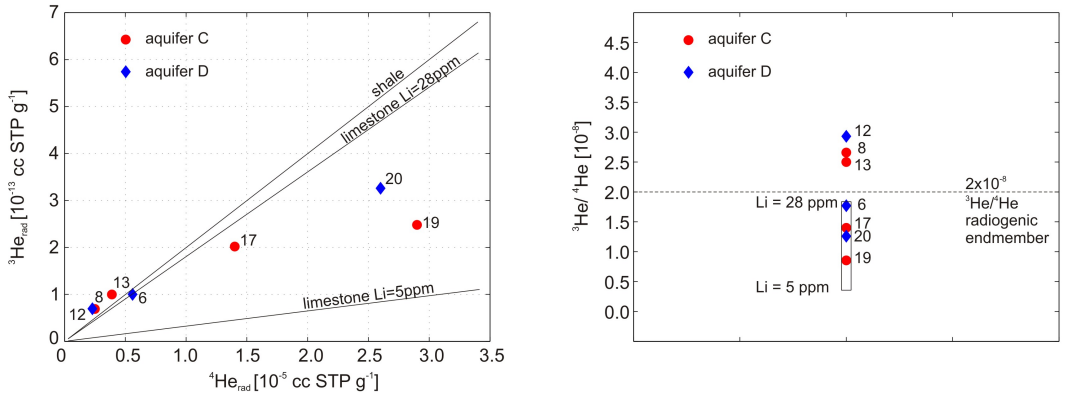

(a) $^3He_{rad}$ plotted against $^4He_{rad}$ (b) $^3He/^4He$ in the interior Najd

Figure 6.11: $^3He/^4He$ production and $^3He/^4He$ in groundwater in the interior Najd. (a) Measured ^3He and ^4He concentrations for the wells outside the recharge area. Straight lines indicate the in-situ production ratios in shale (upper line), limestone with Li of 28 ppm (middle line) and limestone with Li of 5 ppm (lower line). (b) $^3He/^4He$ ratios of the sampled wells in the interior Najd.

value between them would result in a production line that better fits the ^3He and ^4He values in the distant wells. Higher values would cover the steeper increase at the near wells (8, 12, 13). Small lithium values resulting in lower ^3He concentration do not seem to fit the measured values of the wells in the interior.

A possible interpretation could be that the higher values at the wells 8, 12, and 13 result from different rock material. On the other hand, the more distant wells (17, 19, 20) could show the influence of a different rockmatrix with lower lithium concentrations, or mixing effects of different waters (aquifer water, pore water). However, it would fit all wells if limestone with lower Li content and a confining layer with higher Li content were assumed. In our case the latter would be shale. Lehmann et al. (2003) gives Li contents for shale from 24 up to 54 ppm for example.

The lowest measured $^3He/^4He$ ratio was analysed with 8.55 $\times$ 10^{-9} ($\pm$ 6.49 $\times$ 10^{-9}) for well 19 in aquifer C and 1.26$\times$ 10^{-8} for well 20 in aquifer D. Figure 6.11(b) reveals that they are both in the range covered by the calculated $^3He/^4He$ ratios of 3.2$\times$ 10^{-9} to 1.8 $\times$ 10^{-8}. Furthermore, a box supplements the plot with the $^3He/^4He$ ratio of the lower value (5 ppm) and the $^3He/^4He$ ratio of the upper

value (28 ppm) and the line of the radiogenic endmember with $^3He/^4He = 2\times10^{-8}$. The sampled wells are close to the signature of the radiogenic endmember. The grouping of wells (8, 12, 13) closer to the recharge area and the more distant wells (17, 19, 20) is also visible here.

Further explanation or interpretation is limited. In summary, we can say that neither ^3He nor ^4He give a clear indication of where they are coming from. In-situ production, mixing with pore water of adjacent layers or mixing with waters from deeper aquifers could lead to the analysed values. It is likewise possible that the values are the result of a flux from the inner earth (crustal flux).

Other available data fail to further clarify the helium interpretation - in particular if higher $^4He_{rad}$ concentrations along the flowpath can be translated to older ages. Lehmann et al. (1996), for example, compared the chlorine and helium concentrations of groundwaters in different study areas. They observed a correlation of higher helium values with higher chlorine values. They also report that the Cl/He ratios in different aquifers lie within the same range (100:1 to 10,000:1).

In the present study, the data do not show such a correlation. Chlorine concentration in the central Najd does not increase with distance, i.e. some wells in the recharge area (2, 3) display greater values than those in the interior (aquifer D). Well 19 (aquifer C) and 20 (D), with the highest $^4He_{rad}$ concentration, also have a high concentration of chlorine. However, these high values are most likely due to brine water. Al-Mashaikhi (2011) stated that the groundwater in the north-east (well 20) is mixed with brine water originating from the marine deposits.

However, the observed accumulation of $^4He_{rad}$ presented in the Figures 6.10(a) and 6.10(b) shows the expected pattern. $^4He_{rad}$ may therefore be used for the qualitative dating of the Dhofar groundwaters: higher $^4He_{rad}$ indicates a higher groundwater residence time. However, the discussion above showed the uncertainties of the sources of $^4He_{rad}$. The result is that the quantitative dating of the groundwaters can be quite difficult, if not impossible.

With the values for Th and U given in Table 6.2 and a release factor Δ of 1 (assuming equilibrium), the $^4He_{rad}$ release and $^4He_{rad}$ accumulation can be calculated by using Equations 6.6 to 6.9. The density of the limestone aquifer matrix, ρ, was fixed with 2.6 g cm^{-3}. Table 6.5 shows the calculated numbers for the minimum U and Th values (sample B2 at 453 m depth), the maximum values (sample C) and those from the literature. It contains results for a porosity (ϕ) of 20 %.

Table 6.5: Helium release and accumulation for the lower Umm Er Radhuma (samples A to C) and typical limestone values (samples D and E) for a density of ρ=2.6 g cm^{-3}

Sample	U [ppm]	Th [ppm]	Depth [m]	Porosity ϕ [%]	$P_4 \times 10^{-13}$ [cc STP cm^3 a^{-1}]	$A_4 \times 10^{-12}$ [cm^3 g^{-1} H_2O a^{-1}]
A	1.413	0.037	280	20	4.44	1.78
B1	1.314	0.212	332	20	4.27	1.71
B2	0.709	0.013	453	20	2.23	0.89
B3	1.241	0.011	482	20	3.89	1.56
C	1.640	0.285	632	20	5.35	2.14
D	2.0	2.4		10	8.05	7.25
D	2.0	2.4		20	8.05	3.22
D	2.0	2.4		30	8.05	1.88
E	1.3	0.5		10	4.45	4.00
E	1.3	0.5		20	4.45	1.78
E	1.3	0.5		30	4.45	1.04

The calculated $^4He_{rad}$ accumulation rates for the Dhofar samples fall between 5.206$\times$ 10^{-13} cm^3 g^{-1} H_2O a^{-1} (U=0.71 ppm, Th=0.01 ppm, ϕ=30%) and 4.816$\times$ 10^{-12} cm^3 g^{-1} H_2O a^{-1} (U=1.64 ppm, Th=0.28 ppm, ϕ=10%). This is within the range suggested by the literature, for example 3.95$\times$ 10^{-12} to 6.2$\times$ 10^{-12} cm^3 g^{-1} H_2O a^{-1} for the GAB study (Torgersen and Clarke, 1985).

Now, in-situ production can be assumed to be the single source for $^4He_{rad}$ to calculate the age of groundwater with the help of Equation 6.10. For the upper value (sample C, ϕ=10%) of A_4 (4.816$\times$ 10^{-12} cm^3 g^{-1} H_2O a^{-1}), this results in the groundwater ages shown in Table 6.6. With the exception of the wells in the recharge area, the calculated $^4He_{rad}$-ages are significantly higher than ages based on ^{14}C-data. Lower values for A would result in even older ages.

The helium evolution for different depths within an aquifer is calculated with Equation 6.11 taking into consideration the contribution of external sources to the amount of of $^4He_{rad}$ in the aquifers. It requires knowing of the crustal flux F' as well as the parameters flow velocity, porosity, effective diffusion coefficient and position (x and y) in the aquifer.

Table 6.6: Calculated ^{4}He-model age [ka] considering only in-situ production for $^4He_{rad}$.

Recharge area			Central Dhofar			North east Dhofar		
Well	Aqu	^{4}He-age [ka]	Well	Aqu	^{4}He-age [ka]	Well	Aqu	^{4}He-age [ka]
1	D	10	6	D	1160	17	C	2990
2	D	15	8	C	527	19	C	6000
3	D	27	12	D	482	20	D	5360
			13	C	816			

The crustal flux can be calculated analogously to Equations 6.7 and 6.8. Using the values from Torgersen and Clarke (1985) - U=2.8ppm, Th/U=3.8, rock density $\rho = 2.6$ g/cm^3, and the thickness of the upper crust (1-15 km below the Umm Er Radhuma formation) - the production rate in the upper crust turns out to be $2.51\times\ 10^{-6}$cm^3 STP cm^{-3} and a^{-1}. This value is within the range of the values given by Torgersen (2010).

Helium accumulation along the cross-section was calculated for three different depths via Equation 6.11. The assumed depth was 45 m (relative to the top of the LUER) for the wells in the upper part, 125 m for those in the middle of the formation and 200 m depth for the deep wells. Table 6.7 provides the remaining parameters used in the calculation of the Helium evolution curves. The calculation for P_4 and F was performed as shown above. The range of the flow velocity V was derived from the calculated in-situ $^4He_{rad}$-ages and the ^{14}C-age range (up to 30 ka), respectively. The vertical diffusion coefficient K_a was taken from literature sources (Torgersen and Clarke, 1985).

Limitation for the interpretation of the helium evolution is given by the high variability of the parameters, i.e. crustal flux, porosity and diffusion coefficient. Torgersen (2010), for example, gives a variability of crustal flux that is as high as $\pm$ 1.5 orders of magnitude. This same order probably applies to the other parameters as well. Since age range (and with it flow velocity) remains uncertain, the number of degrees of freedom is too great to calculate the concentration of $^4He_{rad}$ with sufficient precision.

Table 6.7: Parameters for calculation of the He evolution curves.

Parameter		Value
Porosity	θ	0.01-0.30
Velocity	V	0.065-7.0 m a^{-1}
Distance	x	variable (0-350 km)
Aquifer thickness	h	250 m
Vertical depth in aquifer	z	45 m, 125 m, 200 m
In-situ accumulation	P_4	5.0×10^{-12} cm^3 STP g^{-1} a^{-1}
Helium flux out of the crust	F	$0.251 - 2.51 \times 10^{-6}$ cm^3 STP cm^{-2} a^{-1}
Effective vertical diffusion coefficient	K_a	4×10^{-9} $m^2 s^{-1}$

The plots in Figure 6.12(a) and 6.12(b) show the accumulation of $^4He_{rad}$ over distance, at three different depths and for two scenarios. In scenario 1, which is represented by Figure 6.12(a), flow velocity V is 7 m a^{-1} (derived from ^{14}C-age range), porosity ϕ=10% and crustal flux F 2.51×10^{-6} cm^3 STP g^{-1}. In scenario 2, which is represented by Figure 6.12(b), flow velocity is defined as 1 m a^{-1} porosity is ϕ=30% and the crustal flux F 5.02×10^{-7} cm^3 STP g^{-1}. Furthermore, the plots show the measured concentrations of $^4He_{rad}$ along the distance.

Both cases reveal that different combinations of parameters result in $^4He_{rad}$ concentrations throughout the range of the sampled wells. However, case 1 (Figure 6.12(a)) results in a wide spread of values for different depths. While for the middle depth (125 m) a good fit between measured and calculated $^4He_{rad}$ could be obtained, the calculated values for a depth of 45 m and 200 m deviate significantly from the respective measured depths. For different depths in the aquifer, the calculated concentrations of helium are spread broadly. The respective measured concentrations, on the other hand, fall within a narrow distribution, indicating mixing of water.

Reducing flow velocity and crustal flux in Equation 6.11 led to a more narrow distribution of helium evolution curves, which is shown in Figure 6.12(b), where, apart from well 12, all wells match the calculated curves of helium evolution for the

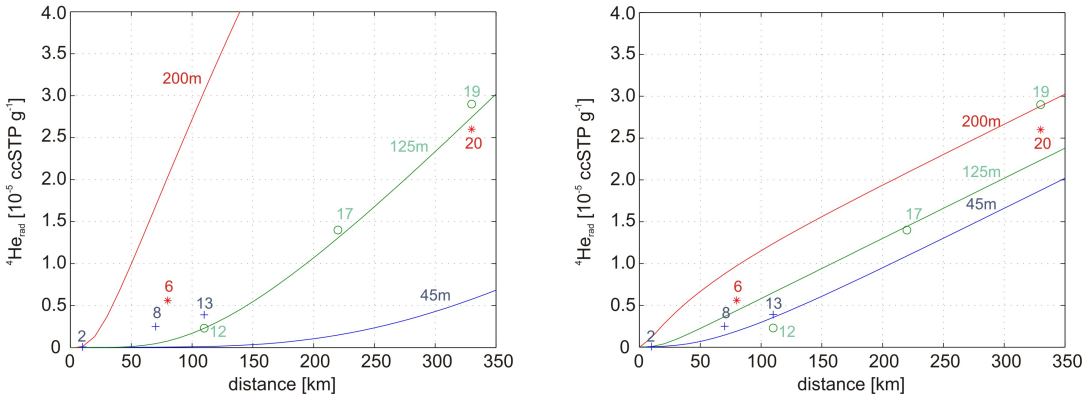

(a) $^4He_{rad}$ accumulation over distance case 1 (b) $^4He_{rad}$ accumulation over distance case 2

Figure 6.12: $^4He_{rad}$ accumulation for three different depth's (45 m, 125 m, 200 m from the top of the formation) over distance by using the Torgersen model (Torgersen, 2010). (a) Case 1: V = 7 m a^{-1} (derived from ^{14}C age range), ϕ=10% and F = 2.51× 10^{-6} ccSTP g^{-1}. (b) Case 2 are V = 1 m a^{-1}, ϕ=30% and F = 5.02× 10^{-7} ccSTP g^{-1}.

three different depths. This might suggest that the external source (F) is below the calculated value of 2.51× 10^{-6} cm^3 STP per cm^{-2} and a^{-1}.

Even though lower rates for the external flux were subject to prior discussion (see, for example, Stute et al. (1992)), the above presented calculations highlight the high degree of uncertainty that arises when helium alone is used for groundwater age estimation.

6.3.3 Dating by using ^{36}Cl-data

10 wells were sampled for ^{36}Cl estimation in January 2012. The location of the sampled wells are shown in Figure 6.5 and Figure 6.6.

Table 6.8 displays the sampled wells with the measured Cl values and the ^{36}Cl/^{35}Cl ratio, the calculated ^{36}Cl atoms and the ^{36}Cl/Cl ratio. The analysis of the chlorine isotopes was done at the Ion Beam Centre at the Helmholtz Zentrum Dresden-Rossendorf. It should be noted that the errors are quite high, in general. A planned second measurement was not conducted when the present study was completed.

Table 6.8: Cl, ^{36}Cl/^{35}Cl and ^{36}Cl/Cl for the wells in aquifer C and D in the Najd, sampled 2012.

Well	Aquifer	Cl [a] (mg l^{-1})	^{36}Cl/^{35}Cl [b] (10^{-15}at at^{-1})	^{36}Cl (10^{8} l^{-1})	^{36}Cl/Cl (10^{-15}at at^{-1})
8	C	536	28.0±31%	1.93	21.2
15	C	273	17.3±41%	0.61	13.1
17	C	307	9.8±51%	0.39	7.5
19	C	2489	1.2±105%	0.38	0.9
2	D	426	29.6±32%	1.63	22.5
4	D	1073	15.7±40%	2.16	11.9
5	D	394	33.1±31%	1.68	25.1
6	D	447	6.8±63%	0.39	5.1
12	D	296	8.5±54%	0.32	6.5
20	D	5245	6.2±60%	4.21	4.7

[a] Measured at the Helmholtz Centre for Environmental Research - UFZ, no error intervals were given

[b] Measured by Accelator Mass Spectrometry at the Helmholtz Zentrum Dresden-Rossendorf

For the classification and evaluation the data were compared to existing ^{36}Cl data from three wells in the Najd (Table 6.9) sampled by I. Clark in the 1980's.

Clark's wells are located in the interior Najd, wells 41 and 64 are located along the principal crosssection under focus in the present study. Well number 64 from Clark is well 10 in the present study. The well was already mentioned before as

the well with the large differences in the measured ^{14}C-activities between 1985 and 2009. Well 41 is located in the far northeast, approximately between well 17 and well 18 of the present study. Only well 55 is away from the principal crosssection, approximately 45 km to the west from well 12.

Table 6.9: Cl, ^{3}H, ^{36}Cl/^{35}Cl and ^{36}Cl/Cl for the wells in aquifer C and D in the Najd, sampled 1985 by I. Clark (Clark, 1987)

Well	depth [m]	^{3}H [TU]	Cl (mg l^{-1})	^{36}Cl/^{35}Cl (10^{-15}at at^{-1})	^{36}Cl (10^{8} l^{-1})	^{36}Cl/Cl (10^{-15} at at^{-1})
41 (C)	385(293)[a]	4	138	59±10	1.350	44.69
55 (C)	250(165)	0	213	32±4	1.160	24.24
64 (D)	553(-)[b]	0	223	56±6	2.120	42.42

[a] cased depth
[a] cased depth unknown

Chloride concentration and evaporation

Chloride was already discussed above, when it was shown that no correlation between chloride and ^{4}He could be observed. Generally, the magnitude of the measured Cl concentrations is quite striking. The concentrations in aquifer C lie between 273 and 536 mg l^{-1}, and in D between 296 and 1073 mg l^{-1}, when neglecting the most distant wells 19 and 20 with the highly mineralized water.

During the monsoon a chlorid concentration of 20 mg l^{-1} was measured in the present study. Fog water in the Dhofar Mountains showed a mean value of 44 mg l^{-1} where the values range between 5.6 mg l^{-1} and 84 mg l^{-1} (Schemenauer and Cereceda, 1992). Precipitation from the cyclone Keila - hitting the Dhofar region in November 2011 - was analysed to 2.1 mg l^{-1} for rain, 47.2 mg l^{-1} for flood water, and 86.7 mg l^{-1} in pond water (the latter sampled about 70 days after the event). Macumber et al. (1994) analysed chloride with 22 mg l^{-1} and 96 mg l^{-1}, respectively, for two surface water bodies originating from a cyclone. The samples were taken 11 days after the event and had therefore been subject

to evaporation. However, it seems unlikely that the Cl concentration in rainfall in the Najd is substantially higher than 20 to 50 mg l^{-1}.

Figure 6.13(a) presents the wells sampled for ^{36}Cl (filled symbols) and those sampled during 2008 and 2009 (open symbols) in aquifers C and D. The chloride concentration in aquifers C and D is higher in the wells at the beginning of the flowpath, the range is (apart from well 4) between 100 and 600 mg l^{-1}. The question is the origin of high Cl concentrations in the groundwater.

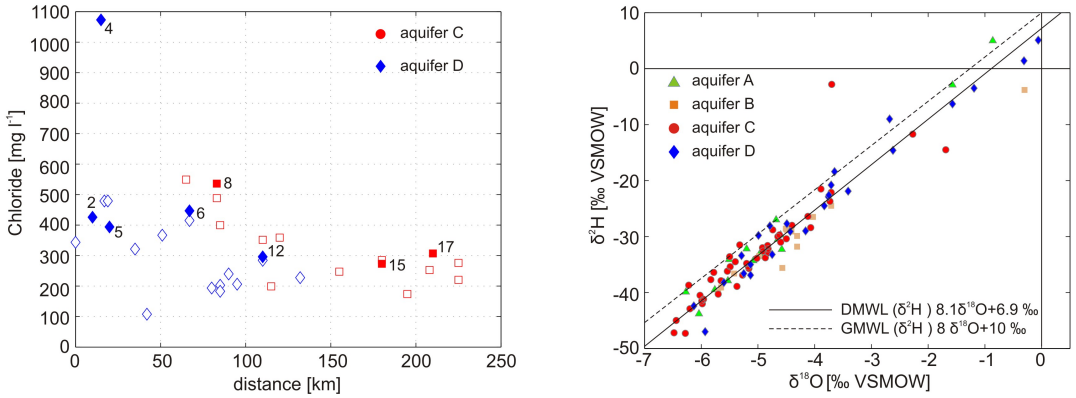

(a) Cl plotted against distance

(b) δH/δO for Najd groundwaters

Figure 6.13: Cl vs. distance (a) and the δ^2H/δ^{18}O diagram for Najd groundwaters (b). (a) Chloride concentration in aquifer C and D. Filled symbols represent wells sampled for ^{36}Cl, open symbols all wells from the sampling campaign 2009. (b) δ^2H against δ^{18}O for the Dhofar groundwaters for all aquifers sampling campaign 2008/2009 (modified from Herb (2011)).

Sources of chloride could be, for example, (i) the dissolution of the evaporites from the Rus formation (see section 2.5.1), or (ii) a concentration of chloride as the result of high evaporation at the land surface. No water samples of the RUS were available in the present study. Therefore it could not be checked if the RUS water show higher mineralization than the water in the UER or if the RUS waters are already leached out. The dissolution of evaporites could therefore not be evaluated. For the UER formation there is no indication for the occurrence of evaporites in the lithological descriptions (see section 2.5.1).

Previous studies concluded that in the Najd and the neighbouring Al-Wusta region the infiltration of surface water is rapid and evaporation negligible (Al-

Mashaikhi, 2011; Clark, 1987; Herb, 2011; Macumber et al., 1994). This was visually observed in the field but can also be seen in the $\delta^2H/\delta^{18}O$ diagramm in Figure 6.13(b). The Dhofar groundwater samples for all aquifers from the sampling campaign 2008/2009 were adapted from Herb (2011). The almost parallel course of the Global Meteoric Water Line (GMWL) and the Dhofar Meteoric Water Line (DMWL) constructed by Herb (2011) indicates that evaporation is negligible for the Dhofar groundwaters. The deuterium excess d of the Dhofar groundwaters varies between 5 and 8 pointing to a precipitation signature without remarkable evaporation. With the $\delta^2H/\delta^{18}O$ plot Herb (2011) furthermore showed that sources other than monsoon and cyclone can be excluded for the Dhofar groundwaters.

Although evaporation seems to be negligible for the infiltrating water, high evaporation rates can be the reason for the accumulation of chloride in the study area. In Figure 4.4 in chapter 4 the yearly rainfall rates for the station Thumrait for the time period 1980 to 2007 were presented. Figure 6.14, below, contains a more detailed record for the years 1980 to 1989 with daily rainfall rates.

Over the whole time period 50 rainfall events took place, 35 of them had rainfall amounts below 10 mm. In the arid Najd of today evaporation rates are high, and potentially reach up to 2200 mm a^{-1} (Al-Mashaikhi, 2011). It can be assumed that smaller rainfall events are not leading to infiltration of water in the subsurface, but evaporate on the land surface. Chloride accumulates on the ground surface, while water evaporates. The accumulated chloride is washed to the subsurface as soon as a strong rainfall event occurs, producing a sufficient amount of water for generating groundwater recharge.

Several assumptions on the threshold of rainfall or the evaporation rates can now be made to calculate the accumulation of chloride. An example is presented for the period 1980 to 1982 and the daily rainfall rates of the station Thumrait (Figure 6.14). 12 events with less than 10 mm rainfall were recorded during this time span. Assuming 20 mg l^{-1} Cl in the rain and complete evaporation, there would be an accumulation of 526 mg m^{-2} of chloride. The event in February 1983 with 23.2 mm rain on the 10th and 21.7 mm rain on the 11th washed the accumulated chloride into the ground. Even though this event might not be strong enough to transport the water (infused with high chloride) directly to the aquifer, the chloride is removed from the surface and shifted to the subsurface. Following rainfall or recharge events transport the chloride to the deeper ground and eventually into

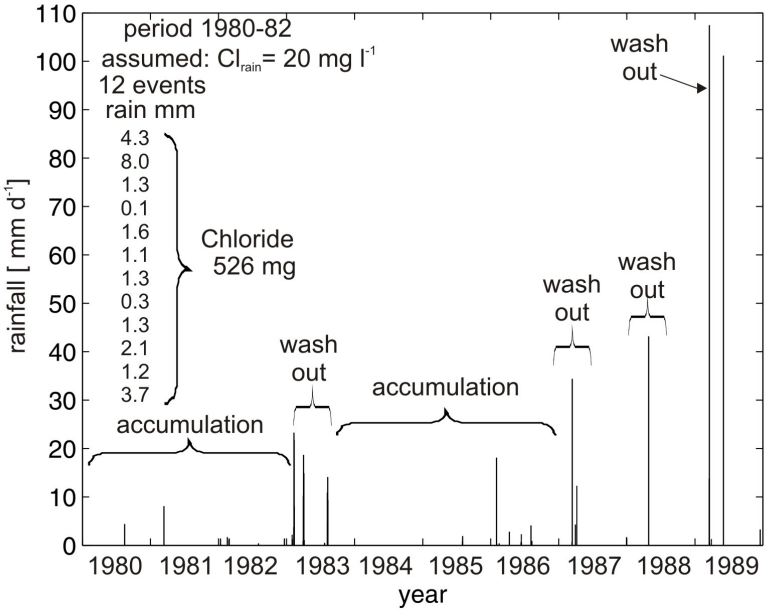

Figure 6.14: Daily rainfall in mm for the station Thumrait for the period 1980 to 1989 and assumed scenario (accumulation and wash out) for the observed high Cl-concentrations in the groundwater.

the aquifer. In summary, small rainfall events become subject to evaporation and are not leading to infiltration of water but to accumulation of chloride; large rainfall events on the other hand lead to infiltration into the deeper ground but are less subject to evaporation. Therefore no evaporatic effects can be observed in the δ^2H/δ^{18}O plot. Under today's climatic condition the observed high Cl-concentrations in the aquifers are best explained by the described scenario.

That the climatic conditions might have been different when the water was recharged is also reflected in the distribution of chloride in Figure 6.13(a). Almost all wells in aquifer D within the first 80 km of the flowpath have Cl values above 300 mg l^{-1}. The wells more downstream are below this threshold. In aquifer C we get a similar picture: high values between 70 and 120 km, and lower values are found more downstream. With the interpretation given above, lower Cl values would represent more humid conditons (and less evaporation).

^{36}Cl/Cl and ^{36}Cl data

Well 8, the first well in aquifer C, is located approximately 80 km away from the Dhofar Mountains and shows the highest ^{36}Cl/Cl ratio in aquifer C with 21.2 × 10^{-15} . Well 19, the most distant well at the northeastern margin of Dhofar, has the lowest ^{36}Cl/Cl ratio of all sampled wells with 0.89 × 10^{-15} . Wells 15 and 17 in between decrease systematically in ^{36}Cl/Cl. ^{36}Cl/Cl in well 8 is the 24-fold of well 19. Altogether, a decreasing trend of ^{36}Cl/Cl over distance can be observed in aquifer C (Figure 6.15(a)).

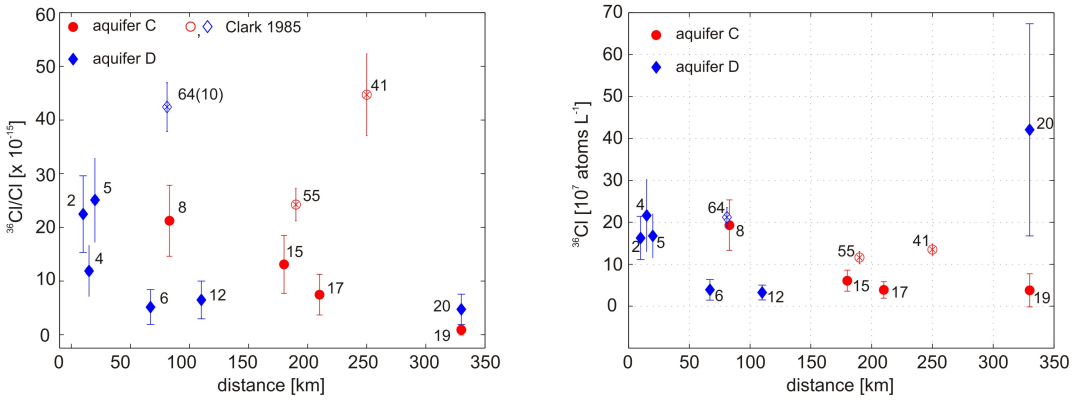

(a) ^{36}Cl/Cl plotted against distance

(b) ^{36}Cl plotted against distance

Figure 6.15: ^{36}Cl/Cl and ^{36}Cl concentration plotted against distance. Displayed are the sampled wells of the campaign 2012 (filled symbols) and the campaign 1985 (open symbols) (Clark, 1987). (a) Decreasing trend for ^{36}Cl/Cl in aquifer C along the whole flow line, and in aquifer D from the recharge area to the interior. (b) ^{36}Cl concentration over distance shows a similar pattern.

In aquifer D wells 2, 4 and 5 in the recharge area have the highest ^{36}Cl/Cl ratios, ranging from 12 to 25 × 10^{-15}. The next well downstream, well 6, has a comparetively low ^{36}Cl/Cl ratio with 5.1 × 10^{-15}. The ^{36}Cl/Cl ratio increases to 6.5 × 10^{-15} at well 12 and then decreases again to 4.7 × 10^{-15} at the far distant well 20. Taking in account the large error intervals, well 12 and well 20 cover almost the same range in their ^{36}Cl/Cl ratio. In aquifer D, a decreasing ^{36}Cl/Cl trend cannot be observed apart from the wells in the recharge area (see Figure 6.15(a)).

The $^{36}Cl/Cl$ ratios analysed by Clark (1987) are up to 1.5 times above the highest value of the 2012 campaign. Well 55 is in the range of the wells 2,5 and 8, for well 41 and 64 $^{36}Cl/Cl$ higher ratios were analysed in 1985. This is interesting especially for the most distant well 41. Apart from having the highest $^{36}Cl/Cl$ ratio, ^{3}H was detected in the well, indicating a recent input to the groundwater.

The concentration of ^{36}Cl over distance is displayed in Figure 6.15(b). Similar to the trend in Figure 6.15(a), a decreasing trend of ^{36}Cl concentration with distance (and the hydraulic gradient) can be observed in aquifer C from well 8 (19.32×10^7 atoms l^{-1}) over well 15 (6.07×10^7 atoms l^{-1}) to well 17 (3.88×10^7 atoms l^{-1}). However, from well 17 to well 19 (3.78×10^7 atoms l^{-1}) the decrease in concentration of ^{36}Cl is quite small.

Clark (1987) stated that in well 41 there is a thermonuclear peak. He interpreted the water in well 41 as a mixture of modern post nuclear groundwater and pre-nuclear water. The higher $^{36}Cl/Cl$ and ^{36}Cl values at the most distant well 41 in Figures 6.15(a) and 6.15(b) would support a mixing of older and more recent water. No anthropogenic contributions were confirmed for the water in wells 55 and 64. According to ^{14}C data these wells contain fossile water. Structural pathways flushing groundwater with higher radioactivity from the depth into the aquifers, were explained to be possible ^{36}Cl sources.

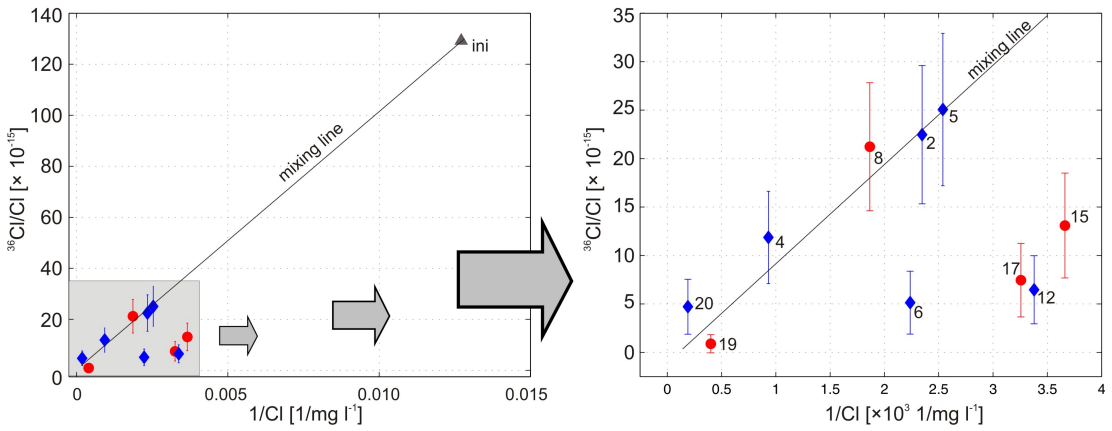

Figure 6.16: $^{36}Cl/Cl$ plotted against 1/Cl. Mixing is represented by the line between an assumed initial value (ini) and the wells 19 and 20 with the lowest $^{36}Cl/Cl$ ratio. A similar grouping of the wells at the beginning of the flowpath (2, 4, 5 and 8) which plot along a line, and the wells downstream (6, 12, 15 and 17) which plot along a line with a lower slope, is observed.

Cl and ^{36}Cl have the following possible sources: (i) water from the assumed recharge area in the Dhofar Mountains, as well as local infiltrations more downstream; (ii) dissolved chloride from overlying layers (for example evaporites in the RUS) with high Cl and ^{36}Cl/Cl ratios close to the secular equilibrum; (iii) pore water from confining layers with low ^{36}Cl/Cl ratios; (iv) water from greater depth which could have high Cl concentrations, but could also produce higher ^{36}Cl because of its depth. In Figure 6.16 a mixing line is plotted between the wells with the lowest ^{36}Cl/Cl ratio (well 19 and 20) and an assumed initial value (ini), where the ^{36}Cl/Cl ratio was taken from the literature (Love et al. (2000): 125 $\times 10^{-15}$ at at^{-1}). Chloride was assumed to be 75 mg l^{-1}. The wells 2, 4, 5 and 8 plot along the mixing line, whereas the wells 6, 12, 15 and 17 are shifted downwards which is interpreted as decay.

When mixing occurs, the interpretation of the evolution of ^{36}Cl/Cl and ^{36}Cl (Figures 6.15(a) and 6.15(b)) becomes speculative, because different processes (for example decay and dissolution) can cancel out each other. In aquifer C, ^{36}Cl/Cl decreases from well 8 to well 19, but there is no observable change in ^{36}Cl from well 17 to well 19 (Figure 6.17). This could be interpreted as radioactive decay along the direction of the groundwater flow (well 8 $\rightarrow$ 15 $\rightarrow$ 17), whereas at well 19, decay equals ^{36}Cl subsurface production (no change in ^{36}Cl/L), and the impact of nonradioactive chlorine is visible since the ^{36}Cl/Cl ratio decreases.

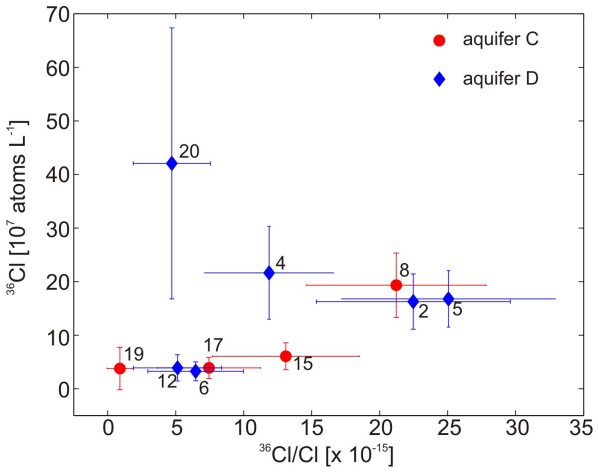

Figure 6.17: ^{36}Cl plotted against ^{36}Cl/Cl. Other factors than radioactive decay dominate ^{36}Cl in the far distant wells.

In aquifer D, one can assume ^{36}Cl/Cl decay from the wells in the recharge area (2, 4, 5) to wells 6 and 12 further downstream. Then again, the almost constant ^{36}Cl/Cl ratio from well 12 to well 20, with a simultaneous strong ^{36}Cl increase, shows that either mixing takes place or other processes than decay dominate the ^{36}Cl concentration. This could be an enhanced subsurface production to which nonradioactive chlorine is added concurrently. Still, other explanations might also fit the high ^{36}Cl at well 20: it could also be an indication for strong evaporation effects.

^{36}Cl initial concentration

Data of ^{36}Cl for rain or shallow groundwater samples were not available for the present study. An estimation of the input value was therefore performed on the theoretical cosmogenic production.

The number of ^{36}Cl atoms (N_{36}) for today's climatic condition in Dhofar can be calculated using equation 6.14 and an average ^{36}Cl fallout of 20 atoms m^{-2} s^{-1} (see Figure 6.4). Since the ratio ^{36}Cl to Cl is not changed by evaporation, ^{36}Cl also accumulates when smaller rainfall events evaporate at the land surface. The fallout (F) in equation 6.14 is then not 20 atoms m^{-2} s^{-1} but the respective concentrated number.

Continuing with the example given above, with Cl=526 mg l^{-1} - corresponding to the 26-fold of the initial concentration of Cl with 20 mg l^{-1}, results for the fallout in 526 atoms m^{-2} s^{-1}. N_{36} is calculated to 6.8×10^{8} atoms per one litre water and to a ^{36}Cl/Cl ratio of about 76×10^{-15} for the event in February 1983, with a precipitation of 23 mm and no assumed evaporation. These values are in the same order as the measured and calculated ones displayed in Table 6.8.

Compared to initial values in the literature the calculated ^{36}Cl/Cl ratio of about 76×10^{-15} at at^{-1} is a bit low, but fits in the range. Love et al. (2000) give a value of 125 $\times10^{-15}$ at at^{-1} for ^{36}Cl/Cl for the Great Artesian Basin for example. The value is confirmed by Sturchio et al. (2004) and validated with ^{81}Kr data. Other studies, for example Bentley et al. (1986) with 110 $\times10^{-15}$ at at^{-1} or Guendouz and Michelot (2006) with 116 $\times10^{-15}$ at at^{-1}, give comparable values for ^{36}Cl/Cl.

Values above those in the literature, but almost in the same order can be obtained when ^{36}Cl is calculated for the fallout above (20 atoms m^{-2} s^{-1}), todays mean annual precipitation in the recharge area (70 mm a^{-1} at station Uyun), a

high evaporation rate of 95% and the concentration of Cl = 50 mg l^{-1}. This would result in 1.8 $\times 10^8$ atoms per one litre water and a $^{36}Cl/Cl$ ratio of about 215×10^{-15} at at^{-1}. The number of atoms then falls within the range of wells (2, 4 and 5) in the recharge area. And the $^{36}Cl/Cl$ ratio lies within the range of the values in the literature.

During all these calculations we need to keep in mind that they hold for present arid conditions. The measured groundwater samples on the other hand represent water which was probably recharged to the aquifers under quite different conditions: more humid times with more precipitation and less evaporation, as well as changes of the atmospheric fallout. Plummer et al. (1997) say, for example, that the fallout was around 30 % above todays values between 12 to 40 ka BP. A raise of 30 % would lead to a $^{36}Cl/Cl$ ratio of approximately about 150×10^{-15} at at^{-1}. In comparison, the analysed values (recharge area) in the present study are 4 to 5 times below a medium value of 125×10^{-15} at at^{-1}.

The difficulty in identifying representative initial $^{36}Cl/Cl$ values also becomes evident when comparing the data for the wells 2 and 5 in aquifer D and well 8 in aquifer C, which show approximately the same ^{36}Cl and $^{36}Cl/Cl$ values. This is somehow surprising since 2 and 5 are wells in the recharge area at the beginning of the flowpath, whereas well 8 is located 80 km downstream. Also, be reminded that aquifer C is not distributed in the recharge area and is most likely filled by aquifer D. The residence time in C should therefore be longer than in D. With respect to ^{36}Cl, lower concentrations in aquifer C would have been expected. One explanation for the comparatively high concentrations in well 8 could be that the transport of the water from the recharge area to well 8 proceeds faster than decay takes place. However, that this cannot be the case is proven by Figure 6.18 where ^{36}Cl is plotted against ^4He.

$^4He_{rad}$ in well 8 is more than 30 times $^4He_{rad}$ in well 2 and is in the same order as wells 6 and 12 in the interior of aquifer D. In well 8 there was a clear radiogenic influence indicating that the residence time is longer than in well 2 where the detected influence was clearly atmospheric (see Figure 6.9). Whereas ^{36}Cl gives the same range for wells 2 and 8, $^4He_{rad}$ clearly shows a longer residence time for the sampled water in well 8. A possible interpretation is that ^{36}Cl refers to old Cl whereas the $^4He_{rad}$ is a sign for old water. This would support the influence of mixing on the $^{36}Cl/Cl$ ratios as discussed before.

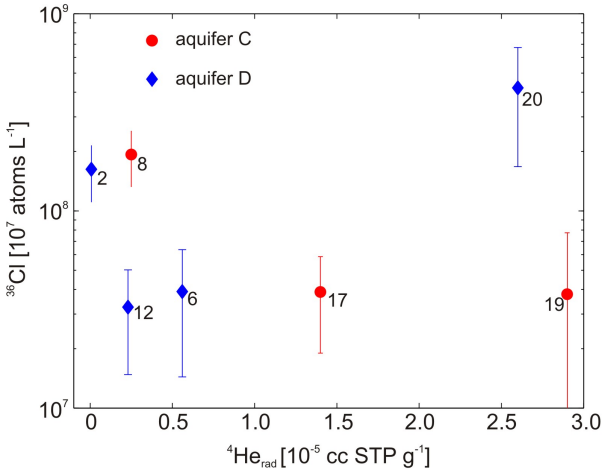

Figure 6.18: ^{36}Cl plotted against $^{4}He_{rad}$. $^{4}He_{rad}$ is increasing in groundwater flow direction in both aquifers. Well 8 in aquifer C has with $^{4}He_{rad} = 2.5\times10^{-6}$ ccSTP g^{-1} more than the 30-fold of well 2 ($^{4}He_{rad} = 7.3\times10^{-8}$ ccSTP g^{-1}, showing a clear radiogenic influence (see also Figure 6.9) and a longer residence time than well 2 in the recharge area in aquifer D.

However, the time span between the sampling of ^{4}He and ^{14}C (November 2009) and ^{36}Cl (January 2012) cannot be ignored. This could be less significant for the wells in aquifer C, since these wells (the ones sampled for ^{36}Cl) are all monitoring wells or artesian wells which are normally not in use. However, there might be relevant influences regarding the origin of the water: for example, the influence of different flowpaths in face of the abstraction in wells further upstream.

In aquifer D where wells 2, 6 and 12 (well 12 since summer 2011) are pumped regularly the situation is more difficult. For the wells at the animal farm (including well 6) discharge between November 2009 and January 2012 was calculated above to be approximately 700,000 to 800,000 m^3. The origin of the waters is therefore most likely different for the two sampling campaigns. Comparing ^{4}He and ^{36}Cl might therefore not be meaningful for the wells in aquifer D. However, it remains a fact that both aquifers show an upstream trend of the isotope tracers increasing in ^{4}He with distance, while decreasing in ^{36}Cl.

^{36}Cl in-situ production

The deep subsurface production can be calculated with Equation 6.15, the neutron flux - as shown before - with Equation 6.5 and the parameters given in Table 6.4. In summary, the following parameters were used for the calculation of R_{36}: a=1.07, b=0.28, τ=7.3×10^{-14} s^{-1} t=1.5 Ma and ϕ from 7.63×10^{-6} to 2.81×10^{-5} (depending on the values for U and Th, see Table 6.2). The secular equilibrium R_{36} was then calculated to have values between 3.47×10^{-15} and 12.8×10^{-15} at at^{-1}.

The secular equilibrium should not be above the smallest measured ^{36}Cl/Cl ratio. As can be seen in Table 6.8, this is the case with the exception of well 19, which has a measured ^{36}Cl/Cl ratio of 0.89×10^{-15}. The difference between the calculated R_{36} and the measured ^{36}Cl/Cl for well 19 might be due to uncertainties in the values for a and b (taken from the literature). Furthermore, consideration needs to be given to the large error interval of well 19. The calculated range for R_{36} nicely fits the values in the literature. Phillips (2000) for example, suggests 8(±3)×10^{-15} at at^{-1} for the secular equilibrum in-situ production in the aquifer when assuming constant Cl concentration.

This calculation was not made for the shale in the confining layers and at the bottom of the LUER since the impact of the confining layers could not really be evaluated in the section on helium above, and since no values for U and Th (as well as on a and b) for the shales in the study area were available.

Calculation of travel times based on ^{36}Cl data

As shown above, there is considerable uncertainty regarding the initial ^{36}Cl/Cl ratio. In addition, the near subsurface production cannot be evaluated on basis of the available data. Theoretical considerations can be made, such as taking in account the elevation of the study region, the aridity and the calcium rich limestone material. However, they are not really meaningful, since they would not narrow the existing uncertainties.

The present study uses relative ages, that is the age difference between the wells at the beginning of the flowpath and the next wells downstream. For aquifer C these are the wells 8 (start) and 15 and 17 (end), for aquifer D the wells 2 (start) and 12 (end).

The residence times were calculated using Equation 6.16 with an initial $^{36}Cl/Cl$ ratio of 125×10^{-15} at at^{-1}, R_{se}= 0 for the calculation of the minimum ages, and R_{se}=0.89×10^{-15} (as the lowest ratio analysed) for the calculation of the maximum ages. Table 6.10 shows the resulting groundwater residence times for the distances between the wells. The calculation of residence times were simplified by excluding analytical uncertainties (see Table 6.8).

Table 6.10: Relative ages based on ^{36}Cl for three wells in the interior Najd.

Well start	$^{36}Cl/Cl$ $[10^{-15}]$	Well end	$^{36}Cl/Cl$ $[\times 10^{-15}]$	distance [km]	^{36}Cl min [a] age [ka]	^{36}Cl max [b] age [ka]
8	21.22	15	13.09	97	210	220
8	21.22	17	7.45	123	450	490
2	22.47	12	6.47	100	540	590

[a] calculated by using R_{se}= 0
[b] calculated by using R_{se}= 0.89×10^{-15}, lowest analysed $^{36}Cl/Cl$ ratio in the present study

The calculated ^{36}Cl tracer model ages in Table 6.10 are between 200,000 and 500,000 years in aquifer C and around 550,000 years in aquifer D. These ages match the ages based on in-situ $^{4}He_{rad}$ production only, as displayed in Table 6.6. However, they are much higher than the residence times reaching up only to 30,000 years based on ^{14}C. For both aquifers the calculated flow velocities are below 0.5 m per year, meaning they vary significantly when compared to velocities based on ^{14}C. For example, the wells in the central Najd (approximate locations of the wells 12 and 13) and a ^{14}C tracer age of 8000 to 10 000 years yield a flow velocity of around 8 to 10 m per year.

In summary, two of the three environmental isotope tracers, namely ^{14}C and ^{36}Cl, disagree significantly in their calculated groundwater residence times and flow velocities for the Dhofar groundwaters. The measured concentrations of the third tracer, ^{4}He, could be the result of different parameter combinations (flow velocity, porosity or the crustal flux) as was shown in Figures 6.12(a) and 6.12(b). However, the relative groundwater ages based on $^{36}Cl/Cl$ data lead to flow velocities below 1 m yr^{-1}, pointing to higher aquifer porosity and lower crustal $^{4}He_{rad}$ flux rates.

6.4 Dating with a combination of tracers and groundwater flow modeling

As mentioned previously, the groundwater ages give us information on the flux in the system. Simply speaking, they tell us how much water is passing the system in a certain time. Besides the available water (the recharge), this depends on the seepage velocity the water is traveling with, and on the porosity, since the seepage velocity is the ratio of Darcian flux (product of the hydraulic gradient between the wells and the hydraulic conductivity of the formation) and effective porosity.

With the groundwater model in Chapter 5 a recharge rate of 4 mm a^{-1} which is sufficient to reproduce the hydraulic heads under todays dry conditions, was obtained.

From the tracer model age, with a focus on ^{36}Cl ages, one can calculate the seepage velocity by dividing distance between the wells by the residence time.

As mentioned in section 4.1.4, a variety of porosity values from 0.5 to 28 % were suggested by different authors for the Umm Er Radhuma. The variance in the values and the limited number of field measurements they are based on, does not permit limiting the porosity with an adequate degree of certainty. Porosity has therefore been an unknown parameter which had to be estimated.

In order to estimate the porosity with the calibrated groundwater model (see chapter 5) the relative ^{36}Cl-age, derived from the age difference of wells 2 and 12, was inserted in the groundwater flow model. It was assumed that well 2 with low $^{4}He_{rad}$ represents water recharged during the last humid period around 10 ka BP. These 10,000 years are short compared to the time span of 550,000 years. Therefore the 550,000 years were set as the tracer model age at well 12. In addition to the head and flow observations "age" was defined as a third observation class in the UCODE input file. The parameter estimation process was executed similar to the procedure described in chapter 5. For the estimation process only the porosity remained adjustable, while all other values were taken from the calibrated model and were fixed. The goal was to estimate the porosity value resulting in a flow model age of 550,000 years at well 12 when the recharge rate is 4 mm yr^{-1}.

The best fit between simulated flow-model age and ^{36}Cl tracer-model age could be obtained with a porosity value of 16.8% for the LUER. Assuming a homogenous porosity of 16.8% for the model layers representing the LUER, results in a

groundwater age distribution from around 0.5 Ma in the interior area to maximum ages of around 3.5 Ma in the far distant wells.

The procedure introduced above includes some necessary simplifications, such as constant (low) recharge values and a system in steady state. We know that in nature circumstances can vary along with recharge rates over time and transient flow conditions. The extent of these variations, say, for example, the duration of humid and dry periods or the difference in recharge amounts, is unknown.

The developed groundwater flow model was calibrated with a recharge rate of 4 mm a^{-1}, representing today's dry conditions. These dry recharge conditions are most likely below a long term average recharge rate which includes wet periods. The estimated 16.8% for the porosity therefore represent "dry" porosity. Assuming a long time average recharge rate above this dry value would inevitably result in a higher porosity value when fitting the flow model age to the tracer model age for well 12.

To prove this theory within the groundwater model, a porosity value of 25% was defined and the recharge rate - the parameter to be estimated - was set to be adjustable. The best fit could be obtained for a recharge value of 21 mm yr^{-1}, which is approximately five times the calibrated value. The maximum calculated groundwater residence times were now approximately 2.5 Myr at the far distant wells (well 19 and 20).

The difference in age distribution between both scenarios changes along the flowpath as can be seen in Figure 6.19(a). Up to a distance of approximately 110 km the age differences lie below 30,000 years, with higher ages in the 25% scenario. But with increasing distance (and time) the age differences reverse and increase with the direction of flow. In the section under focus here (0-350 km), the maximum difference was obtained with around 850,000 years at 350 km distance, i.e. with older ages in the 16.8% scenario.

The reasons are different flow velocities which are the result of different head gradients between the scenarios (see Figure 6.19(b)). An observation of the simulated heads showed much smaller gradients at the beginning of the flowpath, but higher head gradients with increasing distance for the 25% scenario.

Compared to the "dry" scenario with a recharge rate of 4 mm a^{-1}, the recharge rate obtained for the 25% scenario gives a "wet" recharge rate (and a "wet" porosity). Although it might be possible that single periods in the past had five times

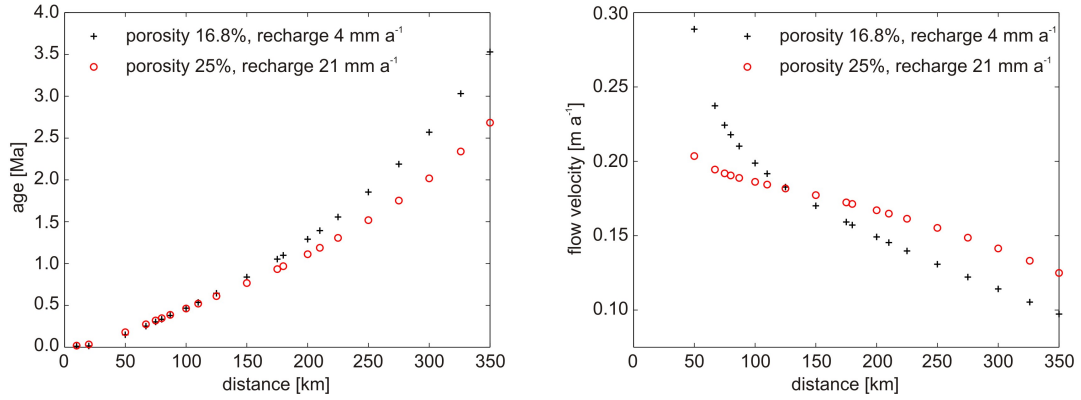

(a) groundwater ages versus distance

(b) flow velocity versus distance

Figure 6.19: Groundwater ages and flow velocity versus distance along the modelled cross-section for two different porosity values. (a) Groundwater age difference between the two scenarios increases with distance. (b) Higher head gradients downstream in the 25% scenario lead to higher flow velocities.

today's recharge rate it is probably too high of a value for a long term mean recharge rate. This raises the questions what the long term mean recharge value could be, and, consequentially, what a likely maximum recharge rate would be.

This question was answered in chapter 5, where maximum groundwater levels were reached for a value of around 10 mm a^{-1}. This value is two to three times that of modern day recharge (4 mm a^{-1}) and half the value of the 25% porosity scenario. The 10 mm a^{-1} rate is sufficient to fill the system and, more importantly, it indicates the long term maximum recharge. The resulting maximum groundwater levels produce the highest gradient caused by the highest recharge value. That is why they also provide the conditions for maximum flow.

This proves that the 21 mm a^{-1} recharge rate is too high for a long term mean value. The long term mean recharge rate has to be between 0, meaning no recharge, and 10 mm a^{-1} being the maximum long term mean.

Re-estimating the porosity with help of the groundwater flow model, for a recharge rate of 10 mm a^{-1} and the calculated ^{36}Cl tracer-model age of well 12 (550,000 years) yields a porosity value of 20 %. The age distribution along the flowline is close to that of the scenario with 25% and the double recharge value (21 mm a^{-1}) as can be seen in Figure 6.20(a).

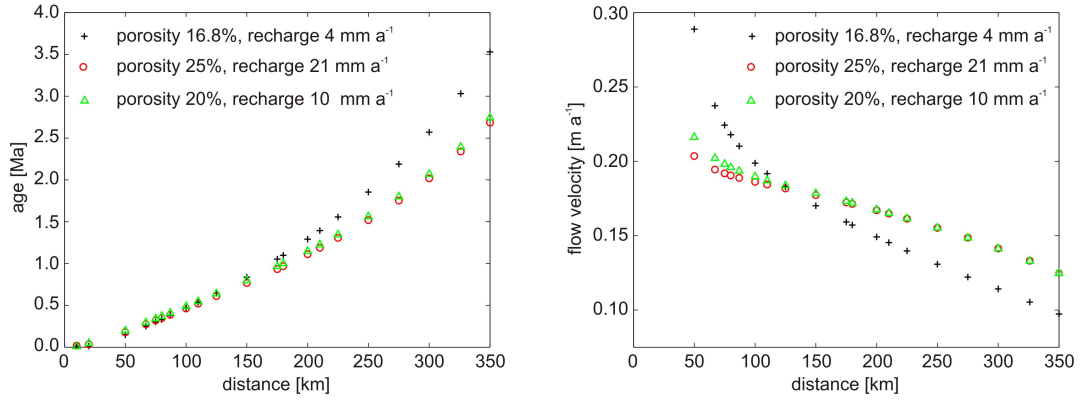

(a) groundwater ages versus distance

(b) flow velocity versus distance

Figure 6.20: Groundwater ages and flow velocity versus distance along the modelled cross-section for three different porosity values. Differences in age (a) and flow velocity (b) are small for the 20% and the 25% scenario.

The velocity versus distance plot in Figure 6.20(b) points in the same direction: compared to the 25% scenario there are slightly higher velocities in the 20% scenario at the beginning of the flowpath but almost no differences with increasing distance. In other words, increasing the recharge above the derived maximum value of 10 mm a^{-1} does not cause the water to flow faster through the aquifer. This strongly suggests that the recharge value of two to three times today's rate of 4 mm a^{-1} is the long term maximum value.

The long term maximum recharge rate of 10 mm a^{-1} represents an upper boundary for recharge. The lower boundary should be somewhere between 0 mm a^{-1} and the 4 mm a^{-1} of today's conditions. Regional porosity values far above 20% seem to be unlikely under the assumptions this study is based on, because they would require recharge rates above the obtained maximum value. It is possible that the 4 mm a^{-1} represent a lower medium value and not the lower boundary for the recharge rate. An indication for this would be that in the Dhofar Mountains today's observed groundwater heads with 550 m amsl are less then 100 m below the possible maximum water levels obtained with the groundwater model.

6.5 Conclusion groundwater residence times

In total 20 wells were used for the analysis and interpretation of environmental isotope tracer concentrations. The wells are located along a principal flowpath through the Najd, from the Dhofar Mountains in the south to the northeastern margin of Dhofar. 17 wells were sampled for ^{14}C and ^{4}He during the campaign in November 2009, ten wells were sampled in January 2012 for the analysis of ^{36}Cl. Seven wells were part of both sampling campaigns and contributed results for all three environmental isotopes.

While the concentration ^{4}He increased along the flowpath and the concentration of ^{36}Cl decreased downstream from the recharge area, the expected trend correlated with distance. A final interpretation for the ^{14}C activities was not possible at this point. In terms of ages, all samples represent mixtures of more or less broadly different waters. This is natural, since not only a single water molecule is analysed, but a quantity of molecules. The quantities compound as a result of increased pumping, borehole losses and mixing between the aquifers due to poorly constructed boreholes in the whole Najd (see section 2.5.4) as well as pumping in the sampled wells and the long open hole intervals of the sampled wells (see section 6.2).

With regard to ^{36}Cl the discussion yielded that mixing might be the reason for the quite low $^{36}Cl/Cl$ ratios in the recharge area. Possible sources for the different waters were suggested. It is not possible to further break down the analysed water in its proportions since the source rate and the mass fraction of the water compartments are unknown. This was already addressed in previous literature, see for example Bethke and Johnson (2008) or Torgersen et al. (2012, in preparation).

In spite of this and all given restrictions by the data, it might still be useful to interpret the isotope data in terms of groundwater residence times for the Najd. Figure 6.9 revealed that wells 1 and 2 are less influenced by $^{4}He_{rad}$ than the wells in the interior, indicating a relatively short residence time of the sampled water. The measured ^{14}C activities of the wells 1 and 2 (22.8 and 18.0 pmC) would confirm the shorter residence times. Herb (2011) calculated 8,000 and 11,500 years respectively based on the ^{14}C data for the two wells. These residence times lie in the same range as the calculated in-situ ^{4}He ages of 10,000 and 15,000 years, respectively, listed in Table 6.6. Since both isotope tracers result in reasonable groundwater

residence times, it could be assumed that mixing is a minor influence in these wells. With regard to the time scale, the water in this area was recharged during the humid period around 10,000 years BP (see chapter 2).

The residence times for the wells in the central Najd (approximately 100 km inland) were calculated to around 550,000 years in aquifer D based on ^{36}Cl. Here the relative age between two wells was calculated. For the wells farther north this would result in even older groundwater residence times up to 2 Ma. For aquifer C the residence times were calculated to 200,000 to 400,000 years for three wells in the interior. For both aquifers the derived flow velocities are below 0.5 m a^{-1}.

On the other hand, the calculated residence times based on ^{36}Cl in combination with the groundwater flow model allowed us to constrain the porosity ϕ, but also the crustal $^{4}He_{rad}$ flux, to a higher degree than shown above. Calculating the crustal $^{4}He_{rad}$ flux along the flowpath results in values between 1.7$\times$ 10^{-8} cm^3 STP cm^{-2} a^{-1} (well 2 to well 12) up to 5.0 $\times$ 10^{-7} cm^3 STP cm^{-2} a^{-1} (interior wells) and fits the range reported in the literature (see section 6.3.2).

The derived porosity values between 16 and 20 % fit the range reported in the literature for limestone, in general, but also for the UER formation in particular (see section 4.1.4). The proportion of fracture porosity and matrix porosity can not be evaluated. Variations in porosity in the UER are also possible in vertical direction (aquifer C, confining layers, aquifer D) as well as in the horizontal direction with up to more than one order of magnitude are possible.

The groundwater residence times of around 550,000 years for the central Najd stand in strong contrast to previous research. Based on ^{14}C, previous research calculated the range of the residence times for the groundwaters in the UER formations in the central Najd 15,000 to 20,000 years and in the far north back to 35,000 years. Concentration of ^{36}Cl and $^{4}He_{rad}$ as well as the parameters porosity and maximum recharge, which were derived with the groundwater flow model are indicative of the older residence times established in the present study.

Chapter 7

Conclusions and Outlook

Results

The question of ongoing and planned groundwater abstractions in the Najd - a problem crucial to the region's overall sustainability (see section 1) - stood at the outset of the present study. Only knowing the existing storage amounts and the possible input sources to the system allows for estimations, predictions and controlled provisions with regard to how much water can and should be abstracted. The general research question for the present study therefore was: *Are the Najd (deep) groundwaters part of an active flow system?*

Chapter 2 showed that with the monsoon and the sporadic cyclonic events in general a source for groundwater recharge is available in the Najd. The rainfall and wadi flow data analysed in chapter 4 provided information on the occurrence, frequency and duration of such events, but it also showed that the available data are not sufficient to draw conclusions about inputs to the groundwater system or about existing correlations of rainfall and wadi flow data.

Since possible modern input processes to the deep groundwater system cannot be directly observed with help of the existing monitoring network, the approach of the present study was to use a combination of groundwater flow modelling and environmental isotope tracer data, while intensifying groundwater level monitoring at the same time. The 2D-model presented in chapter 5 was used to examine the recharge scenarios that are theoretically possible. One model result was that today's observed groundwater heads cannot be the result of groundwater recharge in past humid periods (10,000 years ago) but have to be the result of recent inputs to

the groundwater reservoir, since otherwise the groundwater heads should be below the observed values. This model result was proven correct by the cyclonic storm "Keila" in October/ November 2011, when groundwater levels in the deep aquifers increased as a result of heavy rainfalls in the Najd. The model as well as the installed pressure transducers therefore showed that the deep Najd groundwaters are part of an active flow system.

If a natural depletion of the groundwater levels is ongoing can not be answered definitely. The model results indicate that changes between wet and dry periods can cause transient responses in heads and head gradients lasting for several thousand years.

One of the subquestions in this study was how long the water actually is in the groundwater system. By using environmental isotope tracer data an answer was suggested in chapter 6. In contradiction to previous studies, where, based on ^{14}C, the groundwater residence times were estimated to have been maximally 35,000 years, the ^{36}Cl data indicated groundwater residence times up to more than 2 Myr for the Najd groundwaters. These much older residence times were evaluated with the ^{4}He data and with the groundwater model. The analysed ^{4}He concentrations can be reasonably explained by in-situ production within the aquifer and an external helium flux from the Earth crust. With help of the groundwater flow model it was possible to estimate aquifer porosities which correspond to the tracer based residence times and the flow model based recharge rate.

Finally, information on recharge rates and on porosity is necessary in order to describe the flow in the system. Both parameters were derived in the present study. Today's recharge rate for the deep aquifers can be estimated to be 4 mm yr^{-1} with a maximum value of two to three times this rate. Aquifer porosity was estimated to be 16 to 20 %. These numbers are absolutely possible and comprehensive given the climatic and hydrogeological conditions in the Najd.

However, several factors remain uncertain or unknown at this point: uncertainties remain with regard to the groundwater residence times and the influence the mixing of different waters has on their distribution. Furthermore, the aquifer characteristics probably differ between aquifer C and D and should be investigated. The processes in the unsaturated zone are completely unclear, as is the vertical extent and characteristics of the confining layers (for example the pore volume).

Future activities

Chapter 2.3 presented a description of today's arid climate conditions and a short literature review on the occurrence of humid periods in the past. This dry/wet classification is often used in describing the hydrology of today's arid areas. Consequently, one tends to assume that groundwater recharge only takes place during the humid periods. However, we learned from cyclone Keila that arid phases and extreme rain events ($\rightarrow$ groundwater recharge) are possible at the same time.

Since such cyclonic events seem to affect the area in somewhat regular intervals (3 to 7 years), it is unlikely that the observed event was an isolated outlier. The stable water isotopes of the Najd groundwaters (see Figure 6.13(b)) also indicate strong cyclonic influence, because most of the sampled wells show water with a $\delta^2H/\delta^{18}O$ signature close to today's cyclones.

A fundamental question to ask is the appropriateness or meaningfulness of a dry/wet classification when studying groundwater recharge scenarios and associated periods of time. Against the background of humid, transitional or arid periods shown in Figure 2.5, we also have to ask ourselves in which category today's climate is best placed.

With the large time scale that needs to be considered for the Najd groundwaters now (see chapter 6), a natural follow-up question would be, what the relevance of "short" term climatic fluctuations (below 5,000 years) is for the groundwater reservoir. In the developed groundwater flow model we can now study possible climate and recharge scenarios and their influence on the groundwater regime. Climate scenarios discussed in the literature (see chapter 2.3), the influence of enhanced cyclone activity, or the differences between the long term mean recharge value and the fluctuation of wet and dry periods could be evaluated. Such scenarios become especially interesting when put in relation to studies which are based on other climate proxies such as speleothem growth or tree rings, but also when related to archaeological or geographical research with a focus on the history of settlement or land-use.

The groundwater model can also be used in a more practical way with regard to cyclonic events: cyclone Keila and the resulting observed groundwater level increase could be evaluated with the groundwater model. The observed response time and what it implies for the parameters in the flow model, and the necessary

recharge amount leading to the observed groundwater level increase should be the focus of such a study.

In his paleoclimate study Herb (2011) presents a paleotemperature record for the last 32,000 years. Based on ^{14}C-dating the noble gas temperature differences of around 6.3 °C were associated with a warm holocene and a colder late pleistocene period. Taking into account the groundwater residence times obtained in the present study, the time frame of 32,000 years for the Najd groundwaters is far too limited. A reinterpretation of the noble gas temperatures is therefore required and could also yield new insights on the previous climate conditions in the study area.

Measures

It is common knowledge that a well-designed monitoring network is the basis for the evaluation and characterization of any hydrogeological system. The detailed data description in chapter 4 was intended, *inter alia*, to illustrate the existing gaps in data and understanding. A number of proposals for more systematic and comprehensive monitoring can be made only on the basis of these findings. For example, monitoring of the abstraction rates at the discharge wells is absolutely essential. Besides the information on what is actually taken out of the aquifers, it will provide invaluable information for the parameter estimation of the formations.

Among the difficulties in the interpretation of the analysed environmental isotope concentrations presented in chapter 6 are the definition of initial values, the influence of in-situ production of the isotope, and the mixing of waters with different origins. One approach to partly overcome these problems would be to use another tracer, for example ^{81}Kr, which offers a long dating range (10^6 yr), less uncertainty in the initial value, no underground production and is also insensible to climate variations, since the isotope ratio is analysed (Purtschert et al., 2012, in preparation). Without a doubt some of the open questions could be solved and perhaps an even more accurate age range of the Dhofar groundwaters could be obtained.

On the other hand, instead of three one would have then four tracers. It is likely that other questions and problems would occur when interpreting those tracer concentrations. Also, shortcomings that are due to a system that is irreversibly destroyed and is no longer in its natural state, cannot be overcome by using another tracer.

One could probably also produce good results with less effort, for example by supplementing the existing data by specific sampling campaigns that sometimes presuppose new drilling - preferably in areas which are "black holes" at this point. This would be today's recharge area but also the whole area between well 2 and well 8 (see Figure 6.6) of the present study. Besides the fact that little is known about the groundwater in these areas, it is also of advantage that these areas close to the mountains are less subject to abstraction. Artificial pollution or mixing should therefore have less of an influence. The idea would be to use the groundwater model to detect areas with groundwater residence times fitting the ^{14}C age range, and to consequently sample and analyse wells which are located in these areas. The comparison of predicted and analysed groundwater residence times would, in the best case, further support the results of the present study.

Another focus of study should be mixing processes themselves, since they seem quite influental. In order to reach a better understanding the water would have to be analysed for ^{3}H, ^{14}C and ^{36}Cl again, whereas this time the focus would be on vertical profiles. Shallow water containing ^{3}H could be used for the analysis of evaporation effects on the infiltrating water as well as for the estimation of today's initial value for ^{36}Cl. Deep water containing ^{3}H or high concentrations of ^{14}C would indicate that the vertical distance (more than 300 m into the recharge area) can be overcome quite rapidly. The concentration profiles of all three tracers could be used for mixing calculations and to calculate the fractions of young and old water. This in turn could possibly also contribute to an interpretation of the ^{14}C-data of the 2009 sampling campaign in the present study.

The measures above show, that even though valuable results were gained in the present study, the Najd offers numerous possibilities for future studies.

References

W. Aeschbach-Hertig, F. Peeters, U. Beyerle, and R. Kipfer. Palaeotemperature reconstruction from noble gases in ground water taking into account equilibration with entrapped air. Nature, 405(6790):1040–1044, 2000. [in page nr. : 89]

W. Aeschbach-Hertig, U. Beyerle, J. Holocher, F. Peeters, and R. Kipfer. Excess air in groundwater as a potential indicator of past environmental changes. In International Conference on the Study of Environmental Change Using Isotope Techniques, pages 34–36, 2001. [in page nr. : 89]

L.H. Ahrens. Physics and Chemistry of the Earth, volume 6. Pergamon Press, 1965. [in page nr. : 112]

S. Akhmadaliev, R. Heller, D. Hanf, G. Rugel, and S. Merchel. The new 6 MV AMS-facility DREAMS at Dresden. Nuclear Instruments and Methods in Physics Research Section B: Beam Interactions with Materials and Atoms, (0), 2012. ISSN 0168-583X. doi: 10.1016/j.nimb.2012.01.053. URL `http://www.sciencedirect.com/science/article/pii/S0168583X12000961`. [in page nr. : 95]

M. S. S. Al Lamki and J. J. M. Terken. The role of hydrogeology in Petroleum Development Oman. Middle East Petroleum Geosciences, GeoArabia, 1(4):495–510, 1996. [in page nr. : 21]

A.S. Al-Marshudi. Traditional irrigated agriculture in oman. Water International, 26(2):259–264, 2001. [in page nr. : 7]

Khalid S.A. Al-Mashaikhi. Evaluation of groundwater recharge in Najd aquifers using hydraulics, hydrochemical and isotope evidence. PhD thesis, Helmholtz Centre for Environmental Research - UFZ, 2011. [in page nr. : 3, 10, 11, 13, 14, 17, 19, 26, 30, 40, 102, 104, 107, 108, 114, 121, 122]

J. N. Andrews. The isotopic composition of radiogenic helium and its use to study groundwater movement in confined aquifers. Chemical geology, 49(1-3):339–351, 1985. [in page nr. : 90, 112]

J.N. Andrews and D.J. Lee. Inert gases in groundwater from the Bunter Sandstone of England as indicators of age and palaeoclimatic trends. Journal of Hydrology, 41(3-4):233–252, 1979. [in page nr. : 89]

JN Andrews, J.C. Fontes, J.L. Michelot, and D. Elmore. In-situ neutron flux, 36 Cl production and groundwater evolution in crystalline rocks at Stripa, Sweden. Earth and planetary science letters, 77(1):49–58, 1986. [in page nr. : 88]

W. Bakiewicz, DM Milne, and M. Noori. Hydrogeology of the Umm Er Radhuma aquifer, Saudi Arabia, with reference to fossil gradients. Quarterly Journal of Engineering Geology and Hydrogeology, 15(2):105, 1982. [in page nr. : 22, 40]

A.M.A. Bawain. Influence of Vegetation on Water Fluxes at the Ground Level in a Semi-arid Cloud Forest in Oman. PhD thesis, Chemisch-Geowissenschaftliche Fakultät der Friedrich-Schiller-Universität Jena, 2012. [in page nr. : 11, 30, 34]

J. Beer, H.A. Synal, P.W. Kubik, M. Kaba, and E. Nolte. 36 CL in modern atmospheric precipitation. Geophysical research letters, 26(10):1401–1404, 1999. [in page nr. : 95]

B.B. Benson and D. Krause. Isotopic fractionation of helium during solution: A probe for the liquid state. Journal of Solution Chemistry, 9(12):895–909, 1980. [in page nr. : 90]

H. Bentley, F.M. Phillips, S.N. Davis, MA Habermehl, P.L. Airey, G.E. Calf, D. Elmore, H.E. Gove, and T. Torgersen. Chlorine-36 dating of very old groundwater: The Great Artesian Basin, Australia. Water Resour. Res, 22(13):1991–2001, 1986. [in page nr. : 96, 97, 127]

H.W. Bentley, F.M. Phillips, S.N. Davis, S. Gifford, D. Elmore, L.E. Tubbs, and H.E. Gove. Thermonuclear 36Cl pulse in natural water. 1982. [in page nr. : 95]

C.M. Bethke and T.M. Johnson. Groundwater age and groundwater age dating. Annu. Rev. Earth Planet. Sci., 36:121–152, 2008. [in page nr. : 136]

C.M. Bethke, T. Torgersen, and J. Park. The age of very old groundwater: insights from reactive transport models. Journal of Geochemical Exploration, 69:1–4, 2000. [in page nr. : 98]

P. Blaser. Tracermethoden in der Hydrologie-Kombination verschiedener Methoden und Anwendungen am Beispiel des Ledo-Paniselian-Aquifers in Belgien. 2007. [in page nr. : 91]

D.J. Bourdon. Flow of fossil groundwater. Quarterly Journal of Engineering Geology & Hydrogeology, 10(2):97, 1977. [in page nr. : 22]

G.A. Brook and S.W. Sheen. Article: Rainfall in Oman and the United Arab Emirates: Cyclicity, Influence of the Southern Oscillation, and What the Future May Hold. The Arab World Geographer, 3(2):78–96, 2000. [in page nr. : 30]

S. J Burns, D. Fleitmann, M. Mudelsee, U. Neff, A. Matter, and A. Mangini. A 780-year annually resolved record of Indian Ocean monsoon precipitation from a speleothem from south Oman. Journal of Geophysical Research, 107(D20): 4434–4434, 2002. [in page nr. : 2]

S.J. Burns, D. Fleitmann, A. Matter, U. Neff, and A. Mangini. Speleothem evidence from Oman for continental pluvial events during interglacial periods. Geology, 29(7):623–626, 2001. [in page nr. : 14, 15]

M. C Castro, D. Patriarche, and P. Goblet. 2-D numerical simulations of groundwater flow, heat transfer and 4He transport–implications for the He terrestrial budget and the mantle helium-heat imbalance. Earth and Planetary Science Letters, 237(3-4):893–910, 2005. [in page nr. : 98]

I. D Clark and J. C Fontes. Paleoclimatic reconstruction in northern Oman based on carbonates from hyperalkaline groundwaters. Quaternary Research, 33(3): 320–336, 1990. [in page nr. : 14]

I.D. Clark. Groundwater Resources in the Sultanate of Oman: origin, circulation times, recharge processes and paleoclimatology. Isotopic and geochemical approaches. Unpublished Doctoral thesis, Université de Paris-Sud, Orsay, France, 264pp, 1987. [in page nr. : 2, 10, 14, 15, 19, 104, 105, 107, 108, 120, 122, 124, 125]

I.D. Clark and P. Fritz. Environmental isotopes in hydrogeology. CRC, 1997. [in page nr. : 20, 40, 86]

I.D. Clark, W.T. Bajjali, and G.C. Phipps. Constraining 14C ages in sulphate reducing groundwaters: two case studies from arid regions. In Isotopes in Water Resources Management. IAEA Symposium, volume 336, pages 43–56, 1995. [in page nr. : 2]

I.D. Clark, G.C. Phipps, and W.T. Bajjali. Constraining super (14) c ages in sulphate reducing groundwaters: Two case studies from arid regions. International Atomic Energy Agency. Proceedings Series[PROCEEDINGS SERIES]., pages 43–56, 1996. [in page nr. : 13, 14]

P.G. Cook, A.J. Love, N.I. Robinson, and C.T. Simmons. Groundwater ages in fractured rock aquifers. Journal of Hydrology, 308(1â4):284 – 301, 2005. ISSN 0022-1694. doi: 10.1016/j.jhydrol.2004.11.005. URL `http://www.sciencedirect.com/science/article/pii/S0022169404005360`. [in page nr. : 40]

S.N. Davis, D.W. Cecil, M. Zreda, and P. Sharma. Chlorine-36 and the initial value problem. Hydrogeology Journal, 6(1):104–114, 1998. [in page nr. : 94, 96]

H.JG. Diersch. FEFLOW - Finite Element Subsurface Flow & Transport Simulation System. 2009. [in page nr. : 46]

Nguyen Dinh Chau, Marek Dulinski, Pawel Jodlowski, Jakub Nowak, Kazimierz Rozanski, Monika Sleziak, and Przemyslaw Wachniew. Natural radioactivity in groundwater - a review. Isotopes in Environmental and Health Studies, 47(4):415–437, 2011. doi: 10.1080/10256016.2011.628123. URL `http://www.tandfonline.com/doi/abs/10.1080/10256016.2011.628123`. [in page nr. : 104]

ERSDAC 2011. ERSDAC: ASTER GDEM is a product of METI and NASA *http://www.ersdac.or.jp/GDEM/E/index.html* (30.08.2011). [in page nr. : 9]

RD Faulkner. Fossil water or renewable resource: The case for one Arabian aquifer. Proceedings of the Institution of Civil Engineers. Water, Maritime and Energy, 106(4):325–331, 1994. [in page nr. : 22]

D. Fleitmann. Holocene Forcing of the Indian Monsoon Recorded in a Stalagmite from Southern Oman. Science, 300(5626):1737–1739, June 2003. ISSN

0036-8075. URL http://www.sciencemag.org/cgi/doi/10.1126/science.1083130. [in page nr. : 14, 15]

D. Fleitmann and A. Matter. The speleothem record of climate variability in Southern Arabia. Comptes Rendus Geosciences, 341(8-9):633–642, 2009. [in page nr. : 14]

D. Fleitmann, S.J. Burns, A. Mangini, M. Mudelsee, J. Kramers, I. Villa, U. Neff, A.A. Al-Subbary, A. Buettner, D. Hippler, et al. Holocene ITCZ and Indian monsoon dynamics recorded in stalagmites from Oman and Yemen (Socotra). Quaternary Science Reviews, 26(1-2):170–188, 2007. [in page nr. : 13, 14, 16]

D. Fleitmann, S. J Burns, M. Pekala, A. Mangini, A. Al-Subbary, M. Al-Aowah, J. Kramers, and A. Matter. Holocene and Pleistocene pluvial periods in Yemen, southern Arabia. Quaternary Science Reviews, pages –, 2011. [in page nr. : 2, 14, 15]

Jean-Charles Fontes and Jean-Marie Garnier. Determination of the initial 14C activity of the total dissolved carbon: A review of the existing models and a new approach. Water Resour. Res., 15(2):399–413, 1979. ISSN 0043-1397. doi: 10.1029/WR015i002p00399. URL http://dx.doi.org/10.1029/WR015i002p00399. [in page nr. : 85, 87]

R.A. Freeze and J.A. Cherry. Groundwater. 1977. [in page nr. : 40]

M. Fuchs and A. Buerkert. A 20 ka sediment record from the Hajar Mountain range in N-Oman, and its implication for detecting arid-humid periods on the southeastern Arabian Peninsula. Earth and Planetary Science Letters, 265(3-4):546–558, 2008. [in page nr. : 14, 15]

M.A. Geyh. Handbuch der physikalischen und chemischen Altersbestimmung. Wiss. Buchges., 2005. ISBN 9783534179596. URL http://books.google.de/books?id=0IylAAAACAAJ. [in page nr. : 85]

P.D. Glynn and L.N. Plummer. Geochemistry and the understanding of groundwater systems. Hydrogeology Journal, 13(1):263–287, 2005. [in page nr. : 81, 83]

H. Godwin. Half-life of radiocarbon. Nature, 195:984, 1962. [in page nr. : 86]

D. J Goode. Direct simulation of groundwater age. Water Resources Research, 32 (2):289–296, 1996. [in page nr. : 81, 98]

GRC. Detailed Water Resources Management and Planing Study for the Salalah Region (Part A) - Review. Technical report, Geo Resources Consultancy, 2005a. [in page nr. : 17, 32, 56, 65]

GRC. Drilling and Aquifer Testing Project in the western Al Wusta (Najd) Desert, Oman, Final Report, unpublished. Technical report, Ministry of Regional Municipality and Water Resources (MRMWR), 2005b. [in page nr. : 40]

GRC. Drilling and Aquifer Testing Programme in the Dhofar Governorate. Technical report, Geo Resources Consultancy, 2008. [in page nr. : 11, 12, 17, 19, 21, 32, 34, 38, 40]

A. Guendouz and J.L. Michelot. Chlorine-36 dating of deep groundwater from northern Sahara. Journal of Hydrology, 328(3):572–580, 2006. [in page nr. : 127]

A.W. Harbaugh. MODFLOW-2005: The US Geological Survey Modular Ground-water Model–the Ground-water Flow Process. US Geological Survey, 2005. [in page nr. : 46, 50, 99]

JA Heathcote and S. King. Umm as Samim, Oman: A sabkha with evidence for climate change. In Quaternary deserts and climatic change: proceedings of the International Conference on Quaternary Deserts and Climatic Change: Al Ain, United Arab Emirates, 9-11 December 1995, page 141. Taylor & Francis, 1998. [in page nr. : 14]

William Henry. Experiments on the Quantity of Gases Absorbed by Water, at Different Temperatures, and under Different Pressures. Philosophical Transactions of the Royal Society of London, 93:pp. 29–42+274–276, 1803. ISSN 02610523. URL http://www.jstor.org/stable/107068. [in page nr. : 87]

Christian Herb. Paleoclimate study based on noble gases and other environmental tracers in groundwater in Dhofar (Southern Oman). Master's thesis, Institute

of Environmental Physics, University of Heidelberg, 2011. [in page nr. : 3, 19, 26, 102, 104, 107, 109, 110, 121, 122, 136, 142]

A. Hildebrandt and E.A.B. Eltahir. Using a horizontal precipitation model to investigate the role of turbulent cloud deposition in survival of a seasonal cloud forest in Dhofar. J. Geophys. Res, 113:G04028, 2008. [in page nr. : 34]

A. Hildebrandt, M.A. Aufi, M. Amerjeed, M. Shammas, and E.A.B. Eltahir. Eco-hydrology of a seasonal cloud forest in Dhofar: 1. Field experiment. Water Resources Research, 43(10):10411, 2007. [in page nr. : 12]

M.C. Hill and C.R. Tiedeman. Effective groundwater model calibration: With analysis of data, sensitivities, predictions, and uncertainty. LibreDigital, 2007. [in page nr. : 48, 49, 55, 60, 63, 67]

http://www.fao.org. Food and Agriculture Organization of the United Nations *http://www.fao.org/nr/water/aquastat/countriesregions/oman/index.stm* (24.08.2012). [in page nr. : 7, 21]

E. Ingerson and F.J. Pearson. Estimation of age and rate of motion of ground water by the 14-C method. In Koyama-T. Miyake, Y., editor, Recent researches in the field of hydrosphere, atmosphere and nuclear geochemistry, pages 263–283. Editorial Committee for Sugawara Volume, 1964. [in page nr. : 87]

J. A. Izbicki, C. L. Stamos, T. Nishikawa, and P. Martin. Comparison of ground-water flow model particle-tracking results and isotopic data in the Mojave River ground-water basin, southern California, USA. Journal of Hydrology, 292(1-4): 30–47, 2004. [in page nr. : 98]

R. Kipfer, W. Aeschbach-Hertig, F. Peeters, and M. Stute. Noble gases in lakes and ground waters. Reviews in mineralogy and geochemistry, 47(1):615, 2002. [in page nr. : 88]

D. Lal and B. Peters. Cosmic ray produced radioactivity on the earth. pp 551-612 of Handbuch der Physik. Band XLVI/2. Fluegge, S. Sitte, K.(eds.). Berlin, Heidelberg, New York, Springer-Verlag, 1967., 1968. [in page nr. : 95, 96]

B. E. Lehmann, H. H. Loosli, R. Purtschert, and J. N. Andrews. A comparison of chloride and helium concentrations in deep groundwaters. International Atomic Energy Agency. Proceedings Series[PROCEEDINGS SERIES]., pages 3–17, 1996. [in page nr. : 114]

B.E Lehmann, A Love, R Purtschert, P Collon, H.H Loosli, W Kutschera, U Beyerle, W Aeschbach-Hertig, R Kipfer, S.K Frape, A Herczeg, J Moran, I.N Tolstikhin, and M Groening. A comparison of groundwater dating with 81Kr, 36Cl and 4He in four wells of the Great Artesian Basin, Australia. Earth and Planetary Science Letters, 211(3â4):237 – 250, 2003. ISSN 0012-821X. doi: 10.1016/S0012-821X(03)00206-1. URL `http://www.sciencedirect.com/science/article/pii/S0012821X03002061`. [in page nr. : 112, 113]

J.W. Lloyd and M.H. Farag. Fossil Ground-Water Gradients in Arid Regional Sedimentary Basins. Ground Water, 16(6):388–392, 1978. [in page nr. : 22]

J.W. Lloyd and J.C. Miles. An Examination of the Mechanisms controlling Groundwater gradients in hyper-arid regional sedimentary Basins. JAWRA Journal of the American Water Resources Association, 22(3):471–478, 1986. [in page nr. : 22]

AJ Love, AL Herczeg, L. Sampson, RG Cresswell, LK Fifield, et al. Sources of chloride and implications for 36Cl dating of old groundwater, southwestern Great Artesian Basin, Australia. Water Resources Research, 36(6):1561–1574, 2000. [in page nr. : 126, 127]

P. G. Macumber, B. G. Al-Said, G. A. Kew, and T. B. Tennakoon. Hydrogeologic implications of a cyclonic rainfall event in central Oman. Groundwater Quality: London, Chapman & Hall, pages 87–97, 1994. [in page nr. : 2, 120, 122]

B. A. Mamyrin and I. N. Tolstikhin. Helium isotopes in nature / B.A. Mamyrin and L.N. [i.e. I.N.] Tolstikhin. Elsevier, Amsterdam :, 1984. ISBN 0444421807 0444416358. [in page nr. : 88, 89, 90]

HA McClure. Radiocarbon chronology of late Quaternary lakes in the Arabian Desert. 1976. [in page nr. : 14, 15]

W.G. Mook. Carbon-14 in hydrological studies. In Fontes Ch. Fritz, P., editor, Handbool of Environmental Isotope Geochemistry. The Terrestrial Environment, pages 49–74. Elsevier, Amsterdam, 1980. [in page nr. : 87]

K. O. Muennich. Messungen des C14-Gehaltes von hartem Grundwasser. Naturwissenschaften, 44:32–33, 1957. ISSN 0028-1042. URL http://dx.doi.org/10.1007/BF01146093. 10.1007/BF01146093. [in page nr. : 85]

NASA. http://www.nasa.gov/mission/pages/hurricanes/archives/2011/h2011/Keila.html, 2011. [in page nr. : 77]

U. Neff. Massenspektrometrische Th/U-Datierung von Höhlensintern aus dem Oman: Klimaarchive des asiatischen Monsuns. PhD thesis, Universitätsbibliothek, 2001. [in page nr. : 2, 11, 14, 15]

I. Neretnieks. Age dating of groundwater in fissured rock: Influence of water volume in micropores. Water Resources Research, 17(2):421–422, 1981. [in page nr. : 40]

Brent D. Newman, Karsten Osenbrueck, K.ck, Werner Aeschbach-Hertig, D. Kip Solomon, Peter Cook, Kazimierz Rozanski, and Rolf Kipfer. Dating of young groundwaters using environmental tracers: advantages, applications, and research needs. Isotopes in Environmental and Health Studies, 46(3):259–278, 2010. doi: 10.1080/10256016.2010.514339. URL http://www.tandfonline.com/doi/abs/10.1080/10256016.2010.514339. [in page nr. : 98]

N.N. Groundwater Modelling of the Nejd Aquifers. Technical report, Ministry of Regional Municipalities, Environment and Water Resources, 2007. [in page nr. : 38]

M. Ozima and F.A. Podosek. Noble gas geochemistry. Cambridge Univ Pr, 2002. [in page nr. : 87, 90]

Y. Parrat, W. Hajdas, U. Baltensperger, H.A. Synal, PW Kubik, M. Suter, and HW Gaeggeler. Cross section measurements of proton induced reactions using a gas target. Nuclear Instruments and Methods in Physics Research Section B: Beam Interactions with Materials and Atoms, 113(1):470–473, 1996. [in page nr. : 95, 96]

PAWR. The Najd Exploratory Drilling Investigation. Technical report, Public Authority for Water Resources, 1986. [in page nr. : 17, 19]

F.J. Pearson, W. Balderer, H.H. Loosli, B.E. Lehmann, A. Matter, Tj. Peters, H. Schmassmann, and A. Gautschi. Applied Isotope Hydrogeology: A Case Study in Northern Switzerland. Technischer Bericht NTB. Elsevier, 1991. ISBN 9780444889836. URL http://books.google.de/books?id=fEBs7PudzAEC. [in page nr. : 88, 95, 96, 97, 112]

F.M. Phillips. Environmental Tracers in Subsurface Hydrology, chapter Chlorine-36, pages 299–348. Kluwer Academic Press, Boston, Mass., 2000. [in page nr. : 95, 96, 130]

F.M. Phillips. Isotope Methods for Dating Old Groundwater, chapter Chlorine-36 Dating of Old Groundwater, pages 140–168. IAEA Vienna Austria, 2012, in preparation. [in page nr. : 93, 94, 96, 98]

F.M. Phillips, H.W. Bentley, S.N. Davis, D. Elmore, and G.B. Swanick. Chlorine 36 dating of very old groundwater: 2. Milk River aquifer, Alberta, Canada. Water Resources Research, 22(13):2003–2016, 1986. [in page nr. : 97]

L.N. Plummer and P.D. Glynn. Isotope Methods for Dating Old Groundwater, chapter Radiocarbon Dating in Groundwater Systems, pages 46–101. IAEA Vienna Austria, 2012, in preparation. [in page nr. : 85]

L.N. Plummer, E.C. Prestemon, and D.L. Parkhurst. An interactive code (NETPATH) for modeling geochemical reactions along a flow path. U.S. Geological Survey, version 2.0 water resources investigation report edition, 1994. [in page nr. : 87]

M.A. Plummer, F.M. Phillips, J. Fabryka-Martin, HJ Turin, P.E. Wigand, and P. Sharma. Chlorine-36 in fossil rat urine: an archive of cosmogenic nuclide deposition during the past 40,000 years. Science, 277(5325):538–541, 1997. [in page nr. : 128]

E.P. Poeter, M.C. Hill, E.R. Banta, Steffen Mehl, and Steen Christensen. UCODE2005 and Six Other Computer Codes for Universal Sensitivity Analysis,

Calibration, and Uncertainty Evaluation. U.S. Geological Survey Techniques and Methods 6 - A11, 283p., 2005. [in page nr. : 48, 50]

D.W. Pollock. Users Guide for MODPATH/MODPATH-PLOT, Version 3: A particle tracking post-processing package for MODFLOW, the US Geological Survey finite-difference ground-water flow model. US Geological Survey Open-File Report, 94(464):6, 1994. [in page nr. : 60, 99]

D. Porcelli, C. Ballentine, and R. Wieler. Noble gases in geochemistry and cosmochemistry. Rev. Mineral. Geochem, 47:844, 2002. [in page nr. : 87]

R. Purtschert, R. Yokochi, and N.C. Sturchio. Isotope Methods for Dating Old Groundwater, chapter 81-Kr dating of old groundwater, pages 103–139. IAEA Vienna Austria, 2012, in preparation. [in page nr. : 142]

J. Roger, J. Platel, C. Bourdillon-de Crissac, and Cavelier. Geology of Dhofar (Sultanate of Oman) Geology and geodynamic evolution during the Mesozoic and Cenozoic. Technical report, MInistry of Petroleum and Minerals Sultanate of Oman, 1992. [in page nr. : 17, 18]

TM Rosenberg, F. Preusser, D. Fleitmann, A. Schwalb, K. Penkman, TW Schmid, MA Al-Shanti, K. Kadi, and A. Matter. Humid periods in southern Arabia: Windows of opportunity for modern human dispersal. Geology, 39(12):1115–1118, 2011. [in page nr. : 14, 15]

W.E. Sanford and J.P. Pope. Current challenges using models to forecast seawater intrusion: lessons from the Eastern Shore of Virginia, USA. Hydrogeology Journal, 18(1):73–93, 2010. [in page nr. : 99]

W.E. Sanford and W.W. Wood. Hydrology of the coastal sabkhas of Abu Dhabi, United Arab Emirates. Hydrogeology Journal, 9(4):358–366, 2001. [in page nr. : 65]

W.E. Sanford, L.N. Plummer, D.P. McAda, L.M. Bexfield, and S.K. Anderholm. Hydrochemical tracers in the middle Rio Grande Basin, USA: 2. Calibration of a groundwater-flow model. Hydrogeology Journal, 12(4):389–407, 2004. [in page nr. : 98]

R.S. Schemenauer and P. Cereceda. Monsoon cloudwater chemistry on the Arabian Peninsula. Atmospheric Environment. Part A. General Topics, 26(9):1583–1587, 1992. [in page nr. : 120]

D.K. Solomon, A. Hunt, and R.J. Poreda. Source of radiogenic helium 4 in shallow aquifers: Implications for dating young groundwater. Water Resources Research, 32:1805–1814, 1996. doi: 10.1029/96WR00600. [in page nr. : 89, 91]

NC Sturchio, X. Du, R. Purtschert, BE Lehmann, M. Sultan, LJ Patterson, ZT Lu, P. Müller, T. Bigler, K. Bailey, et al. One million year old groundwater in the Sahara revealed by krypton-81 and chlorine-36. Geophys. Res. Lett, 31(5): L05503, 2004. [in page nr. : 127]

M. Stute, C. Sonntag, J. Déak, and P. Schlosser. Helium in deep circulating groundwater in the Great Hungarian Plain: Flow dynamics and crustal and mantle helium fluxes. Geochimica et cosmochimica acta, 56(5):2051–2067, 1992. [in page nr. : 118]

Tamers. Surface-Water Infiltration and Groundwater Movement in Arid Zones of Venezuela. Isotopes in Hydrology, Proceedings Symposium of International Atomic Energy Agency and International Union Geodesy and Geophysics, Vienna:339–353, 1967. [in page nr. : 87]

T. Torgersen. Controls on pore-fluid concentration of 4He and 222Rn and the calculation of 4He/222Rn ages. Journal of Geochemical Exploration, 13(1):57–75, 1980. [in page nr. : 91]

T. Torgersen. Continental degassing flux of 4He and its variability. Geochemistry Geophysics Geosystems, 11(6):Q06002, 2010. [in page nr. : 116, 118]

T. Torgersen and W. B. Clarke. Helium accumulation in groundwater, I: An evaluation of sources and the continental flux of crustal 4He in the Great Artesian Basin, Australia. Geochimica et Cosmochimica Acta, 49(5):1211–1218, 1985. [in page nr. : 91, 92, 115, 116]

T. Torgersen and G. N. Ivey. Helium accumulation in groundwater. II: A model for the accumulation of the crustal 4He degassing flux. Geochimica et Cosmochimica Acta, 49(11):2445–2452, 1985. [in page nr. : 91, 93]

T. Torgersen and M. Stute. Isotope Methods for Old Groundwater, chapter Helium (and other Noble Gases) as a Tool for Understanding Long Time-Scale Groundwater Transport, pages 196–233. IAEA Vienna Austria, 2012, in preparation. [in page nr. : 112]

T. Torgersen, R. Purtschert, F. Phillips, L. Plummer, W. Sanford, and A. Suckow. Isotope Methods for Dating Old Groundwater, chapter Defining Groundwater Age, pages 33–45. IAEA Vienna Austria, 2012, in preparation. [in page nr. : 82, 136]

A. Visser. Trends in groundwater quality in relation to groundwater age. Netherlands Geographical Studies, 384, 2009. [in page nr. : 98]

J.C. Vogel. Investigation of groundwater flow with radiocarbon. Isotopes in Hydrology, Vienna, 1967. [in page nr. : 87]

C. E. Weyhenmeyer. Cool Glacial Temperatures and Changes in Moisture Source Recorded in Oman Groundwaters. Science, 287(5454):842–845, February 2000. ISSN 00368075. URL http://www.sciencemag.org/cgi/doi/10.1126/science.287.5454.842. [in page nr. : 2, 14, 15]

R. Yokochi, T. Torgersen, A. Suckow, M. Stute, N.C. Sturchio, W. Sanford, R. Purtschert, L.N. Plummer, F. Phillips, P. Glynn, K. Froehlich, and P.K. Aggarwal. Isotope Methods for Dating Old Groundwater, chapter Introduction, pages 11–15. IAEA Vienna Austria, 2012, in preparation. [in page nr. : 85]

C. Zhu. Estimate of recharge from radiocarbon dating of groundwater and numerical flow and transport modeling. Water Resources Research, 36(9):2607–2620, 2000. [in page nr. : 98]